


ไฮโดรจิเนชันของคาร์บอนไดออกไซด์โดยตัวเร่งปฏิกิริยาโคบอลต์บนวัสดุเชิงประกอบ  
อะลูมินาซีลิกา



นางสาว ธมลวรรณ เจษฎานุรักษ์

ศูนย์วิทยทรัพยากร  
จุฬาลงกรณ์มหาวิทยาลัย

วิทยานิพนธ์นี้เป็นส่วนหนึ่งของการศึกษาตามหลักสูตรปริญญาวิศวกรรมศาสตรมหาบัณฑิต

สาขาวิชาวิศวกรรมเคมี ภาควิชาวิศวกรรมเคมี

คณะวิศวกรรมศาสตร์ จุฬาลงกรณ์มหาวิทยาลัย

ปีการศึกษา 2553

ลิขสิทธิ์ของจุฬาลงกรณ์มหาวิทยาลัย

CARBON DIOXIDE HYDROGENATION OVER ALUMINA-SILICA  
COMPOSITES-SUPPORTED COBALT CATALYST

Miss Thamonwan Jetsadanurak

ศูนย์วิทยทรัพยากร

A Thesis Submitted in Partial Fulfillment of the Requirements  
for the Degree of Master of Engineering Program in Chemical Engineering  
Department of Chemical Engineering  
Faculty of Engineering  
Chulalongkorn University  
Academic Year 2010  
Copyright of Chulalongkorn University

Thesis Title            CARBON DIOXIDE HYDROGENATION OVER ALUMINA-SILICA  
COMPOSITES-SUPPORTED COBALT CATALYST


By                         Miss Thamonwan Jetsadanurak

Field of Study         Chemical Engineering


Thesis Advisor        Associate Professor Bunjerd Jongsomjit, Ph.D.

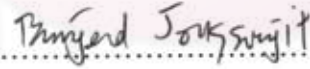
---

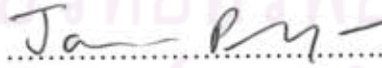
Accepted by the Faculty of Engineering, Chulalongkorn University in Partial  
Fulfillment of the Requirements for the Master's Degree

  
.....Dean of the Faculty of Engineering  
(Associate Professor Boonsom Lerdhirunwong, Dr.Ing.)

#### THESIS COMMITTEE

  
.....Chairman  
(Assistant Professor Anongnat Somwangthanaroj, Ph.D.)

  
.....Thesis Advisor  
(Associate Professor Bunjerd Jongsomjit, Ph.D.)

  
.....Examiner  
(Assistant Professor Joongjai Panpranot, Ph.D.)

  
.....External Examiner  
(Assistant Professor Okorn Mekasuwandamrong, Ph.D.)

ชมลวรรณ เจษฎานุรักษ์ : ไฮโดรเจนชั้นของคาร์บอนไดออกไซด์โดยตัวเร่งปฏิกิริยา  
โคบอลต์บนวัสดุเชิงประกอบอะลูมินาซิลิกา (CARBON DIOXIDE HYDRO  
GENATION OVER ALUMINA-SILICA COMPOSITES-SUPPORTED  
COBALT CATALYST) อ. ที่ปริกษาวิทยานิพนธ์หลัก: รศ. ดร. บรรเจิด จงสมจิตร, 88  
หน้า

งานวิจัยนี้ได้ศึกษาคุณลักษณะของตัวรองรับวัสดุเชิงประกอบอะลูมินาซิลิกาที่ถูกปรับปรุง  
ด้วยการเคลือบฝั่งของอนุภาคอะลูมินาบนพื้นผิวของซิลิกาทรงกลมโดยใช้ปฏิกิริยาไฮโดรลิซิสของ  
อะลูมิเนียมไฮดรอกไซด์ โดยการเปลี่ยนปริมาณอะลูมินาบนซิลิกา หรือ AISSP รวมทั้งการ  
เผาไหม้ในอากาศที่อุณหภูมิ 650 และ 1000 องศาเซลเซียส นอกจากนี้ศึกษาคุณลักษณะของตัวเร่ง  
ปฏิกิริยาโคบอลต์บนซิลิกาหรือ CoSSP และวัสดุเชิงประกอบอะลูมินาซิลิกาหรือ CoAISSP รวมทั้ง  
ศึกษาความว่างและค่าการเลือกเกิดมีเทนของตัวเร่งปฏิกิริยาโคบอลต์บนซิลิกาหรือ CoSSP และ  
วัสดุเชิงประกอบอะลูมินาซิลิกาหรือ CoAISSP สำหรับปฏิกิริยาคาร์บอนไดออกไซด์ไฮโดรเจนชั้น  
ที่อุณหภูมิของปฏิกิริยา 220 องศาเซลเซียส ตัวอย่างทั้งหมดถูกตรวจสอบคุณลักษณะโดยใช้การดูด  
ซับทางกายภาพด้วยไนโตรเจน การกระเจิงรังสีเอกซ์ การวิเคราะห์เชิงความร้อน การส่องผ่านด้วย  
กล้องจุลทรรศน์อิเล็กตรอน การวัดการกระจายตัวของโลหะ การส่องกราดด้วยกล้องจุลทรรศน์  
อิเล็กตรอน การวัดกัมมันตภาพรังสีแบบโปรแกรมหุณหภูมิและการดูดซับด้วยคาร์บอนมอนอกไซด์ ผล  
การศึกษาพบความสัมพันธ์ระหว่างอุณหภูมิเริ่มต้นเมื่อเติมอะลูมินาบนซิลิกา อีกทั้งการเพิ่มปริมาณ  
อะลูมินามีผลให้ขนาดของโครงสร้างผลึกใหญ่ขึ้นเมื่อเปลี่ยนปริมาณอะลูมินาบนซิลิกา ยิ่งกว่านั้น  
การกระจายตัวของอนุภาคอะลูมินาบนพื้นผิวของซิลิกามีลักษณะดี และพบว่าอะลูมินาช่วยขัดขวาง  
การเกิดซินเทอร์ริง เมื่อเผาไหม้ในอากาศที่อุณหภูมิสูง นอกจากนั้นความสามารถในการวัดตัวของ  
ตัวเร่งปฏิกิริยาโคบอลต์คือๆ ลดลงบนตัวรองรับชนิดวัสดุเชิงประกอบอะลูมินาซิลิกา สำหรับผล  
การศึกษาปฏิกิริยาคาร์บอนไดออกไซด์ไฮโดรเจนชั้น พบว่า ร้อยละการเปลี่ยนแปลงสูงสุดและค่า  
การเลือกเกิดมีเทนของตัวเร่งปฏิกิริยาโคบอลต์บนวัสดุเชิงประกอบอะลูมินาซิลิกา คือ 26.12  
เปอร์เซ็นต์ และ 94.02 เปอร์เซ็นต์ ตามลำดับ ที่อุณหภูมิของปฏิกิริยา 220 องศา เซลเซียส

ภาควิชา.....วิศวกรรมเคมี..... ลายมือชื่อนิสิต..... น.ศ. ชมลวรรณ เจษฎานุรักษ์  
สาขาวิชา.....วิศวกรรมเคมี..... ลายมือชื่อ อ. ที่ปริกษาวิทยานิพนธ์หลัก.....  
ปีการศึกษา.....2553.....

##5271485021: MAJOR CHEMICAL ENGINEERING

KEYWORDS: ALUMINA SILICA COMPOSITES/ COBALT CATALYST/  
CARBON DIOXIDE HYDROGENATION

THAMONWAN JETSADANURAK: CARBON DIOXIDE  
HYDROGENATION OVER ALUMINA-SILICA COMPOSITES-  
SUPPORTED COBALT CATALYST. THESIS ADVISOR: ASSOC. PROF.  
BUNJERD JONGSOMJIT, Ph.D., 88 pp.

This research focused on investigation of characteristics of the  $\text{Al}_2\text{O}_3$ - $\text{SiO}_2$  composite supports that were prepared by deposition of  $\text{Al}_2\text{O}_3$  particles on the spherical silica particle (SSP) surface using hydrolysis of aluminium isopropoxide with loading variation of  $\text{Al}_2\text{O}_3$  onto  $\text{SiO}_2$  to obtain AISSP with calcination temperature at 650 and 1000 °C. Furthermore, the characteristics of the impregnated cobalt on spherical silica particle support (CoSSP) and alumina-silica composite support (CoAISSP) were investigated. In addition, the catalytic activity and selectivity to methane of CoSSP and all of CoAISSP samples for carbon dioxide hydrogenation with reaction temperature at 220°C was also investigated. All samples were characterized by BET surface area, XRD, DTA/TG, EDX, SEM, TEM, TPR, and CO chemisorptions methods. It was found that thermal stability of alumina can be enhanced with adding to silica. Besides, at various compositions of alumina-silica, increased amount of alumina exhibited a larger crystalline size of alumina. Moreover, the alumina distribution on the silica surface was good. In addition, at high calcination temperature, it was found that sintering effect was impeded by alumina addition. Furthermore, the reducibilities of cobalt supported on  $\text{Al}_2\text{O}_3$ - $\text{SiO}_2$  composites catalysts were slightly decreased. Based on the  $\text{CO}_2$  hydrogenation reaction results, the  $\text{CO}_2$  conversion and selectivity to methane of the cobalt supported on  $\text{Al}_2\text{O}_3$ - $\text{SiO}_2$  composite are 26.12% and 94.02%, respectively upon the reaction temperature at 220°C.

Department : .....Chemical Engineering....

Student's Signature...Thamonwan J.

Field of Study : ...Chemical Engineering....

Advisor's Signature...Bunjerd Jongsomjit

Academic Year : .....2010.....

## ACKNOWLEDGEMENTS

The author would like to express her greatest gratitude and appreciation to her advisor, Assoc. Prof. Dr. Bunjerd Jongsojmit for his invaluable guidance, providing value suggestions and his kind supervision throughout this study. In addition, she is also grateful to Assistant Professor Anongnat Somwangthanaroj, as the chairman, Assistant Professor Joongjai Panpranot and Assistant Professor Okorn Mekasuwandamrong as the members of the thesis committee. The author would like to thank the Thailand Research Fund (TRF).

Many thanks for kind suggestions and useful help to Mr. Jakrapan Janlamool, Mr. Benjapol Nitijalornwong, and many friends in the laboratory who always provide the encouragement and co-operate along the thesis study.

Most of all, the author would like to express her highest gratitude to her parents who always pay attention to her all the times for suggestions, support and encouragement.



ศูนย์วิทยทรัพยากร  
จุฬาลงกรณ์มหาวิทยาลัย

# CONTENTS

	<b>Page</b>
ABSTRACT (IN THAI).....	iv
ABSTRACT (IN ENGLISH).....	v
ACKNOWLEDGEMENTS.....	vi
CONTENTS.....	vii
LIST OF TABLES.....	x
LIST OF FIGURES.....	xi
CHAPTER	
I INTRODUCTION.....	1
II LITERATER REVIEWS.....	5
2.1 The silica supported metals.....	5
2.2 The alumina-silica composites supported metals.....	6
2.3 The supported metal catalysts in CO and CO <sub>2</sub> hydrogenation system.....	8
III THEORY.....	11
3.1 CO <sub>2</sub> Hydrogenation Reactions.....	11
3.2 Silicon dioxide .....	12
3.3 Alumina.....	16
3.4 Cobalt.....	20
3.4.1 General.....	20
3.4.2 Physical properties.....	21
IV EXPERIMANTAL.....	24
4.1 Research Methodology.....	24
4.2 Catalyst preparation.....	26
4.2.1 Chemicals.....	26
4.2.2 Preparation of the spherical silica particle (SSP).....	26
4.2.3 Preparation of the Al <sub>2</sub> O <sub>3</sub> -SiO <sub>2</sub> composites supports.....	26

CHAPTER	Page
4.2.4 Cobalt Loading.....	27
4.2.5 Catalysts Nomenclature.....	27
4.3 Catalyst characterization.....	28
4.3.1 X-ray diffraction (XRD).....	28
4.3.2 N <sub>2</sub> physisorption .....	28
4.3.3 Scanning electron microscopy(SEM) and energy dispersive X-ray spectroscopy (EDX).....	29
4.3.4 Transmission electron microscope (TEM).....	29
4.3.5 Temperature-programmed reduction (TPR).....	29
4.3.6 Thermogravimetry analysis (TGA).....	29
4.3.7 Carbon monoxide chemisorptions.....	30
4.4 Reaction study in CO <sub>2</sub> hydrogenation.....	30
4.4.1 Material.....	30
4.4.2 Apparatus.....	30
4.4.3 Procedures.....	34
V RESULTS AND DISCUSSION .....	35
5.1 Support preparation and characterization.....	35
5.1.1 Preparation of spherical silica particle (SSP).....	35
5.1.2 Preparation and characterization of alumina-spherical silica particles composites supports (AlSSP).....	37
5.2 Preparation and characterization of spherical silica (SSP) and alumina-spherical silica composites (AlSSP) supported cobalt catalyst.....	43
VI CONCLUSIONS AND RECOMMENDATIONS.....	64
6.1 Conclusions.....	64
6.2 Recommendations.....	65



	<b>Page</b>
REFERENCES.....	66
APPENDICES.....	69
APPENDIX A: CALCULATION FOR CATALYST PREPARATION.....	70
APPENDIX B: CALCULATION FOR TOTAL CO CHEMISORPTION AND DISPERSION.....	72
APPENDIX C: CALCULATION FOR REDUCIBILITY.....	73
APPENDIX D: CALIBRATION CURVES .....	75
APPENDIX E: CALCULATION OF CO <sub>2</sub> CONVERSION, REACTION RATE AND SELECTIVITY.....	80
APPENDIX F: PORE SIZE DISTRIBUTION CURVES.....	81
APPENDIX G: LIST OF PUBLICATION.....	88
VITA .....	95



ศูนย์วิทยทรัพยากร  
จุฬาลงกรณ์มหาวิทยาลัย

## LIST OF TABLES

<b>Table</b>	<b>Page</b>
3.1 Physical properties of silica.....	13
3.2 Physical of aluminium oxide.....	19
3.3 Physical properties of cobalt.....	22
4.1 Operating condition for gas chromatograph.....	32
5.1 BET surface area, pore volume and pore diameter of spherical silica particles.....	36
5.2 BET Surface areas, pore volume and pore diameter of alumina-spherical silica particle composites.....	40
5.3 BET Surface areas, pore volume and pore diameter of silica and alumina- silica composites-supported cobalt catalysts.....	45
5.4 H <sub>2</sub> consumption from TRP profiles of silica and alumina-silica composites- supported cobalt catalysts.....	60
5.5 Amount of carbon monoxide adsorbed on silica and alumina-silica composites-supported cobalt catalysts.....	61
5.6 Activity and product selectivity of spherical silica and alumina-silica composites supported cobalt catalysts.....	62
D.1 Conditions use in Shimadzu modal GC-8A and GC-14B. ....	76

## LIST OF FIGURES

Figure	Page
3.1 Reaction mechanisms for CH <sub>3</sub> OH formation from H <sub>2</sub> /CO <sub>2</sub> over Cu-ZnO/SiO <sub>2</sub> catalyst.....	12
3.2 Desorption of water from alumina surface.....	18
3.3 Lewis acid and Lewis basic sites on alumina.....	18
3.4 Illustration of Al and O atom packing the basal plan.....	20
4.1 Flow diagram of CO <sub>2</sub> hydrogenation system.....	33
5.1 The SEM images of the spherical silica particles.....	36
5.2 DTA/TG curve of the AlSSP composites.....	38
5.3 XRD patterns of spherical silica and alumina-silica composite supports.....	38
5.4 SEM micrograph and EDX mapping of AlSSP650 (3:1) composites.....	41
5.5 A typical spectrum of the AlSSP650 (3:1) composites from EDX analysis.....	42
5.6 TEM micrographs of the AlSSP650 (1:3) composites.....	43
5.7 XRD patterns of silica and alumina-silica composites supported cobalt catalysts.....	44
5.8 SEM micrograph and EDX mapping of CoSSP550 catalyst.....	46
5.9 A typical spectrum of the CoSSP550 catalyst from EDX analysis.....	47
5.10 SEM micrograph and EDX mapping of AlCoSSP650 (1:3) catalyst .....	48
5.11 SEM micrograph and EDX mapping of AlCoSSP1000 (1:3) catalyst.....	49
5.12 SEM micrograph and EDX mapping of AlCoSSP650 (1:1) catalyst.....	50
5.13 SEM micrograph and EDX mapping of AlCoSSP1000 (1:1) catalyst.....	51
5.14 SEM micrograph and EDX mapping of AlCoSSP650 (3:1) catalyst.....	52
5.15 SEM micrograph and EDX mapping of AlCoSSP1000 (3:1) catalyst.....	53
5.16 A typical spectrum of the CoAlSSP650 (3:1) catalyst from EDX analysis.....	54
5.17 TEM micrograph for the silica and alumina-silica composites supported cobalt catalysts.....	58

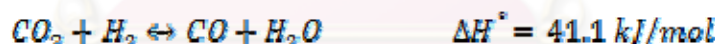
<b>Figure</b>	<b>Page</b>
5.18 TPR patterns of the silica and alumina-silica composites supported cobalt catalysts.....	59
5.19 Reaction rate at 220°C vs. time on stream of silica and alumina-silica composites supported cobalt catalysts.....	63
D.1 The calibration curve of carbon dioxide .....	76
D.2 The calibration curve of carbon monoxide .....	77
D.3 The calibration curve of methane.....	77
D.4 The calibration curve of ethane.....	78
D.5 The calibration curve of propane.....	78
D.6 The chromatograms of catalyst sample from thermal conductivity detector, gas chromatography Shimadzu model 8A (Molecular sieve 5A column).....	79
D.7 The chromatograms of catalyst sample from flame ionization detector, gas chromatography Shimadzu model 14B (VZ10 column).....	79
F.1 The pore size distribution of SSP550 and CoSSP550.....	81
F.2 The pore size distribution of AlSSP650 (1:3) and CoAlSSP650 (1:3).....	82
F.3 The pore size distribution of AlSSP1000 (1:3) and CoAlSSP1000 (1:3).....	83
F.4 The pore size distribution of AlSSP650 (1:1) and CoAlSSP650 (1:1).....	84
F.5 The pore size distribution of AlSSP1000 (1:1) and CoAlSSP1000 (1:1).....	85
F.6 The pore size distribution of AlSSP650 (3:1) and CoAlSSP650 (3:1).....	86
F.7 The pore size distribution of AlSSP1000 (3:1) and CoAlSSP1000 (3:1).....	87

# CHAPTER I

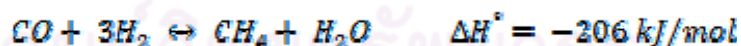
## INTRODUCTION

Carbon dioxide (CO<sub>2</sub>) is a greenhouse gas that occurs naturally in the atmosphere. Human activities are increasing the concentration of CO<sub>2</sub> in the atmosphere, thus contributing to Earth global warming. This is an important and urgent problem causing acid rain and the loss of oxygen-carrying molecule in the red blood cell. CO<sub>2</sub> is emitted when fuel is burnt. It can be also emitted by some other industrial processes. In contrast, chemical CO<sub>2</sub> fixation has become of greater interest in recent years, primarily because of its impact on the environment through the greenhouse gases appeared to warm up the atmosphere [Riedel et al., 1999]. In addition, catalytic hydrogenation of CO<sub>2</sub> has been considered as one of the chemical fixation and recycling technologies for emitted CO<sub>2</sub> [Kusuma et al., 2001]. The current interest in CO<sub>2</sub> hydrogenation (Fischer-Tropsch synthesis) has been extensively studied for years [Suzuki et al., 1993; Saib et al., 2002; Dagle et al., 2007; Panagiotopoulou et al., 2008].

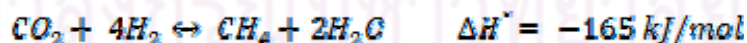
Considering the mechanism of CO<sub>2</sub> hydrogenation Fischer-Tropsch synthesis, the general view is a first RWGS reaction as follow;



to produce CO which is subsequently consumed in the FT conversion as;



However, the additional reaction of a direct CO<sub>2</sub> hydrogenation occurs as;



In general, the catalyst properties depend on reaction conditions, catalyst compositions, metal dispersion, and types of inorganic supports used. Cobalt catalysts represent the optimal choice for low temperature, because of higher stability, higher conversion and relatively small negative effect of water on conversion [Khodakov, 2009], preferring for synthesis of high molecular weight paraffins [Dry, 2002; Chu et al., 2007], and lower price compared to those of noble metal. Furthermore, the

research has emphasized that the supports, such as  $\text{Al}_2\text{O}_3$ ,  $\text{SiO}_2$ , and  $\text{TiO}_2$  can significantly enhance the activity, selectivity and catalytic properties as well [Storsaeter et al., 2005].  $\text{SiO}_2$  has been considered to be very attractive because of high surface area, thermal stability and improving the reduction degree of supported cobalt [Khodakov et al., 1997; Backman et al., 1998]. Moreover,  $\text{Al}_2\text{O}_3$  is one of the most supports for cobalt catalyst because of its favorable mechanical properties and adjustable surface properties. In addition, it significantly improved the catalytic activity of FTS by increasing the dispersion [Zhang et al., 2006]. Furthermore, the effect of  $\text{SiO}_2$  modification to  $\text{Co}/\text{Al}_2\text{O}_3$  catalyst was widely studied by improving the properties of the supports and supported cobalt. In reversible, alumina-doped silica was also investigated [Marie et al., 2009; Sun et al., 2010].

The main objective of this present study was to investigate the catalytic behaviors of carbon dioxide hydrogenation over alumina-silica composites-supported cobalt catalyst. The composites supports and catalysts were prepared and characterized by several techniques, such as XRD, BET, DTA/TG, SEM/EDX, TEM, TPR, and CO chemisorptions methods, and then tested for  $\text{CO}_2$  hydrogenation reaction in order to measure activity and selectivity under methanation condition.

### **Motivation**

The  $\text{Al}_2\text{O}_3$ - $\text{SiO}_2$  composites supports can exhibit the novel properties that are not finding in a single oxide support. With combination, the benefit of  $\text{Al}_2\text{O}_3$  support provided the mechanical properties and adjustable surface properties. In addition, it significantly improved the catalytic activity of FTS by increasing the dispersion and  $\text{SiO}_2$  has a sufficiently high surface area, thermal stability and improving the reduction degree of supported cobalt. In this work, I intended to improve activity and selectivity of the cobalt based  $\text{Al}_2\text{O}_3$ - $\text{SiO}_2$  composites catalyst over  $\text{CO}_2$  hydrogenation.

## Objective

This research objective was to investigate the effect of different  $\text{Al}_2\text{O}_3\text{-SiO}_2$  composites supports on their characteristics by varying composition between  $\text{Al}_2\text{O}_3$  and  $\text{SiO}_2$ . Cobalt supported on  $\text{Al}_2\text{O}_3\text{-SiO}_2$  composites catalysts for  $\text{CO}_2$  hydrogenation was further investigated with regard to activity and selectivity.

## Research scopes

- Preparation of submicrosphere silica support.
- Characterization of silica support samples by BET surface area X-ray diffraction (XRD), scanning electron microscopy (SEM) and transmission electron microscope (TEM).
- Preparation of  $\text{Al}_2\text{O}_3\text{-SiO}_2$  composites supports with 25 to 75 wt% of  $\text{Al}_2\text{O}_3$  on the composites support using hydrolysis of aluminium isopropoxide method.
- Characterization of  $\text{Al}_2\text{O}_3\text{-SiO}_2$  composites supports by BET surface area, X-ray diffraction (XRD), scanning electron microscope (SEM), energy dispersive X-ray spectroscopy (EDX), transmission electron microscope (TEM), and differential thermal analysis and thermogravimetric (DTA/TG).
- Preparation of supported Co catalyst on the  $\text{Al}_2\text{O}_3\text{-SiO}_2$  composites supports, which were calcined at 500 to 1000°C, using the incipient wetness impregnation method.
- Characterization of the catalyst samples using BET surface area, X-ray diffraction (XRD), CO chemisorptions, temperature programmed reduction (TPR), scanning electron microscope (SEM), energy dispersive X-ray spectroscopy (EDX) and transmission electron microscope (TEM).
- Investigation of the catalytic activity of Co/  $\text{Al}_2\text{O}_3\text{-SiO}_2$  catalyst in the hydrogenation of carbon dioxide ( $\text{CO}_2$ ) at 220°C and 1 atm and a  $\text{H}_2/\text{CO}_2$  ratio of 10 under methanation condition.

**Benefits**

- Develop the cobalt base  $\text{Al}_2\text{O}_3$ -SiO composites catalyst for  $\text{CO}_2$  hydrogenation.

- Enhance  $\text{CO}_2$  fixation system.

- Produce research article based on the results obtained.



ศูนย์วิทยทรัพยากร  
จุฬาลงกรณ์มหาวิทยาลัย



## CHAPTER II

### LITERATURE REVIEWS

This chapter reviews the work about alumina-silica composites supported Co catalyst that is also of great interest in the field of heterogeneous catalysis, while it has been used for catalytic application. The last section of this review shows a few research investigate supported metal catalyst in CO and CO<sub>2</sub> hydrogenation system.

#### 2.1 The silica supported metals

Kogelbauer et al. [1995] studied the formation of cobalt silicates on Co/SiO<sub>2</sub> under hydrothermal conditions. Hydrothermal treatment at 220°C led to a catalyst with lower reducibility due to the formation of both reducible and nonreducible (at temperature < 900°C) Co silicates. They also showed that silicate was formed in catalysts which had been used for FT synthesis. No significant change occurred upon hydrothermal treatment of calcined catalyst. The presence of air during the hydrothermal treatment inhibited the formation of silicate and they proposed that the formation of silicate was linked to the presence of metallic cobalt.

Choi [1995] investigated the reduction of cobalt catalysts supported on Al<sub>2</sub>O<sub>3</sub>, SiO<sub>2</sub>, and TiO<sub>2</sub> and the effect of metal loading on the reduction. The activation energy of reduction increased in following order: Co/SiO<sub>2</sub> > Co/Al<sub>2</sub>O<sub>3</sub> > Co/TiO<sub>2</sub>. For different metal loading, the catalyst with the higher loading is more readily reducible than with the lower metal loading.

Jacobs et al. [2002] investigated the effect of support, loading and promoter on the reducibility of cobalt catalysts. They have reported that significant support interactions on the reduction of cobalt oxide species were observed in the order Al<sub>2</sub>O<sub>3</sub> > TiO<sub>2</sub> > SiO<sub>2</sub>. Addition of Ru and Pt exhibited a similar catalytic effect by decreasing the reduction temperature of cobalt oxide species, and for Co species where a significant surface interaction with the support was present, while Re impacted mainly the reduction of Co species interaction with the support. They also

suggested that, for catalysts prepared with a noble metal promoter and reduced at the same temperature, the increase in the number of active sites was due to mainly to improvements in the percentage reduction rather than the actual dispersion (cluster size). Increasing the cobalt loading, and therefore the average Co cluster size, was found to exhibit improved reducibility by decreasing interactions with the support.

Okabe et al. [2004] investigated Fischer-Tropsch synthesis was carried out in slurry phase over uniformly dispersed Co-SiO<sub>2</sub> catalysts prepared by the sol-gel method. When 0.01-1 wt% of noble metals were added to the Co-SiO<sub>2</sub> catalysts, a high and stable catalytic activity was obtained over 60 h of the reaction at 503 K and 1 MPa. The addition of noble metals increased the reducibility of surface Co on the catalysts, without changing the particle size of Co metal significantly. High dispersion of metallic Co species stabilized on SiO<sub>2</sub> was responsible for stable activity. The uniform pore size of the catalysts was enlarged by varying the preparation conditions and by adding organic compounds such as *N,N*-dimethylformamide and formamide. Increased pore size resulted in decrease in CO conversion and selectivity for CO<sub>2</sub>, a byproduct, and an increase in the olefin/paraffin ratio of the products. By modifying the surface of wide pore silica with Co-SiO<sub>2</sub> prepared by the sol-gel method, a bimodal pore structure catalyst was prepared. The bimodal catalyst showed high catalytic performance with reducing the amounts of the expensive.

## **2.2 The alumina-silica composites supported metals**

The research has emphasized that the supports such as Al<sub>2</sub>O<sub>3</sub>, SiO<sub>2</sub>, and TiO<sub>2</sub> can significantly enhanced the activity, selectivity and catalytic properties as well [Storsaeter et al., 2005]. SiO<sub>2</sub> has been considered to be very attractive because of high surface area, thermal stability and improving the reduction degree of supported cobalt [Khodakov et al., 1997; Backman et al., 1998]

Nowadays, the alumina-silica composites supported metal catalysts have attracted the scientists attention in the catalyst filed. Recently, it was reported that alumina-silica modified supports exhibited better catalytic properties than classical oxides such as alumina or silica.

Daniell et al. [2000] investigated the modification of  $\gamma$ -alumina with silica led to the creation of both highly acidic Lewis and Brønsted acid sites (BASs); the former through isomorphous substitution of  $\text{Si}^{4+}$  ions by  $\text{Al}^{3+}$  ions at tetrahedral lattice sites; and the latter through formation of bridged hydroxy groups, similar to those found in zeolites. The relative strength and quantity of these sites reached a maximum with 40 wt.% silica content, above which the surface of the samples became silica coated and exhibited acidity approximating that of pure silica.

Baca et al. [2008] synthesized multiple grafting of Al isopropoxide, the mesoporous aluminas of controlled pore sizes, in organic solvents on mesoporous silica SBA-15. The results show that the chemical nature of the Al-grafted materials varies continuously with the number of grafting from pure silica to pure alumina. Typically, after three graftings, this original method of synthesis allows one to prepare ordered mesoporous alumina with specific surface areas above  $300 \text{ m}^2 \text{ g}^{-1}$  and a narrow pore size distribution centered on ca.  $60 \text{ \AA}$ .

Gu et al. [2009] studied the mesoporous silica with modified alumina through one-pot synthesis, solvent-free solid grinding and gel-mixing methods, in order to optimize the adsorptive capability of mesoporous composite. Modification with alumina significantly increased the ability of MCM-41 to trap NPYR, and among various preparations the solvent-free solid grinding method was able to disperse alumina guest with high accessibility and to reserve surface silanol groups on MCM-41. Typically, the  $\text{Al}_2\text{O}_3/\text{MCM-41}$  composite synthesized by solvent-free method with 12 wt.% alumina exhibited a capacity comparable to zeolite NaY for trapping NPYR in airflow but four times superior to NaY for adsorbing bulky nitrosamine NNN in solution.

Marie et al. [2009] studied the structure and catalytic performance in fixed bed reactor at 20 bars of cobalt Fischer-Tropsch catalysts supported by commercial alumina (Puralox) and silica-doped alumina (Siralox) by varied cobalt loading between 8 and 15 wt.%; both alumina and silica-doped alumina supports had similar textural properties. The presence of small amounts of silica in alumina (5 wt.%  $\text{SiO}_2$ ) enhanced cobalt reducibility and hindered formation of hardly reducible cobalt

aluminate species. Higher Fischer-Tropsch reaction rate over cobalt catalysts supported on silica-doped alumina was attributed to better cobalt reducibility.

Sun et al. [2010] studied the reversible promotional effect of SiO<sub>2</sub> modification to Co/Al<sub>2</sub>O<sub>3</sub> catalyst for Fischer-Tropsch synthesis. The addition of a small amount of SiO<sub>2</sub> to Al<sub>2</sub>O<sub>3</sub>-supported cobalt catalyst significantly increased the reduction degree of the supported cobalt oxides and the metallic cobalt surface area. Compared with the Al<sub>2</sub>O<sub>3</sub>-promoted Co/SiO<sub>2</sub> catalyst, the present catalyst exhibited a reversible promotional effect in slurry-phase FTS. Either Al<sub>2</sub>O<sub>3</sub> modification to Co/SiO<sub>2</sub> or SiO<sub>2</sub> addition to Co/Al<sub>2</sub>O<sub>3</sub> exhibited highest CO conversion at 10 wt.% extra addition amount, indicating the precise balance among dispersion, reduction degree, BET surface area and metallic Co surface area.

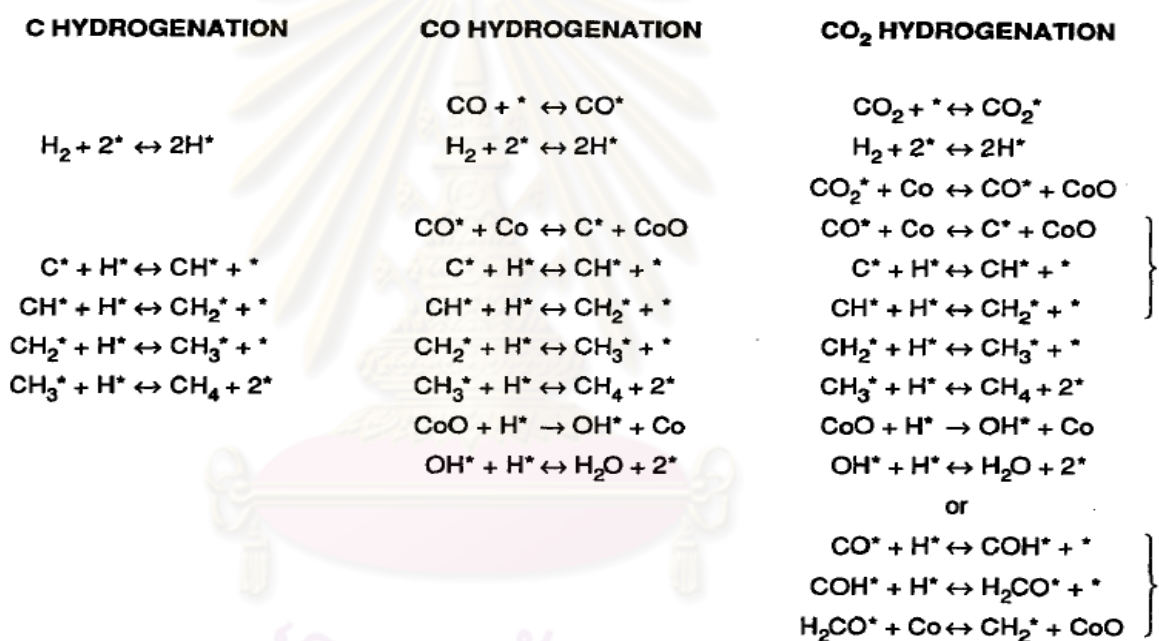
### **2.3 The supported metal catalysts in CO and CO<sub>2</sub> hydrogenation system**

Development of catalyst for CO and CO<sub>2</sub> hydrogenation is the key technology of gas to liquid (GTL) process. The catalytic hydrogenation of carbon monoxide and carbon dioxide produces a large variety of products ranging from methane and methanol to higher molecular weight alkanes, alkenes and alcohols. [Somorjai, 1994; Dry, 1996; Adesina, 1996; Iglesia, 1997].

Frohlich et al. [1996] investigated the activation and deactivation of Co foils during hydrogenation of carbon dioxide in dependence on pretreatment of the catalyst and time on stream, temperature and composition of the educt gas by means of a combination of various methods. Both oxidation/reduction of the surface and incorporation of oxygen and carbon in the bulk lead to marked changes in the surface structure and a considerable increase in surface area. The catalytic activity of the oxidized surface concerning the hydrogenation of CO<sub>2</sub> is small, but increases strongly with reduction. Deactivation is accompanied with structural changes and proved to be reversible. Chemical poisoning was only observed after addition of hydrogen sulfide to the educt gas.

Lahtinen et al. [1994] investigated C, CO and CO<sub>2</sub> hydrogenation on cobalt foil model catalysts. It was found that the reactions produce mainly methane, but with selectivities of 98, 80, and 99 wt% at 525 K for C, CO and CO<sub>2</sub>, respectively. The rate of methane formation on cobalt foil shows zero order partial pressure dependence on CO<sub>2</sub> and first order partial pressure dependence on H<sub>2</sub>. The reaction proceeds via dissociation of C-O bonds and formation of CoO on the surface. The reduction of CoO is the rate limiting step in the CO and CO<sub>2</sub> hydrogenation reaction. These authors also proposed the reaction mechanisms for C, CO and CO<sub>2</sub> hydrogenation.

The reaction mechanisms proposed for C, CO and CO<sub>2</sub> hydrogenation.



Yongqing et al. [2002] investigated CO and CO<sub>2</sub> hydrogenation on silica and alumina supported cobalt Fischer-Tropsch synthesis catalysts. It found that CO and CO<sub>2</sub> hydrogenation obtained similar catalytic activity but the selectivity was very different, FTS product distributions were observed with an  $\alpha$  of about 0.8; in contrast, the CO<sub>2</sub> hydrogenation products contained about 70% or more of methane and propose reaction pathway for CO and CO<sub>2</sub> hydrogenation.

Okabe et al. [2004] investigated the Fischer-Tropsch synthesis that was carried out in slurry phase over uniformly dispersed Co/SiO<sub>2</sub> catalysts prepared by sol-gel method. When 0.01-1 wt% of noble metals were added to the Co/SiO<sub>2</sub> catalysts, a high and stable catalytic activity was obtained over 60 h of the reaction at 503 K and 1 MPa. The addition of noble metals increased the reducibility of surface Co on the catalysts, without changing the particle size of Co metal. The uniform pore size of the catalysts was enlarged by varying the preparation conditions. Increase pore size resulted in decreased CO conversion and selectivity for CO<sub>2</sub> and increased olefin/paraffin ratio of the products.

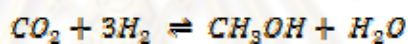
Panagiotopoulou et al. [2008] investigated that the catalytic performance of Al<sub>2</sub>O<sub>3</sub> supported noble metal catalysts for the methanation of CO, CO<sub>2</sub> and their mixture with respect to nature of the dispersed metallic phase (Ru, Rh, Pt, Pd). It has been found that, for all experimental conditions investigated, Ru and Rh are significantly more active than Pt and Pd. Selectivity towards hydrogenation products depends strongly on the noble metal catalyst employed as on whether solo- or co-methanation of CO/CO<sub>2</sub> is occurring. In presence of water in the feed, catalytic activity of Ru is not affected, while that of Rh is reduced. On the other hand, the performance of Pt and Pd is poor since they promote the undesired water-gas shift reaction.

## CHAPTER III

### THEORY

#### 3.1 CO<sub>2</sub> Hydrogenation Reactions

In recently, several reaction mechanisms for the CO<sub>2</sub> hydrogenation have been proposed. First, the catalytic hydrogenation over promoted Cu-ZnO catalysts under pressurized conditions produces mainly CH<sub>3</sub>OH, CO and H<sub>2</sub>O. A small amount of CH<sub>4</sub> was produced. At higher temperature, a very small amount of CH<sub>3</sub>OCH<sub>3</sub> was also produced. Therefore, main reactions are shown in the following equations [Arakawa et al., 1992].



An in situ F-IR observation of surface species over 5 wt% Cu-ZnO/SiO<sub>2</sub> as model catalyst showed the presence of bidentate carbonate species on both Cu and ZnO at the condition of 3MPa, 30°C and 100 ml/min. Also a small amount of adsorbed CO on Cu site was observed. These bidentate carbonate species were rapidly transformed to the bidentate formate species with the increase of reaction temperature up to 150°C under 3 MPa. However, a small amount of adsorbed CO species has diminished at 100°C and it was never observed under the reaction conditions. The experimental dynamic in situ FT-IR spectra of adsorbed species over the catalyst at various reaction conditions, this observation also suggests the direct formation of CH<sub>3</sub>OH from CO<sub>2</sub> via bidentate carbonate species, formate species and methoxy species as shown in Figure.

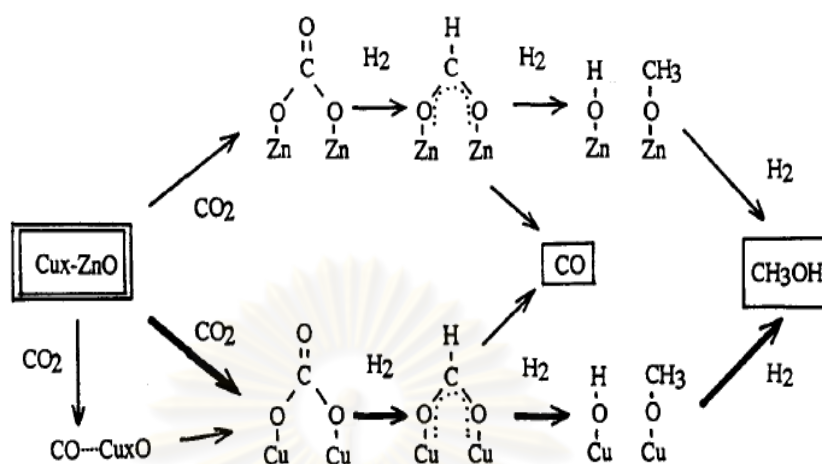
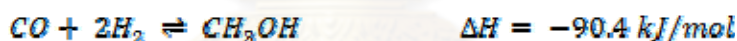
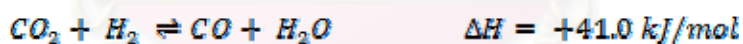


**Figure 3.1** Reaction mechanisms for  $\text{CH}_3\text{OH}$  formation from  $\text{H}_2/\text{CO}_2$  over  $\text{Cu-ZnO/SiO}_2$  catalyst [Arakawa et al., 1992].

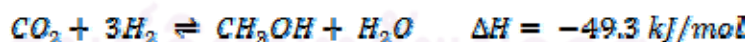
The fibrous  $\text{Cu/Zn/Al/Zr}$  catalyst showed high activity for producing methanol from  $\text{CO}_2$  hydrogenation [Xin et al., 2009]. Thus, there are three independent reactions present in methanol synthesis from  $\text{CO}_2$ , namely Methanol synthesis from  $\text{CO}$ :



Reverse water gas shift:



Methanol synthesis from  $\text{CO}_2$ :



### 3.2 Silica dioxide

In its many forms, silica has been used in all stages of civilization, from the ancient flints of the Stone Age to the modern silica laboratory ware. Because of its many uses, and of the many varied forms in which it occurs, silica has been called by more name than any other mineral. Many of the older names of flints are now so obsolete that repetition is needless, but many of the present-day names for quartz gems are unknown save to a few jewelers. Then, the exact research of the modern laboratory has shown



several distinct crystallographic varieties of silica; some of which are closely connected with the temperature experienced in their life-history.

**Table 3.1** Physical properties of silica

Other name	Silica
Molecular formula	SiO <sub>2</sub>
Molar mass	60.0843 g/mol
Appearance	White powder
Density	2.643 g/cm <sup>3</sup>
Melting point	1650(±75) °C
Boiling point	2230 °C
Solubility in water	0.012 g/ 100mL

The many different names, and their different connotations, which are now in use for silica minerals, call for a classification and arrangement in a more ample, yet more concise manner than is to be found in the usual discussion of the varieties of silica. This article is written with the hope of making a scientific classification of these names, so that the use of the different terms will no longer be a cause for tedious searching for definitions.

These varieties are named in the order formed with descending temperature. Recrystallization changes occur at the temperature noted when ample time is allowed for the action, often in the laboratory only in the presence of catalysts. Besides the changes at these critical temperatures, there are probably similar changes from unstable forms towards quartz at atmospheric temperature, especially after long time intervals. With fairly rapid cooling or heating intermediate forms may not occur in their stable zone, but a direct change from one to another without the intermediate product may take place.

Most of the recrystallization changes noted is found to occur at ascending and descending temperatures.

(A) SILICA GLASS – amorphous, a true non-crystalline glass, stable below the melting point and above the “gc” temperature. Quartz Glass Fused Silica, fused Quartz, are the other names for this supercooled liquid. In most forms at atmospheric temperature there are traces of cristobalite.

(B) CRISTOBALITE – isomeric, or pseudo-isometric, “gc” range is at 1710°C where cristobalite changes to glass as temperature rise or glass to cristobalite as they fall. Cristobalite, an alternate spelling, Beta Cristobalite, also called High Cristobalite, is the high temperature product, forming in the “gc” range in cooling. It is isometric, and in cooling recrystallizes to Alpha Cristobalite, or Low Cristobalite, at 200-275°, providing cooling through the “ct” and “tq” ranges has been too rapid for recrystallization. It is tetragonal.

(C) TRIDYMITE – hexagonal, bipyramidal. “ct” range is at 1470°, where cristobalite changes to tridymite on cooling. Glass may crystallize as tridymite at 1670° if the cooling was too rapid through the “gc” range. Beta Second Tridymite, or Upper High Tridymite, is the high temperature product, forming in the “ct” range in cooling, and which recrystallizes to Beta First Tridymite, also called Lower High Tridymite, at 163° if cooling was too rapid for the “tq” transformation. This in turn alters to Alpha Tridymite, or Low Tridymite, at 117°C, which is the usual tridymite of nature.

- Asmanite - a meteoric tridymite, relate to the above series.
- Vestan - a doubtful silica mineral, probably to be ascribed to tridymite.
- Granuline - a doubtful pulverescent mineral which seems allied to tridymite on optical grounds.

(D) QUARTZ – hexagonal, forms from tridymite in the “tq” range at 870° in cooling. Glass may change to crystalline quartz at about 1400° providing cooling was too rapid for the “gc”, “gt” and “ct” transformations. Beta Quartz, or High Quartz, is the high temperature product, forming at the “tq” point. It is hemihedral. On cooling it recrystallizes to Alpha Quartz, also called Low Quartz, at 573°, yielding the stable low temperature mineral. It is tetartohedral, showing polarity along the c axis and is divisible into Right Hand Quartz and Left Hand quartz

(E) CHALCEDONY – a cryptocrystalline, or very finely fibrous mineral, which has not been successfully located in the thermal equilibrium diagram. Heating to 725-850° usually results in an alteration to tridymite, which thereafter acts as normal tridymite. Chalcedony is usually found as a deposit from solutions, and may be a mixture of glass and quartz, or more probably an intermediate product in the dehydration of the opal colloid. Various subdivisions of chalcedony have been made on optical grounds.

Chalcedony	-	biaxial, positive, elongation positive.
Chalcedonite	-	biaxial, negative.
Lussatite	-	biaxial, positive, parallel, elongation.
Quartzine	-	biaxial, positive, negative, elongation pseudochalcedonite, Lutecite.
Jenzschite	-	differently soluble, but of same S. G. as chalcedony.
Melanophlogite	-	possibly impure chalcedony.
Sulfuricin	-	probably a chalcedony rich in sulphur.

(F) COLLOIDAL SILICA – is usually hydrous, and is commonly described under opal. Silicon occurs in nature combined with oxygen in various forms of silica and silicates. Silicates have complex structures consisting of SiO<sub>4</sub> tetrahedral structural units incorporated to a number of metals. Silicon is never found in nature in free elemental form. Among all elements silicon forms the third largest number of compounds after hydrogen and carbon. There are well over 1000 natural silicates including clay, mica, feldspar, granite, asbestos and hornblende. Such natural silicates have structural units

containing orthosilicates,  $\text{SiO}_4^{4-}$ , pyrosilicates  $\text{Si}_2\text{O}_7^{6-}$  and other complex structural units, such as,  $(\text{SiO}_3)_n^{2n-}$  that have hexagonal rings arranged in chains or pyroxene  $(\text{SiO}_3^{2-})_n$  and amphiboles,  $(\text{Si}_4\text{O}_{11}^{6-})_n$  in infinite chains. Such natural silicates include common minerals such as tremolite,  $\text{Ca}_2\text{Mg}_5(\text{OH})_2\text{Si}_8\text{O}_{22}$ ; diopsid,  $\text{CaMg}(\text{SiO}_3)_2$ ; kaolin,  $\text{H}_8\text{Al}_4\text{Si}_4\text{O}_{18}$ ; montmorillonite,  $\text{H}_2\text{Al}_2\text{Si}_4\text{O}_{12}$ ; tale,  $\text{Mg}_3[(\text{OH})_2\text{SiO}_{10}]$ ; muscovite (a colorless form of mica),  $\text{H}_2\text{KAl}_3(\text{SiO}_4)_3$ ; hemimorphite,  $\text{Zn}_4(\text{OH})_2\text{Si}_2\text{O}_7 \cdot \text{H}_2\text{O}$ ; beryl,  $\text{Be}_3\text{Al}_2\text{Si}_6\text{O}_{18}$ ; zircon,  $\text{ZrSiO}_4$ ; benitoite,  $\text{BaTiSi}_3\text{O}_9$ ; feldspars,  $\text{KAlSi}_3\text{O}_8$ ; zeolites,  $\text{Na}_2\text{O} \cdot 2\text{Al}_2\text{O}_3 \cdot 5\text{SiO}_2 \cdot 5\text{H}_2\text{O}$ ; nephrite,  $\text{Ca}(\text{Mg},\text{Fe})_3(\text{SiO}_3)_4$ ; enstatite,  $(\text{MgSiO}_3)_n$ ; serpentine,  $\text{H}_4\text{Mg}_3\text{Si}_2\text{O}_{10}$ ; jadeite,  $\text{NaAl}(\text{SiO}_3)_2$ ; topaz,  $\text{Al}_2\text{SiO}_4\text{F}_2$ ; and tourmaline,  $(\text{H}, \text{Li}, \text{K}, \text{Na}) \cdot \text{Al}_3(\text{BOH})_2\text{SiO}_{19}$ . Silica, the other most important class of silicon compounds, exists as sand, quartz, flint, amethyst, agate, opal, jasper and rock crystal.

### 3.3 Alumina

Alumina which is  $\text{Al}_2\text{O}_3$  in general form is a polymorphic material. Alumina can be easily synthesized small particles and obtained desirous surface area and pore distribution. Commercial alumina have surface area between 100-600  $\text{m}^2/\text{g}$ . High porosity solid cause high intra surface area, good metal dispersion and increasable effective of catalytic. There are many forms of alumina ( $\alpha$ -,  $\gamma$ -,  $\delta$ -,  $\eta$ -,  $\kappa$ -,  $\chi$ -,  $\theta$ -,  $\rho$ -, and  $\iota$ - $\text{Al}_2\text{O}_3$ ) but the  $\alpha$ - $\text{Al}_2\text{O}_3$  is the only stable form. The thermodynamically stable phase is alpha alumina ( $\alpha$ - $\text{Al}_2\text{O}_3$ , corundum) where all Al ions are equivalent in octahedral coordination in a hep oxide array.  $\alpha$ - $\text{Al}_2\text{O}_3$  (corundum) powders are applied in catalysis as supports, for example, of silver catalysts for ethylene oxidation to ethylene oxide, just because they have low Lewis acidity, low catalytic activity, and conversely, they are mechanically and thermally very strong. All other alumina polymorphs are metastable [Evans, 1993].

The other forms are frequently termed 'transition' aluminas. These transition aluminas are frequently termed 'activated' or 'active' aluminas.  $\rho$ - $\text{Al}_2\text{O}_3$  is amorphous but the other forms have reasonably well-defined X-ray diffraction patterns. The activated aluminas use as an adsorbent. Even though the surface of an activated alumina

has a strong affinity for water, it makes very effective as a desiccant. Activated alumina can be used for removing water from a very wide range of compounds including acetylene, benzene, alkanes, alkenes and other hydrocarbons, air, ammonia, argon, chlorinated hydrocarbons, chlorine, natural gas and petroleum fuels, oxygen, sulfur dioxide and transformer oils [Evans, 1993].

Activated alumina can dry a gas to water content lower than that achievable with any other commercially available desiccant. In addition to water removal, activated alumina can be used selectively to adsorb certain other chemical species from gaseous or liquid streams. Polar molecules such as fluorides or chlorides are readily adsorbed and so activated alumina is used in petroleum refining to adsorb HCl from reformed hydrogen and organic fluorides from hydrocarbons produced by the HF-alkylation process [Evans, 1993].

Activated aluminas find widespread application as both catalysts in their own right and as catalyst substrates. The more significant applications are summarized as the claus catalyst for the removal of the hydrogen sulfide in natural gas processing, petroleum refining and coal treatment, as alcohol dehydration to give olefins or ethers, as hydrotreating to remove oxygen, sulfur, nitrogen and metal (V and Ni) impurities from petroleum feedstocks and to increase the H/C ratio, as reforming catalysts: Pt and Re catalysts on a  $\gamma$ - $\text{Al}_2\text{O}_3$  substrate are used to raise the octane-number of petrol, as automotive exhaust catalysts [Evans, 1993].

Activated alumina has a surface with both Lewis and Bronsted acidic and basic sites. Acidity is derived from the  $\text{Al}^{3+}$  ions and  $\text{H}_2\text{O}$  molecules coordinated to cationic sites, while basicity is due to basic hydroxide groups and  $\text{O}^{2-}$  anion vacancies [Evans, 1993].

If alumina contact to humidity, surface are adsorped water molecules and when alumina were dried at 100 °C to 150 °C, water molecules are desorbed but remain hydroxyl group (-OH) cause acidity of alumina are weak Bronsted acid (Figure 3.2).

Calcination temperatures below 300 °C, the acid strength and concentration of alumina are low and at 500 °C reduce Bronsted acid sites [Wittayakhun et al., 2004].

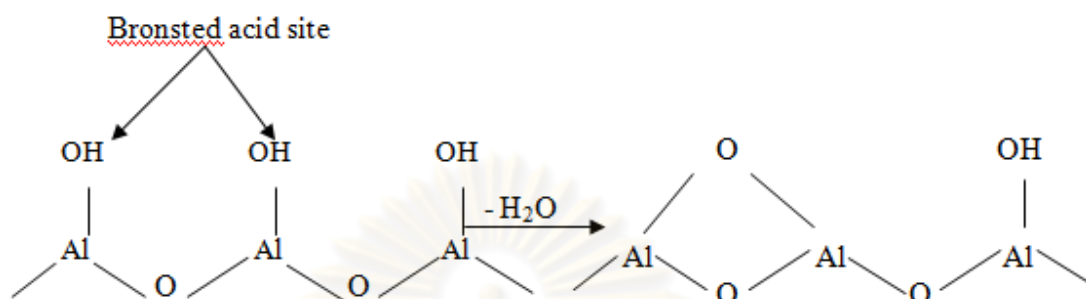


**Figure 3.2** Desorption of water from alumina surface [Wittayakhun et al., 2004].

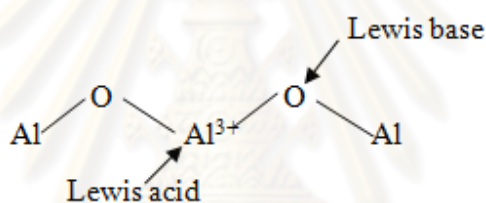


**Figure 3.3** Lewis acid and Lewis basic sites on alumina [Wittayakhun et al., 2004].

As shown in Figure 3.3, further increasing temperatures above 600 °C, adjacent –OH combine and more emit H<sub>2</sub>O and contribute to Al<sup>3+</sup> are Lewis acid sites and O<sup>2-</sup> are Lewis basic sites. Hardness of surface bring about no reaction between Lewis acid and Lewis base which both sites have high activity in various reaction such as Dehydration of alcohol and isomerization of alkene. The decline in acidity for calcination temperatures above 800 °C can be attributed to the collapse in surface area as the alumina is converted to its alpha form [Wittayakhun et al., 2004].

**Table 3.2** Physical of aluminium oxide

Other name	Alumina
Molecular formula	Al <sub>2</sub> O <sub>3</sub>
Molar mass	101.96 g/mol
Appearance	White solid (very hygroscopic)
Density	3.95 – 4.10 g/cm <sup>3</sup>
Melting point	2072 °C
Boiling point	2977 °C
Solubility in water	Insoluble
Solubility	Insoluble in diethyl ether practically insoluble in ethanol

The structure of  $\alpha$ -alumina consists of close packed planes of the large oxygen ions stacking in A-B-A-B sequence, thus forming hexagonal close packed array of anions. The aluminium cations are located at octahedral sites of this basic array and from another type of close packed planes between the oxygen layers. To maintain neutral charge, however, only two third of the available octahedral sites are filled with cation. Figure 3.4 illustrates the packing of Al and O atom in the basal plane. Since the vacant octahedral sites also from regular hexagonal array, three different types of cation layer can be defined, namely a, b, and c layer, depending on the position of the vacant cation site within the layer. These layers are stacked in a-b-c-a-b-c sequence in the structure of alumina.

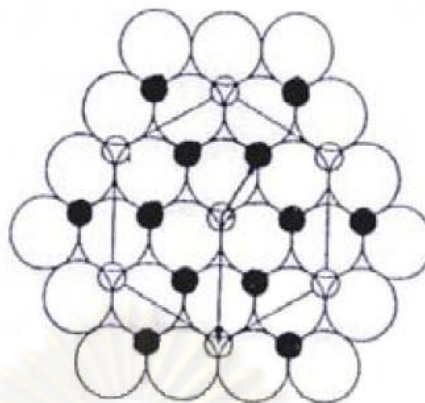


**Figure 3.4** Illustration of Al and O atom packing the basal plan.

Alumina can exist in many metastable phase before transforming to the stable  $\alpha$ -alumina (corundum form). There are six principle phase designated by The Greek letters chi, kappa, eta, theta, delta and gamma. The nature of the product obtained by calcinations depends on the starting hydroxide (Gibbsite, boehmit and others) and on the calcinations conditions. Normally, transition alumina starts to lose their surface areas even at temperature below  $800^{\circ}\text{C}$  due to the elimination of micro-pores. However, drastic loss occurs at temperature higher than  $1000^{\circ}\text{C}$  when the crystallization to the thermodynamically stable  $\alpha$ -alumina occurs.

### 3.4 Cobalt

#### 3.4.1 General

Cobalt, a transition series metallic element having atomic number 27, is similar to silver in appearance. Cobalt and cobalt compounds have expended from use colorants in glasses and ground coat frits for pottery to drying agents in paints and lacquers, animal and human nutrients, electroplating materials, high temperature alloys, hard facing alloys, high speed tools, magnetic alloys, alloys used for prosthetics and used in radiology. Cobalt is also as a catalyst for hydrocarbon refining from crude oil for the synthesis of heating fuel.



### 3.4.2 Physical Properties

The electronic structure of cobalt is  $[\text{Ar}] 3d^7 4s^2$ . At room temperature the crystalline structure of the  $\alpha$  (or  $\epsilon$ ) form, is close-packed hexagonal (cph) and lattice parameters are  $a = 0.2501$  nm and  $c = 0.4066$  nm. Above approximately  $417^\circ\text{C}$ , a face-centered cubic (fcc) allotrope, the  $\gamma$  (or  $\beta$ ) form, having a lattice parameter  $a = 0.3544$  nm, becomes the stable crystalline form. Physical properties of cobalt are listed in Table 3.3.

The scale formed on unalloyed cobalt during exposure to air or oxygen at high temperature is double-layered. In the range of  $300$  to  $900^\circ\text{C}$ , the scale consists of a thin layer of mixed cobalt oxide,  $\text{Co}_3\text{O}_4$ , on the outside and cobalt (II) oxide,  $\text{CoO}$ , layer next to metal. Cobalt (III) oxide,  $\text{Co}_2\text{O}_3$ , may be formed at temperatures below  $300^\circ\text{C}$ . Above  $900^\circ\text{C}$ ,  $\text{Co}_3\text{O}_4$  decomposes and both layers, although of different appearance, are composed of  $\text{CoO}$  only. Scales formed below  $600^\circ\text{C}$  and above  $750^\circ\text{C}$  appear to be stable to cracking on cooling, whereas those produced at  $600$ - $750^\circ\text{C}$  crack and flake off the surface.

Cobalt forms numerous compounds and complexes of industrial importance. Cobalt, atomic weight 58.933, is one of the three members of the first transition series of Group 9 (VIII B). There are thirteen known isotopes, but only three are significant,  $\text{Co}$  is the only stable and naturally occurring isotope,  $\text{Co}$  has a half-life of 5.3 years and is a common source of  $\gamma$ -radioactivity; and  $^{57}\text{Co}$  has a 270-d half-life and provides the  $\gamma$ -source for Mossbauer spectroscopy.

**Table 3.3** Physical properties of cobalt

Property	Value
Atomic number	27
Atomic weight	58.93
Transformation temperature, °C	417
Heat of transformation, J/ga	251
Melting point, °C	1493
Latent heat of fusion, $\Delta H_{fus}$ J/ga	395
Boiling point, °C	3100
Latent heat of vaporization at bp, $\Delta H_{vap}$ kJ/ga	6276
Specific heat, J/(g· °C) <sup>a</sup>	
15-100 °C	0.442
Molten metal	0.560
Coefficient of thermal expansion, °C <sup>-1</sup>	12.5
C <sub>ph</sub> at room temperature	14.2
Fcc at 417 °C	69.16
Thermal neutron absorption, Bohr atom	34.8
Resistivity, at 20 °C, 10 <sup>-8</sup> Ω·m	6.24
Curie temperature, °C	1121
Saturation induction, 4πI <sub>s</sub> , T <sup>c</sup>	1.870
Permeability, μ	
Initial	68
Max	245
Residual induction, T <sup>e</sup>	0.490
Coercive force, A/m	708
Young's modulus, G <sub>pac</sub>	211

Cobalt exists in the +2 or +3 valance states for the major of its compounds and complexes. A multitude of complexes of the cobalt (III) ion exists, but few stable simple salt are known. Octahedral stereo chemistries are the most common for cobalt (II) ion as well as for cobalt (III). Cobalt (II) forms numerous simple compounds and complexes, most of which are octahedral or tetrahedral in nature; cobalt (II) forms more tetrahedral complex than other transition-metal ions. Because of the small stability difference between octahedral and tetrahedral complexes of cobalt (II), both can be found equilibrium for a number of complexes. Typically, octahedral cobalt (II) salts and complexes are pink to brownish red; most of the tetrahedral Co (II) species are blue.

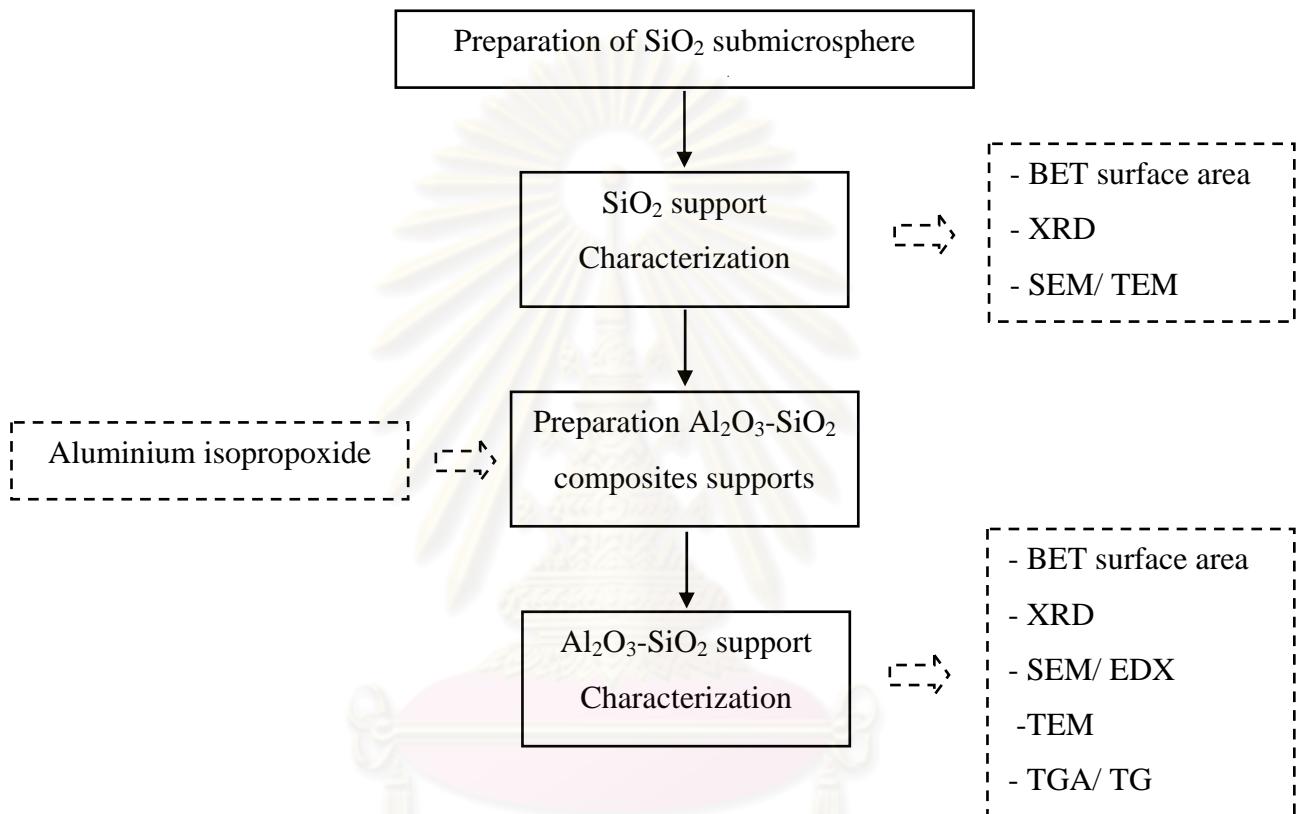


ศูนย์วิทยทรัพยากร  
จุฬาลงกรณ์มหาวิทยาลัย

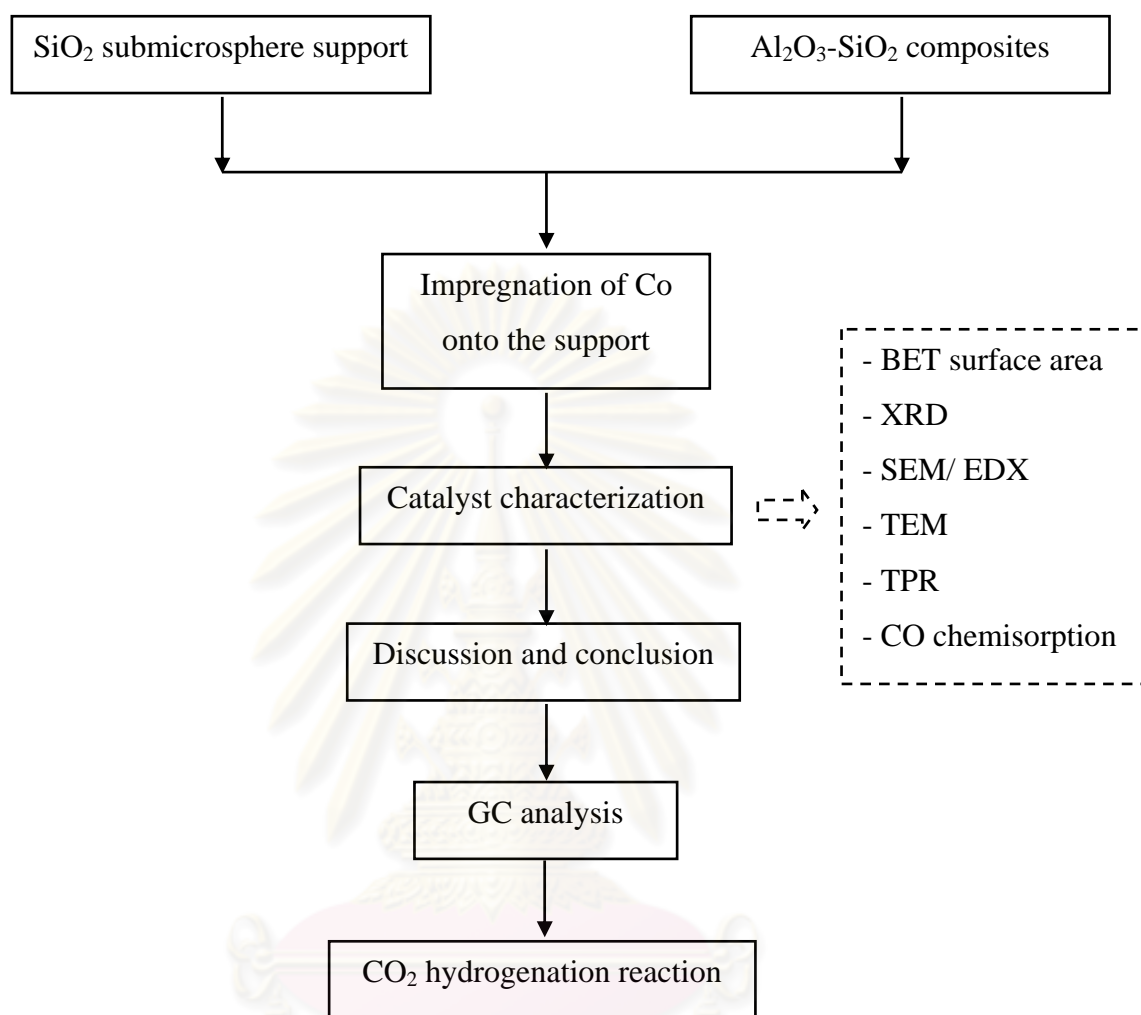
# CHAPTER IV

## METHODOLOGY

### 4.1 Research methodology



**Scheme 4.1** Flow diagram of research methodology for support preparation.



**Scheme 4.2** Flow diagram of research methodology for catalyst preparation and characterization.

## 4.2 Catalyst preparation

### 4.2.1 Chemicals

1. Tetraethoxysilane 98% (TEOS) available from Aldrich
2. Aluminium isopropoxide 98% ( $\text{Al}(\text{OPr}^i)_3$ ) from Aldrich
3. Cetyltrimethylammonium bromide (CTAB) from Aldrich
4. Cobalt (II) nitrate hexahydrate 98% [ $\text{Co}(\text{NO}_3)_2 \cdot 6\text{H}_2\text{O}$ ] available from Aldrich
5. Ammonia 30% available from Panreac
6. Ethanol 99.99% available from J.T. Baker
7. Isopropanol available from QReC
8. De-ionized water

### 4.2.2 Preparation of spherical silica particle (SSP) [Liu et al., 2003]

1. The composition of the synthesis gel had following molar ratio: 1 TEOS : 0.3  $\text{C}_{16}\text{TMABr}$  : 11  $\text{NH}_3$  : 58 Ethanol : 144  $\text{H}_2\text{O}$
2. The solution was further stirred for 2 h at room temperature.
3. The white precipitate was then collected by filtration and washed with distilled water.
4. Dried samples were calcined at  $550^\circ\text{C}$  for 6 h with a heating rate of  $10^\circ\text{C min}^{-1}$  in air.

### 4.2.3 Preparation of the $\text{Al}_2\text{O}_3$ - $\text{SiO}_2$ composites supports [Grzechowiak, 2008; Liu et al., 2009]

1. The desired amount of aluminium isopropoxide was dissolved in isopropanol (using 1:3 w/w of support: isopropanol).
2. The silica from 4.2.2. was added to the solution and stirred for 1 h.
3. Hydrolysis was performed by addition of ammonia ( $\text{H}_2\text{O} : \text{Al}(\text{OPr}^i)_3 = 4:1$ ). The sol was further stirred for 20 h at room temperature. Then, the sample was dried at  $110^\circ\text{C}$  for 24 h.
4. Dried sample was calcined in air for 2 h at temperature up to  $1000^\circ\text{C}$ .

#### 4.2.4 Cobalt loading

In this experiment, incipient wetness impregnation was the one method used for loading cobalt. Cobalt (II) nitrate hexahydrate  $[\text{Co}(\text{NO}_3)_2 \cdot 6\text{H}_2\text{O}]$  was used as precursor in this method.

The incipient wetness impregnation procedure was as follows:

1. The certain amount of cobalt (20 %wt loading) was introduced into the de-ionized water which its volume equals to pore volume of catalyst.
2. Spherical silica particle (SSP) and  $\text{Al}_2\text{O}_3$ - $\text{SiO}_2$  composites support were impregnated with aqueous solution of cobalt. The cobalt solution was dropped slowly to the spherical silica particle (SSP) and  $\text{Al}_2\text{O}_3$ - $\text{SiO}_2$  composites support, respectively.
3. The catalyst was dried in the oven at  $110^\circ\text{C}$  for 12 h.
4. The catalyst was calcined in air at  $500^\circ\text{C}$  for 4 h.

#### 4.2.5 Catalysts nomenclature

The nomenclature was used for the catalyst samples in this study are as follows:

- $\text{CoSSPXXX}$
- $\text{CoAlSSPXXX (a:b)}$

**CoSSPXXX** refers to cobalt supported on spherical silica composites (CoSSP) was calcined at  $\text{XXX}^\circ\text{C}$ .

**CoAlSSPXXX** refers to cobalt supported on alumina-spherical silica composites (CoAlSSP) was calcined at  $\text{XXX}^\circ\text{C}$ .

*a* refers to the weight ratio of  $\text{Al}_2\text{O}_3$

*b* refers to the weight ratio of  $\text{SiO}_2$

### 4.3 Characterization

#### 4.3.1 X-ray diffraction (XRD)

XRD was performed to determine the bulk phase of catalysts by SIEMENS D 5000 X-ray diffractometer connected with a computer with Diffract ZT version 3.3 programs for fully control of the XRD analyzer. The experiment was carried out by using  $\text{CuK}_\alpha$  radiation with Ni filter in the  $2\theta$  range of 20-80 degrees resolution  $0.04^\circ$ . The crystallite size was estimated from line broadening according to the Scherrer equation and  $\alpha\text{-Al}_2\text{O}_3$  was used as standard.

#### 4.3.2 $\text{N}_2$ physisorption

BET apparatus for the single point method, the reaction apparatus of BET surface area measurement consisted of two feed lines for helium and nitrogen. The flow rate of the gas was adjusted by means of fine-metering valve on the gas chromatograph. The sample cell made from pyrex glass. The mixture gases of helium and nitrogen were flowed through the system at the nitrogen relative of 0.3. The catalyst sample (ca. 0.3 to 0.5 g) was placed in the sample cell, which was then heated up to  $160^\circ\text{C}$  and was held at this temperature for 2 hours. After the catalyst sample was cooled down to room temperature, nitrogen uptakes were measured as follows.

1. Adsorption step: The sample that set in the sample cell was dipped into liquid nitrogen. Nitrogen gas that was flowed through the system was adsorbed on the surface of the sample until equilibrium was reached.

2. Desorption step: The sample cell with nitrogen gas-adsorption catalyst sample was dipped into the water at room temperature. The adsorbed nitrogen gas was desorbed from the surface of the sample. This step was completed when the indicator line was in the position of base line.

3. Calibration step: 1 ml of nitrogen gas at atmospheric pressure was injected through the calibration port of the gas chromatograph and the area was measured. The area was the calibration peak.



#### **4.3.3 Scanning Electron Microscope: SEM and Energy Dispersive X-ray Spectroscopy (EDX)**

Scanning electron microscopy (SEM) and energy dispersive X-ray spectroscopy (EDX) was used to determine the morphology and elemental distribution of the catalyst particles. Model of SEM: JEOL mode JSM-5800LV and EDX were performed using Link Isis Series 300 program at the Scientific and Technological Research Equipment Center, Chulalongkorn University (STREC).

#### **4.3.4 Transmission Electron Microscope (TEM)**

The particle size and distribution of catalyst samples were observed using JEOL-JEM 200CX transmission electron microscope operated at 100 kV.

#### **4.3.5 Temperature Programmed Reduction (TPR)**

TPR was used to determine the reducibility of catalysts. The catalyst sample 0.1 g was used in the operation and temperature ramping from 35°C to 800°C at 10 °C/min. The carrier gas will be 5% H<sub>2</sub> in Ar. During reduction, a cold trap was placed to before the detector to remove water produced. A thermal conductivity detector (TCD) was measured the amount of hydrogen consumption. The calibration of hydrogen consumption was performed with bulk cobalt oxide (Co<sub>3</sub>O<sub>4</sub>) at the same conditions.

#### **4.3.6 Thermogravimetry Analysis (TGA)**

TGA was used to determine the weight loss pattern and the reducibility of catalysts by Shimadzu TGA model 50. The catalyst sample of ca. 10-20 mg and temperature ramping from 35°C to 1000°C at 10°C/min were used in the operation. The carrier gas was H<sub>2</sub>UHP.

### 4.3.7 Carbon monoxide Chemisorptions

Static CO chemisorption at room temperature on the reduce catalysts were used to determine the number of reduced surface cobalt metal atoms. The total CO chemisorption was calculated from the number of injection of a known volume. CO chemisorptions was carried out following the procedure using a Micromeritics Pluse Chemisorb 2750 instrument at the Analysis Center of Department of Chemical Engineering, Faculty of Engineering, Chulalongkorn University. In an experiment, about 0.10 g of the catalyst sample was places in a glass tube. Prior to chemisorptions, the catalysts will be reduced at 350°C for 3 hours after ramping up at a rate of 10°C/min. After, carbon monoxide 30 microlite was injected to catalyst and repeated until desorption peak constant. Amount of carbon monoxide adsorption on catalyst is relative amount of active site.

## 4.4 Reaction study in CO<sub>2</sub> hydrogenation

### 4.4.1 Material

CO<sub>2</sub> hydrogenation was performed using 0.1 g of catalyst packed in the middle of the stainless steel microreactor, which is located in the electrical furnace. The total flow rate was 30 ml/min with H<sub>2</sub>/CO<sub>2</sub> ratio of 10/1. The catalyst sample was re-reduced *in situ* in flowing H<sub>2</sub> at 350°C for 3 h prior to CO<sub>2</sub> hydrogenation. CO<sub>2</sub> hydrogenation will be carried out at 220°C and 1 atm total pressure. The effluent was analyzed using gas chromatography technique [ Thermal conductivity detector (TCD), molecular sieve 5 °A was used for separation of carbon dioxide (CO<sub>2</sub>) and methane (CH<sub>4</sub>) and flame ioinization detector (FID), VZ-10 was used for separation of light hydrocarbon such as methane (CH<sub>4</sub>), ethane (C<sub>2</sub>H<sub>6</sub>), propane (C<sub>3</sub>H<sub>8</sub>), etc.].

### 4.4.2 Apparatus

Flow diagram of CO<sub>2</sub> hydrogenation system was shown in Figure 4.1. The system consists of a reactor, an automatic temperature controller, an electrical furnace and a gas controlling system.

#### **4.4.2.1 Reactor**

The reactor was made from a stainless steel tube (O.D. 3/8"). Two sampling points were provided above and below the catalyst bed. Catalyst was placed between two quartz wool layers.

#### **4.4.2.2 Automation Temperature Controller**

This unit consisted of a magnetic switch connected to a variable voltage transformer and a solid-state relay temperature controller model no. SS2425DZ connected to a thermocouple. Reactor temperature was measured at the bottom of the catalyst bed in the reactor. The temperature control set point is adjustable within the range of 0-800°C at the maximum voltage output of 220 volt.

#### **4.4.2.3 Electrical Furnace**

The furnace supplied heat to the reactor for CO hydrogenation. The reactor could be operated from temperature up to 800°C at the maximum voltage of 220 volt.

#### **4.4.2.4 Gas Controlling System**

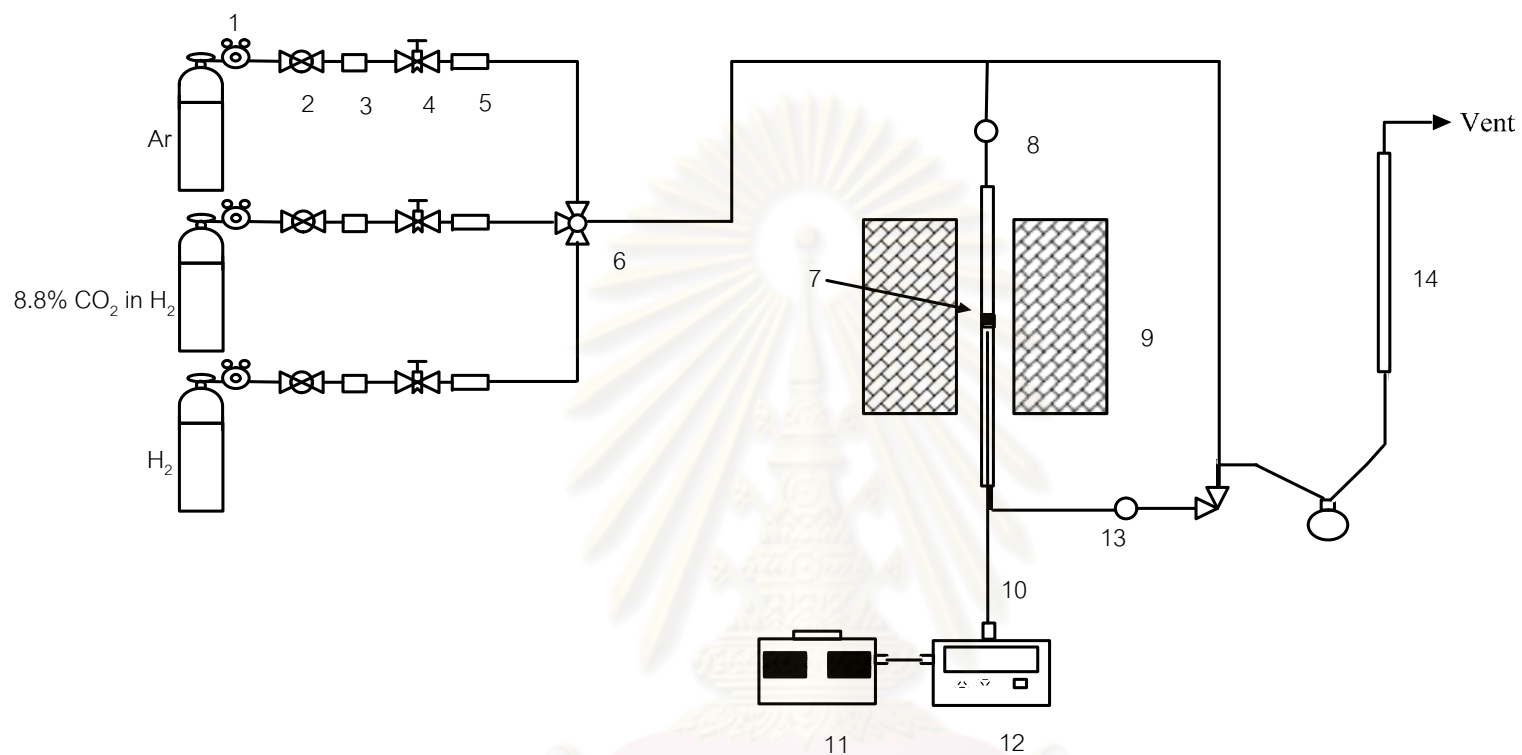
Reactant for the system was each equipped with a pressure regulator and an on-off valve and the gas flow rates were adjusted by using metering valves.

#### **4.4.2.5 Gas Chromatography**

The composition of hydrocarbons in the product stream was analyzed by a Shimadzu GC14B (VZ10) gas chromatograph equipped with a flame ionization detector. A Shimadzu GC8A (molecular sieve 5A) gas chromatography equipped with a thermal conductivity detector was used to analyze CO and H<sub>2</sub> in the feed and product streams. The operating conditions for each instrument were shown in the Table 4.1.

**Table 4.1** Operating condition for gas chromatograph

<b>Gas Chromatograph</b>	<b>SHIMADZU GC-8A</b>	<b>SHIMADZU GC-14B</b>
Detector	TCD	FID
Column	Porapak Q	VZ10
- Column material	SUS	-
- Length	2 m	-
- Outer diameter	4 mm	-
- Inner diameter	3 mm	-
- Mesh range	60/80	60/80
- Maximum temperature	350°C	80°C
Carrier gas	He (99.999%)	He (99.999%)
Carrier gas flow	40 cc/min	-
Column gas	He (99.999%)	Air, H <sub>2</sub>
Column gas flow	40 cc/min	-
Column temperature		
- Initial (°C)	60	70
- Final (°C)	60	70
Injection temperature	100	100
Detector temperature	100	150
Current (mA)	80	-
Analysed gas	Ar, CO, H <sub>2</sub>	Hydrocarbon C <sub>1</sub> -C <sub>4</sub>



- |                            |                   |                       |                   |                                  |                |
|----------------------------|-------------------|-----------------------|-------------------|----------------------------------|----------------|
| 1. Pressure Regulator      | 2. On-Off Valve   | 3. Gas Filter         | 4. Metering Valve | 5. Back Pressure                 | 6. 3-way Valve |
| 7. Catalyst Bed            | 8. Sampling point | 9. Furnace            | 10. Thermocouple  | 11. Variable Voltage Transformer |                |
| 12. Temperature Controller | 13. Heating Lin   | 14. Bubble Flow Meter |                   |                                  |                |

**Figure 4.1** Flow diagram of CO<sub>2</sub> hydrogenation system

#### 4.4.3 Procedures

1. Using 0.05 g of catalyst packed in the middle of the stainless steel microreactor, which was located in the electrical furnace.

2. A flow rate of Ar = 8 CC/min, 8.8% CO<sub>2</sub> in H<sub>2</sub> = 22 CC/min and H<sub>2</sub> = 50 CC/min in a fixed-bed flow reactor. A relatively high H<sub>2</sub>/CO<sub>2</sub> ratio was used to minimize deactivation due to carbon deposition during reaction.

3. The catalyst sample was re-reduced *in situ* in flowing H<sub>2</sub> at 350°C for 3 h prior to CO<sub>2</sub> hydrogenation.

4. CO<sub>2</sub> hydrogenation was carried out at 220°C and 1 atm total pressure in flowing 8.8% CO<sub>2</sub> in H<sub>2</sub>.

5. The effluent was analyzed using gas chromatograph technique. [Thermal conductivity detect (TDC) was used for separation of carbon dioxide (CO<sub>2</sub>) and methane (CH<sub>4</sub>) and flame ionization detector (FID) were used for separation of light hydrocarbon such as methane (CH<sub>4</sub>), ethane (C<sub>2</sub>H<sub>6</sub>), propane (C<sub>3</sub>H<sub>8</sub>), etc.]. In all case, steady-state was reached within 6 h.

## CHAPTER V

### RESULTS AND DISCUSSIONS

This chapter was conducted in order to investigate the characteristic and catalytic properties of spherical silica and alumina-silica composites-supported cobalt catalysts for carbon dioxide hydrogenation reaction. This chapter is divided into two sections. The first section describes the preparation and characterization of spherical silica and alumina-silica composites supports. The second section shows characteristics and catalytic activity of spherical silica and alumina-silica composites supported cobalt catalysts.

#### 5.1 Support preparation and characterization

This section described the preparation and characterization of spherical silica and alumina-silica composite supports by deposition of  $\text{Al}_2\text{O}_3$  particles on the spherical silica particle (SSP) surface using hydrolysis of aluminium isopropoxide to obtain AlSSP.

##### 5.1.1 Preparation of spherical silica particle (SSP)

Scanning electron microscopy (SEM) characterization was used to investigate the morphology of spherical silica support. Figure 5.1 shows images of spherical particles, with an average size of about  $0.5 \mu\text{m}$ .

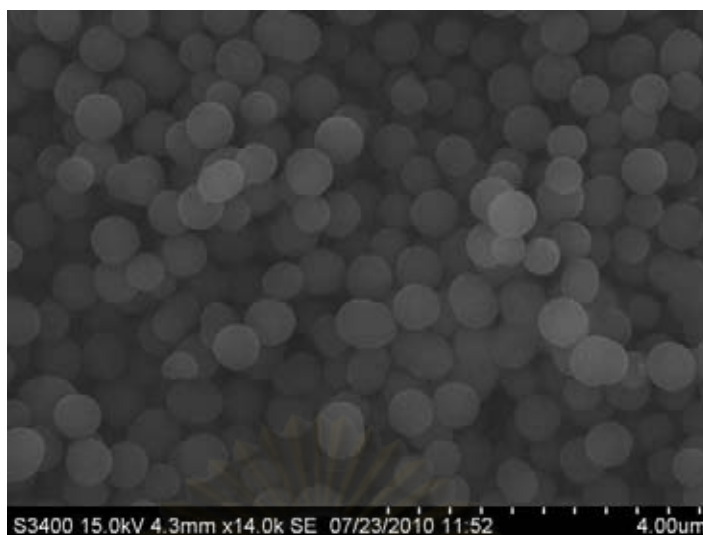


**Figure 5.1** The SEM images of the spherical silica particles.

The specific surface area, pore size and pore volume of spherical silica particles were measured by nitrogen physisorption technique. The results are summarized in Table 5.1.

**Table 5.1** BET surface area, pore volume and pore diameter of spherical silica particles

Sample	Surface area (m <sup>2</sup> /g)	Pore volume (cm <sup>3</sup> /g)	Pore diameter (nm)
SSP550	927	0.7508	2.18



### **5.1.2 Preparation and characterization of alumina-spherical silica particles composites supports (AISSP)**

This section described the characterization of spherical silica and alumina-silica composite supports by deposition of  $\text{Al}_2\text{O}_3$  particles on the spherical silica particle (SSP). The structure and crystallinity of the alumina-silica composite supports (AISSP) were measured by BET surface area, X-ray diffraction, scanning electron microscopy (SEM), energy dispersive X-ray spectroscopy (EDX) and transmission electron microscope (TEM) were used to study the morphology of the alumina-silica composites supports. The thermal properties of the alumina-silica composites supports were characterized by differential thermal analysis and thermogravimetric (DTA/TG).

#### **5.1.2.1 Differential thermal analysis and thermogravimetric (DTA/TG)**

The thermal property was characterized by thermogravimetric and differential thermal analysis (TG-DTA). Figure 5.2 shows the endothermic peaks of differential thermal analysis (DTA) curve of AISSP below  $600^\circ\text{C}$ . The weight loss corresponding to dehydration was observed in the thermal analysis TG curve. The noticeable exothermic peak at  $992^\circ\text{C}$  was related to the XRD patterns as mentioned after. The DTA curve indicated the exothermic peak that was due to the phase transformation of amorphous to  $\gamma$ -alumina at  $992^\circ\text{C}$ . The TG curve had shown a largest weight loss about 12.5% in AISSP.

ศูนย์วิทยทรัพยากร  
จุฬาลงกรณ์มหาวิทยาลัย

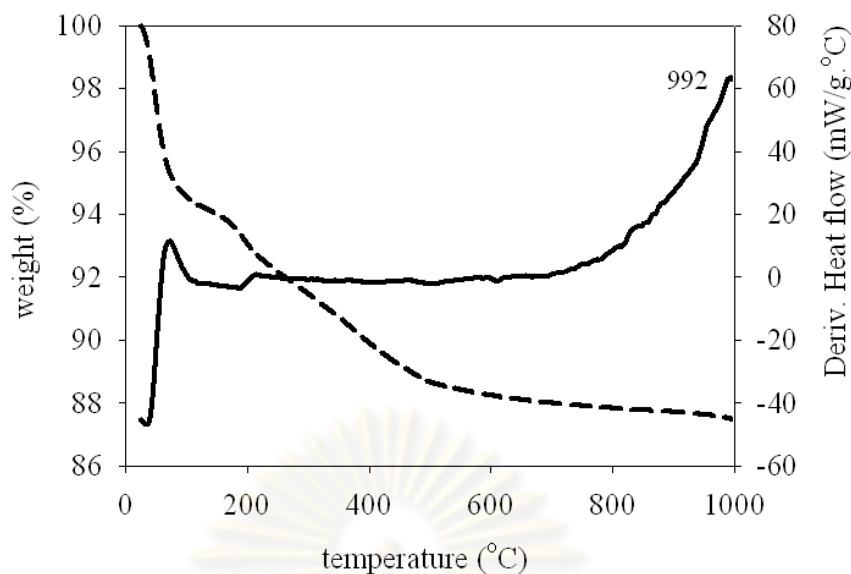


**Figure 5.2** DTA/TG curve of the AlSSP (1:3) composites.

### 5.1.2.2 X-Ray Diffraction

Bulk crystal structure and chemical phase composition of a crystalline material having crystal domain of greater than 3-5 nm can be determined by X-ray diffraction. The measurements were carried out at the diffraction angles ( $2\theta$ ) between  $20^\circ$  and  $80^\circ$ .

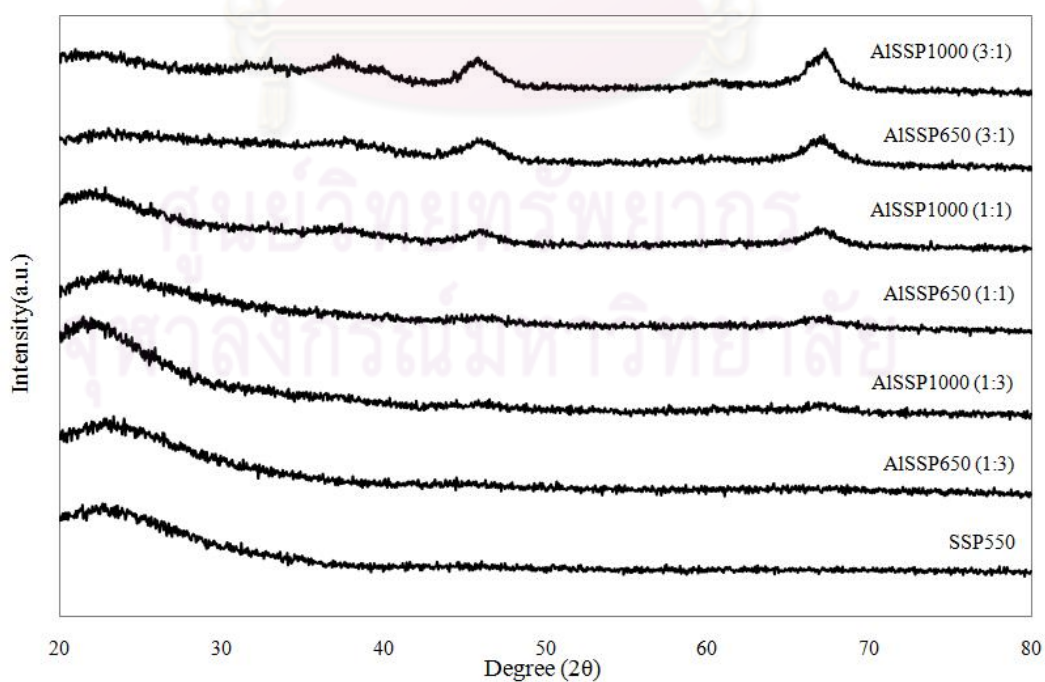


**Figure 5.3** XRD patterns of spherical silica and alumina-silica composite supports.

XRD patterns of spherical silica (SSP) and alumina-silica composite supports (AISSP) before impregnation with the cobalt metal at various calcination temperatures for 2 h and various compositions between alumina and silica are shown in Figure 5.3. After calcined at 550°C for 2 h, the XRD patterns of SSP550 exhibited only amorphous silica. At 650 and 1000°C, the slight diffraction peak of Al<sub>2</sub>O<sub>3</sub> crystallite can be observed at 33.08, 37.2, 45.84, and 67.28°. This demonstrates that Al<sub>2</sub>O<sub>3</sub> had a small significant crystalline size of  $\gamma$ -alumina. Therefore, thermal stability of  $\gamma$ -alumina can be enhanced by adding spherical silica. At various composition between alumina and silica, AISSP1000 (3:1) had a highest large  $\gamma$ -alumina crystallite size compared with AISSP1000 (1:3).

### 5.1.2.3 Nitrogen physisorption

The BET surface area, pore volume and average pore diameter analysis of alumina-silica composite supports (AISSP) at various calcination temperatures for 2 h and various compositions between alumina and silica are listed in Table 5.2, which are measured by nitrogen physisorption technique.

From the result, it can be observed that the surface areas of all AISSP supports were less than the pure spherical silica particle. This was in accordance with the larger pore sizes of AISSP supports than those of pure spherical silica support. This is probably due to the increase of alumina amount in the spherical silica particle. At various calcination temperatures, AISSP650 (1:3) exhibited the best possible BET surface area of 769 m<sup>2</sup>/g. Moreover, the BET surface area and pore volume dramatically decreased to 23 m<sup>2</sup>/g for AISSP1000 (1:3). This is probably due to the sintering effect. However, BET surface area increased with alumina loading from 23 m<sup>2</sup>/g of AISSP1000 (1:3) to 76 and 134 m<sup>2</sup>/g of AISSP1000 (1:1) and AISSP1000 (3:1), respectively as shown in Table 5.2. This can be attributed to grain growth from phase transformation of amorphous to  $\gamma$ -alumina and the particles sintering. The smaller  $\gamma$ -alumina crystallites grow into bigger  $\gamma$ -alumina crystallites through the phase transformation as the results from Figure 5.3, leading to the decrease of the voids among  $\gamma$ -alumina crystallites.

**Table 5.2** BET Surface areas, pore volume and pore diameter of alumina-spherical silica particle composites.

<b>Samples</b>	<b>Surface area (m<sup>2</sup>/g)</b>	<b>Pore Volume (cm<sup>3</sup>/g)</b>	<b>Pore Diameter (nm)</b>
AlSSP650 (1:3)	769	0.6247	2.56
AlSSP1000 (1:3)	23	0.0452	6.92
AlSSP650 (1:1)	529	0.5282	3.69
AlSSP1000 (1:1)	76	0.2362	9.09
AlSSP650 (3:1)	443	0.7278	5.62
AlSSP1000 (3:1)	134	0.4762	9.35

#### **5.1.2.4 Scanning electron microscopy (SEM) and energy dispersive X-ray spectroscopy (EDX)**

Scanning electron microscopy (SEM) and energy dispersive X-ray spectroscopy (EDX) was also conducted in order to study surface texture, morphology and elemental distribution of the materials, respectively. In the backscattering scanning mode, the electron beam focused on the sample is scanned by a set of deflection coils. Backscattered electrons or secondary electrons emitted from the sample are detected. The typical SEM micrograph, EDX mapping and a typical spectrum from EDX analysis for AlSSP650 (3:1) was illustrated in Figure 5.4 and Figure 5.5. The external surface of support granule was shown in this figure and light or white patches on the support granule surface representing high concentration of silica, alumina and oxygen distribution on the surface. It indicated that the alumina distribution on the spherical silica surface is uniform.

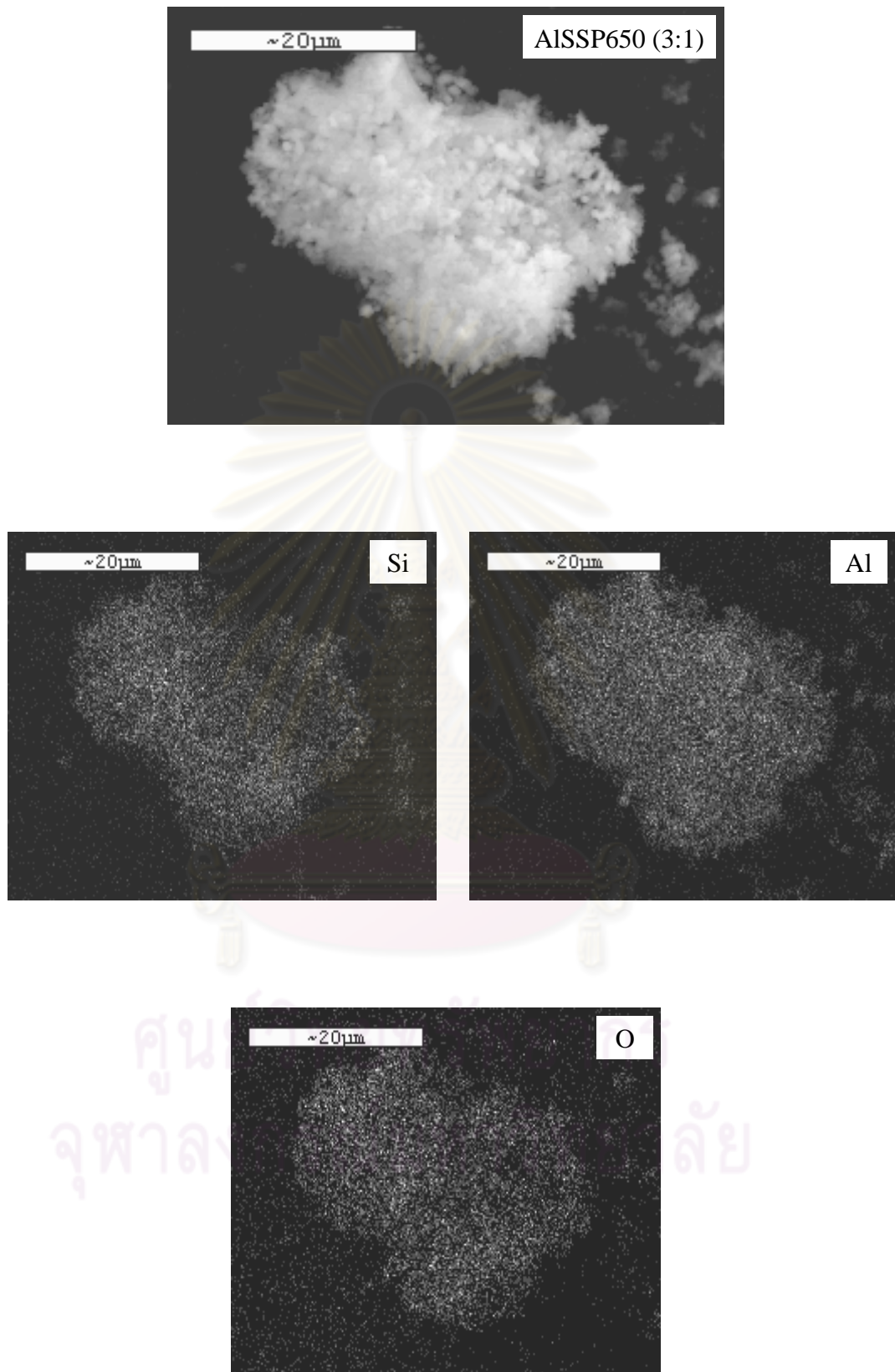
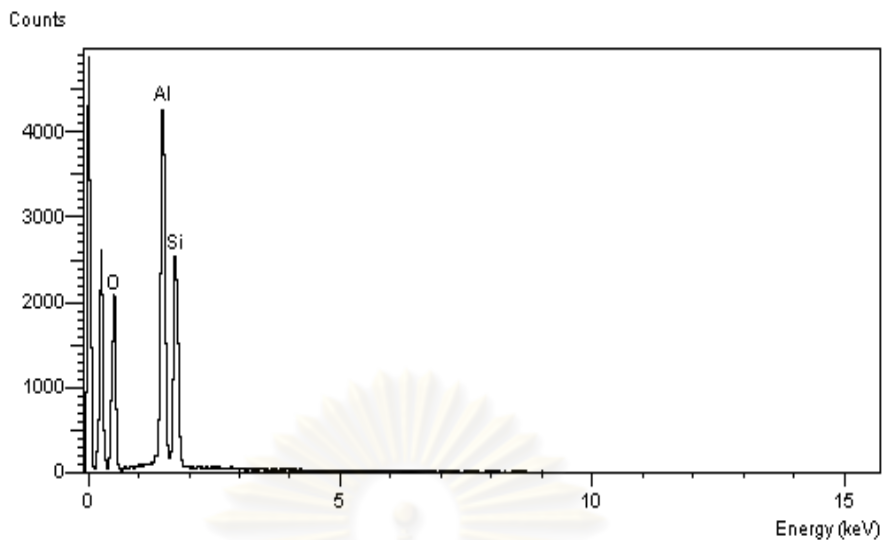


**Figure 5.4** SEM micrograph and EDX mapping of AlSSP650 (3:1) composites.



Element	Element (%)	Atomic (%)
Si	17.42	12.67
Al	25.87	20.01
O	56.71	67.32

**Figure 5.5** A typical spectrum of the AlSSP650 (3:1) composites from EDX analysis.

#### 5.1.2.5 Transmission electron microscope (TEM)

In order to determine the dispersion of alumina on the spherical silica employed, the high resolution TEM was used. The TEM micrographs for alumina-silica composites support, AlSSP650 (1:3) is shown in Figure 5.6. As seen in this figure, the dark spots representing the alumina on the spherical silica was well dispersed. TEM image was found to be similar with the results from SEM/ EDX.

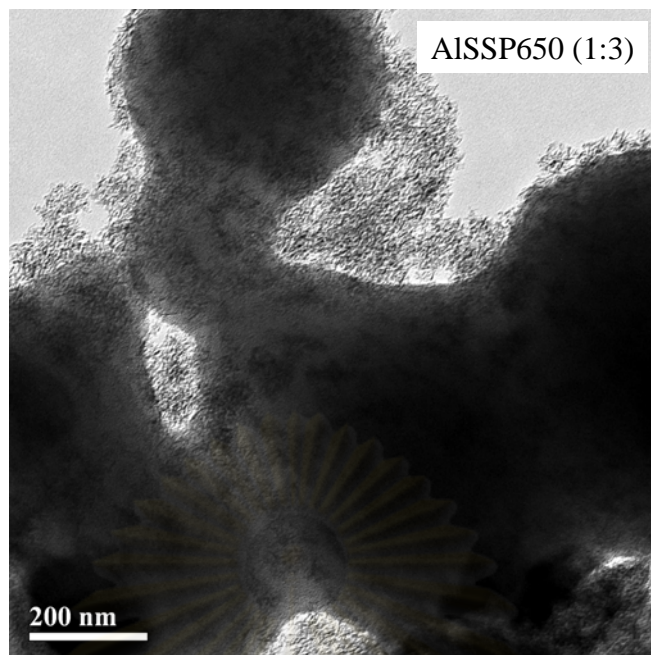


**Figure 5.6** TEM micrographs of the AlSSP650 (1:3) composites.

## **5.2 Preparation and characterization of spherical silica (SSP) and alumina-spherical silica composites (AlSSP) supported cobalt catalyst.**

This section presented the characterization of silica and alumina-silica composites supported cobalt catalyst by incipient wetness impregnation of cobalt (II) nitrate hexahydrate. The various analytical techniques had been performed including BET surface area, X-ray diffraction, scanning electron microscopy (SEM), energy dispersive X-ray spectroscopy (EDX), transmission electron microscope (TEM), temperature programmed reduction (TPR), CO chemisorptions and CO<sub>2</sub> hydrogenation reaction performance.

### **5.2.1 X-ray diffraction**

The phase identification was carried out on the basis of data from X-ray diffraction. A 20% wt of cobalt was impregnated onto spherical silica (SSP) and alumina-silica composite supports (AlSSP). After calcination in air at 500°C for 4 h, the XRD patterns for the calcined Co catalysts for all supports are shown in Figure 5.7. The XRD peaks of Co<sub>3</sub>O<sub>4</sub> were observed at 31°, 37°, 45°, 59°, and 65°

[Jakrapan, 2009]. XRD peaks of  $\gamma$ - $\text{Al}_2\text{O}_3$  were not observed due to high intensity of the  $\text{Co}_3\text{O}_4$  peaks.

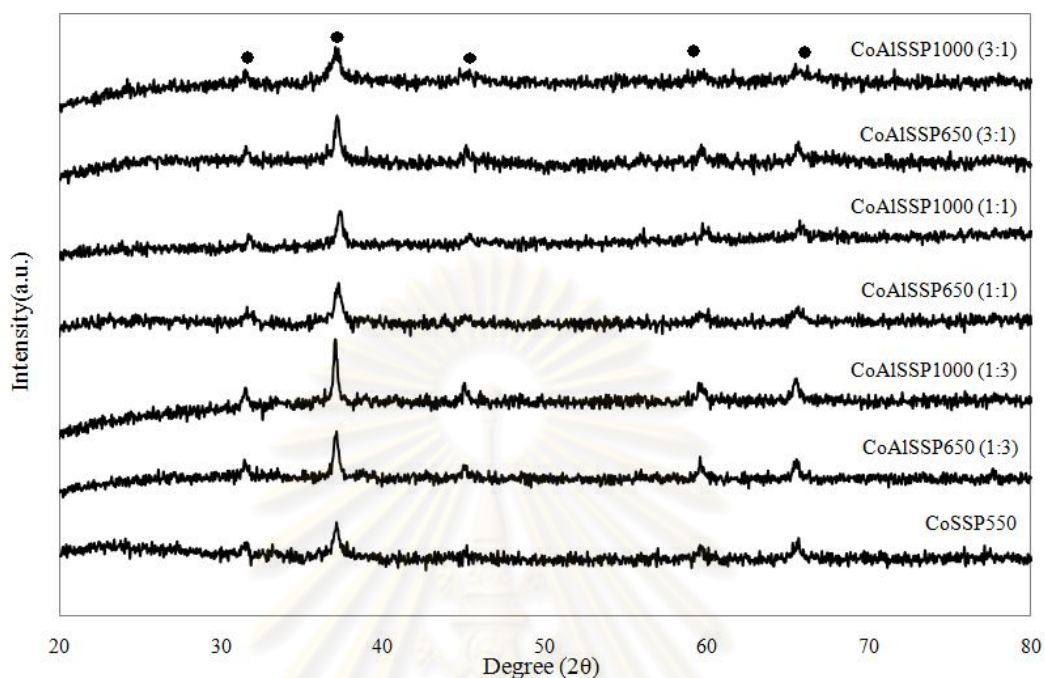


**Figure 5.7** XRD patterns of silica and alumina-silica composites supported cobalt catalysts.

### 5.2.2 Nitrogen physisorption

The BET surface areas, pore volume and average pore diameter analysis of cobalt impregnated onto SSP and AlSSP after calcination for 6 hours at  $500^\circ\text{C}$  were measured by nitrogen physisorption technique as shown in Table 5.3. The surface areas of CoSSP and all CoAlSSP were less than the corresponding supports. This was in accordance with the smaller pore sizes of CoSSP550, CoAlSSP650 and CoAlSSP1000 catalysts than those of pure support particles.



**Table 5.3** BET Surface areas, pore volume and pore diameter of silica and alumina-silica composites-supported cobalt catalysts.

<b>Samples</b>	<b>Surface area (m<sup>2</sup>/g)</b>	<b>Pore Volume (cm<sup>3</sup>/g)</b>	<b>Pore Diameter (nm)</b>
CoSSP550	631	0.4578	2.46
CoAlSSP650 (1:3)	490	0.2528	2.36
CoAlSSP1000 (1:3)	25	0.0405	5.16
CoAlSSP650 (1:1)	380	0.2818	3.66
CoAlSSP1000 (1:1)	63	0.1715	8.15
CoAlSSP650 (3:1)	244	0.2998	4.69
CoAlSSP1000 (3:1)	102	0.2979	8.81

### 5.2.3 Scanning electron microscopy (SEM) and energy dispersive X-ray spectroscopy (EDX)

Scanning electron microscopy (SEM) and energy dispersive X-ray spectroscopy (EDX) were also conducted in order to study the morphologies and elemental distribution of the samples, respectively. The SEM micrographs and EDX mapping for spherical silica supported cobalt catalyst; CoSSP550 was illustrated in Figure 5.9 and Figure 5.10. The external surface of catalyst granule was shown. In all figures, the light or white patches on the catalyst granule surface represent high concentration of cobalt oxides on the surface. It can be seen that cobalt is well distributed on the external surface.

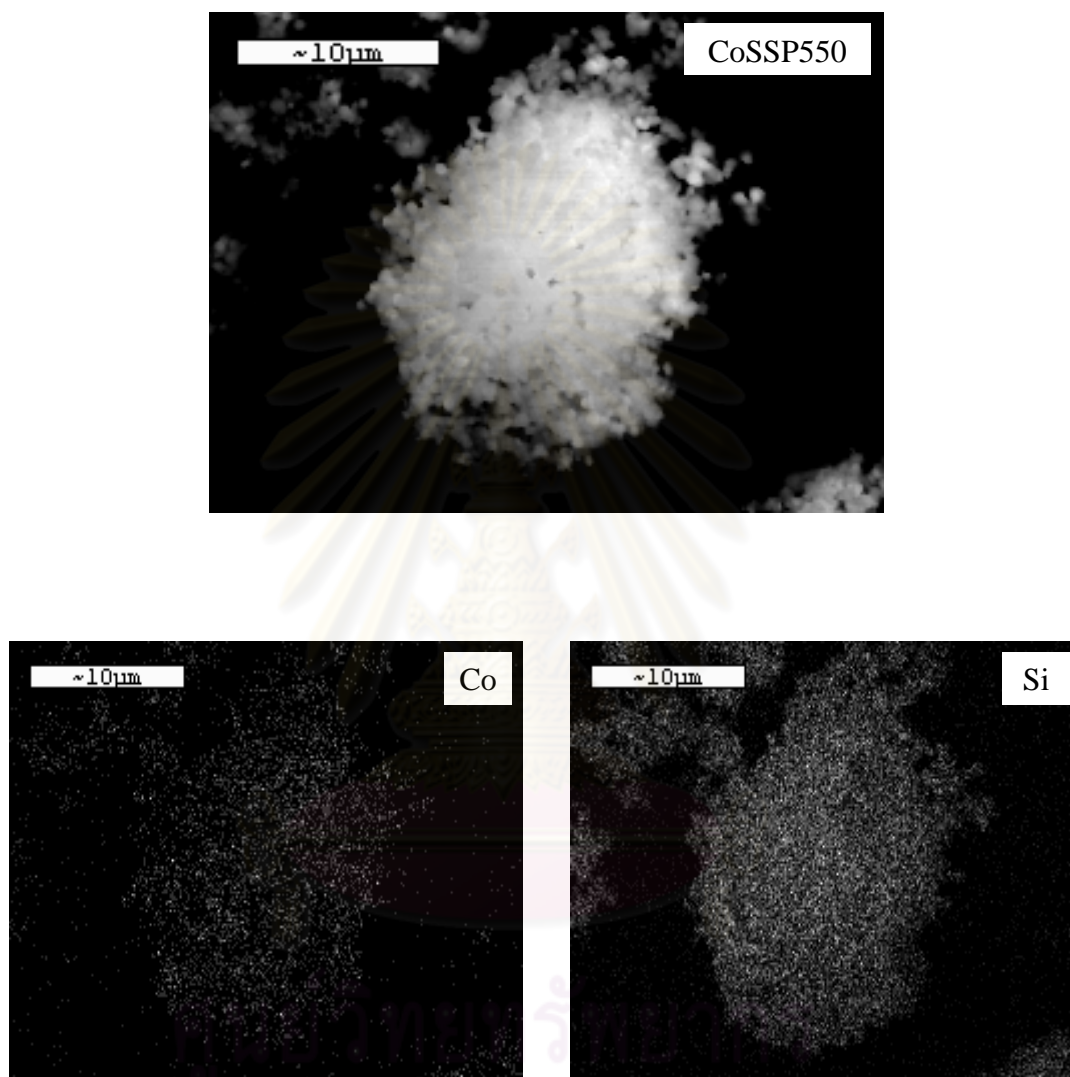
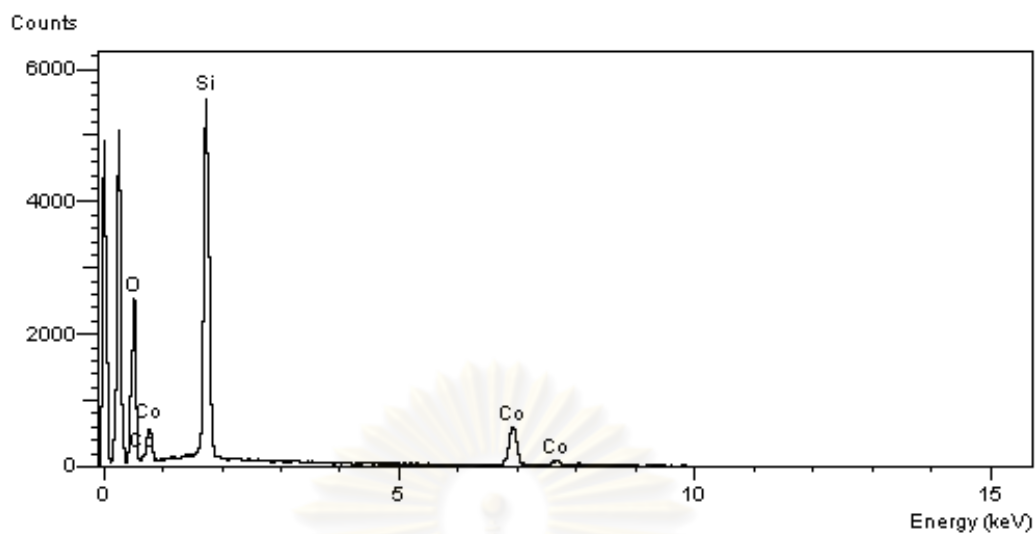


**Figure 5.8** SEM micrograph and EDX mapping of CoSSP550 catalyst.



Element	Element (%)	Atomic (%)
Si	30.37	22.88
Co	15.55	5.58
O	54.08	71.53

**Figure 5.9** A typical spectrum of the CoSSP550 catalyst from EDX analysis.

Figures 5.10- 5.15 are shown the morphologies and elemental distribution of the samples. Figure 5.16 presents a typical spectrum and element quantity of CoAlSSP650 (3:1) surface from EDX analysis. It can be seen that the cobalt oxide species was well dispersed on alumina-silica composite supports.

จุฬาลงกรณ์มหาวิทยาลัย

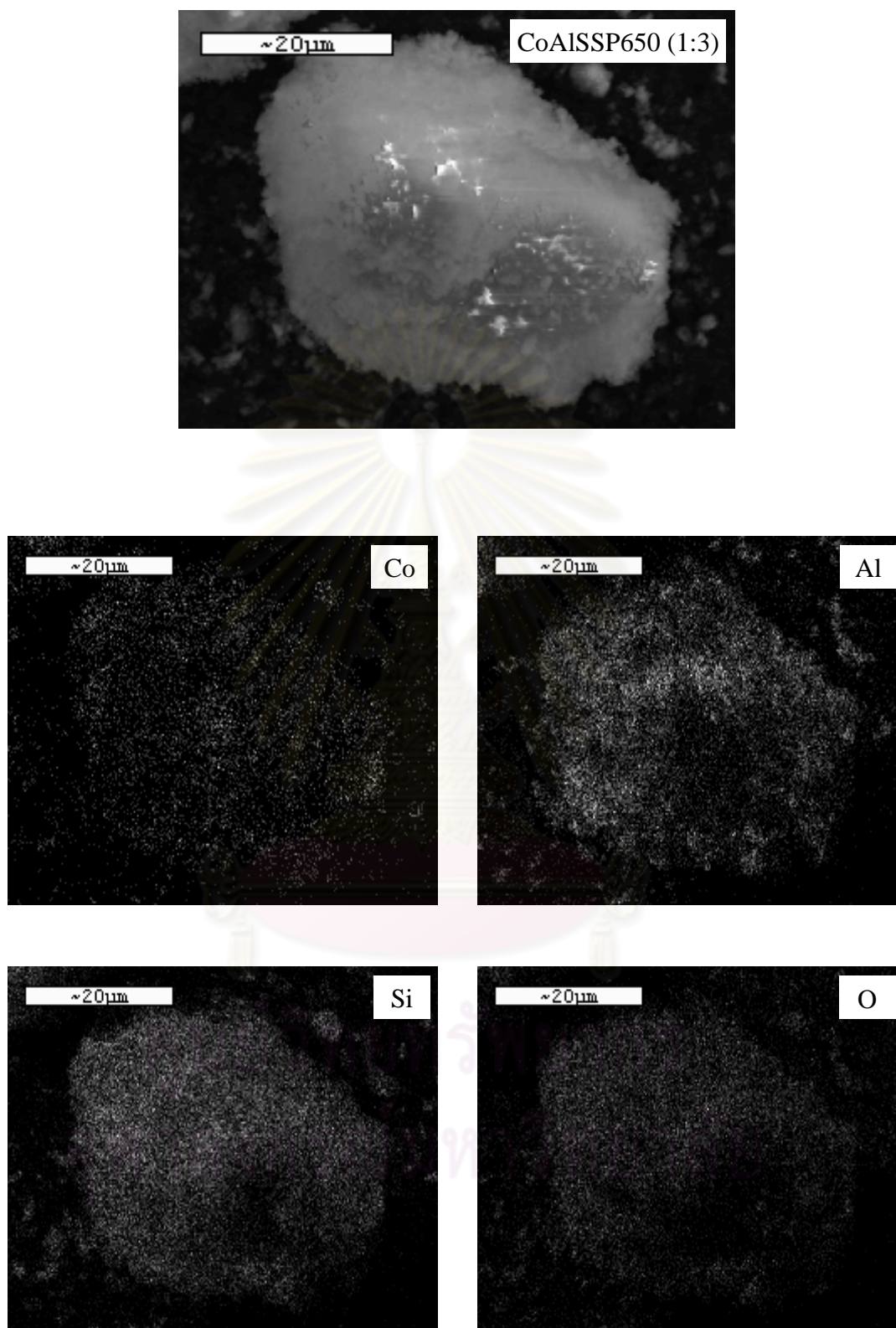


**Figure 5.10** SEM micrograph and EDX mapping of CoAlSSP650 (1:3) catalyst.

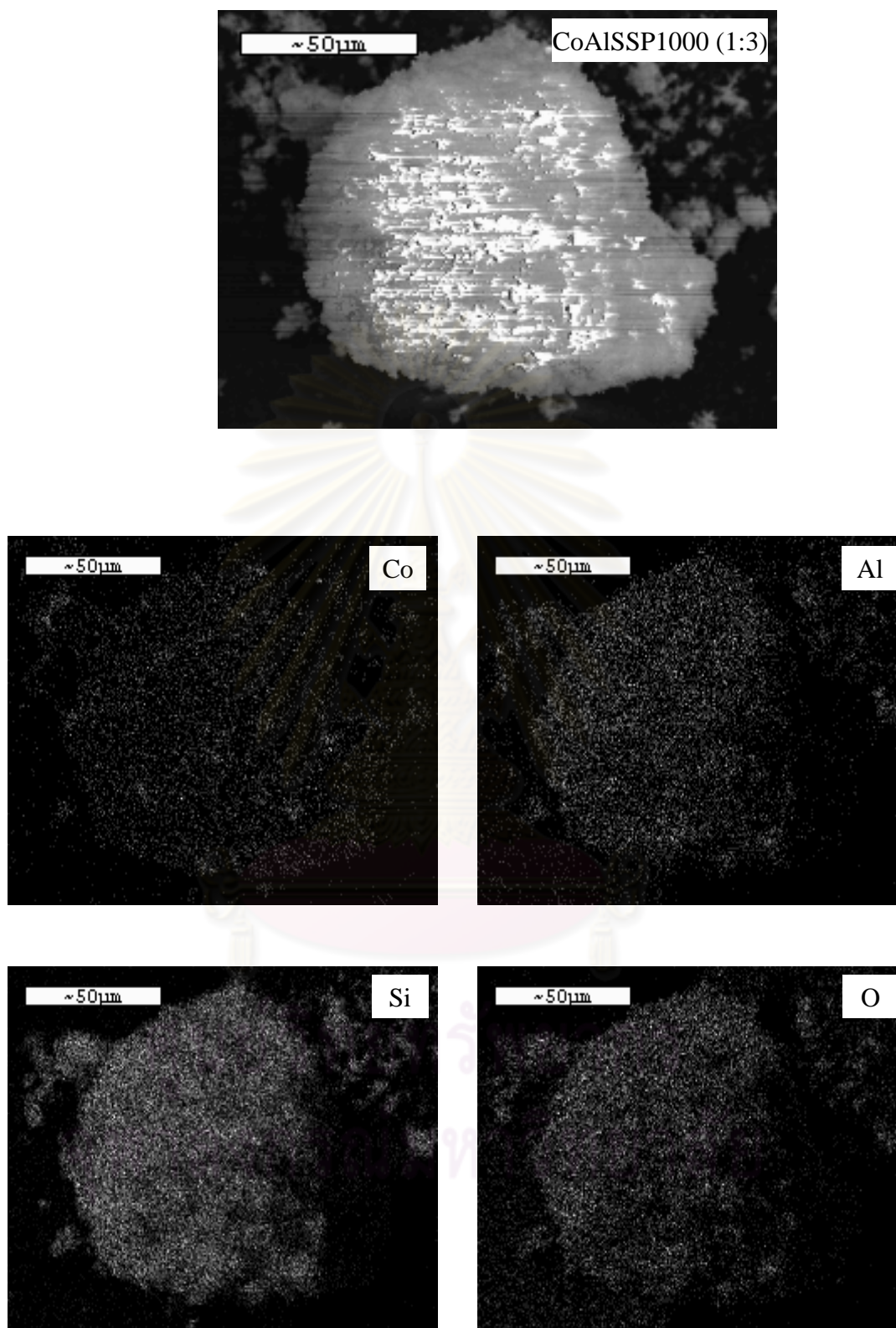


**Figure 5.11** SEM micrograph and EDX mapping of CoAlSSP1000 (1:3) catalyst.

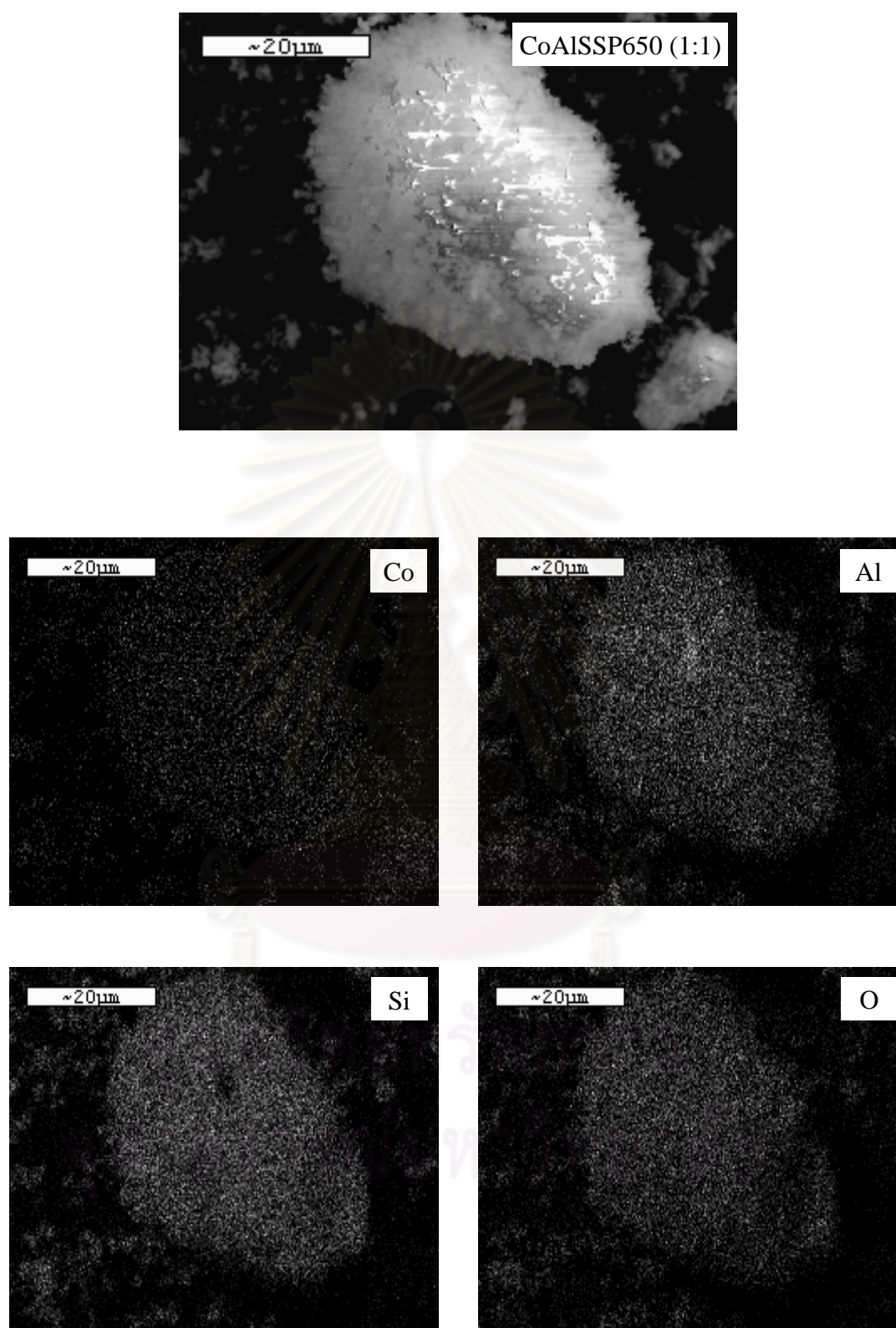


**Figure 5.12** SEM micrograph and EDX mapping of CoAlSSP650 (1:1) catalyst.

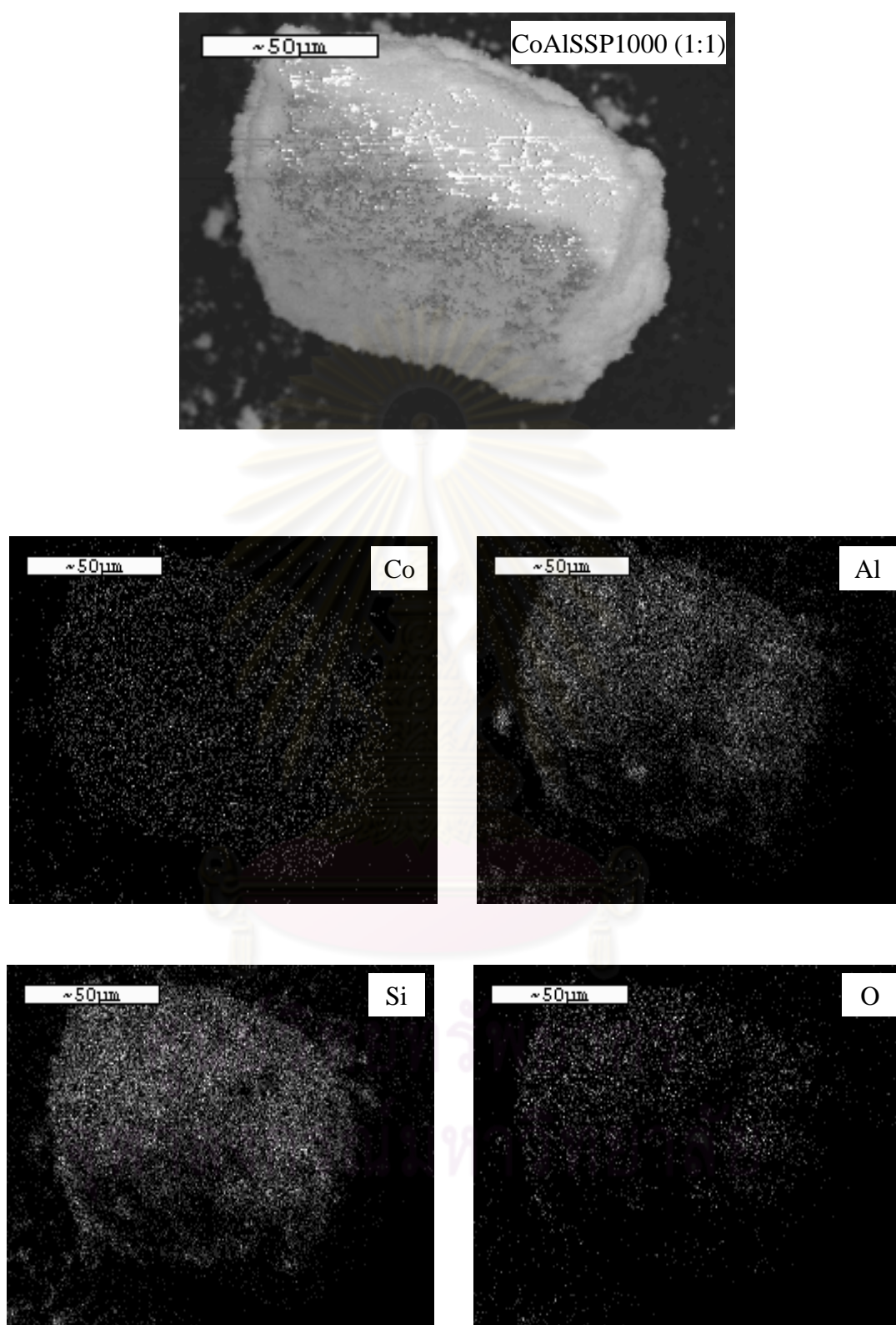


**Figure 5.13** SEM micrograph and EDX mapping of CoAlSSP1000 (1:1) catalyst.

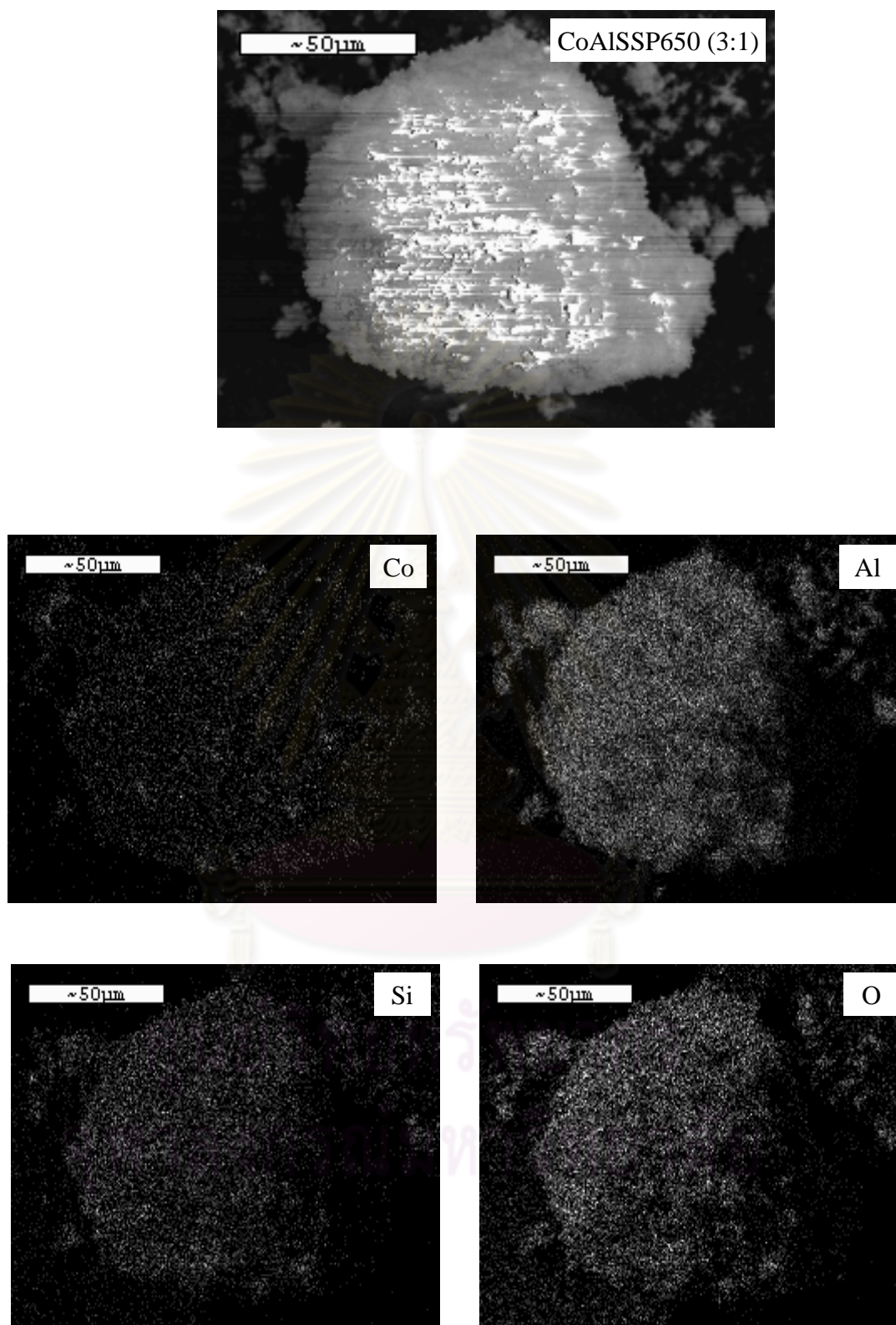


**Figure 5.14** SEM micrograph and EDX mapping of CoAlSSP650 (3:1) catalyst.



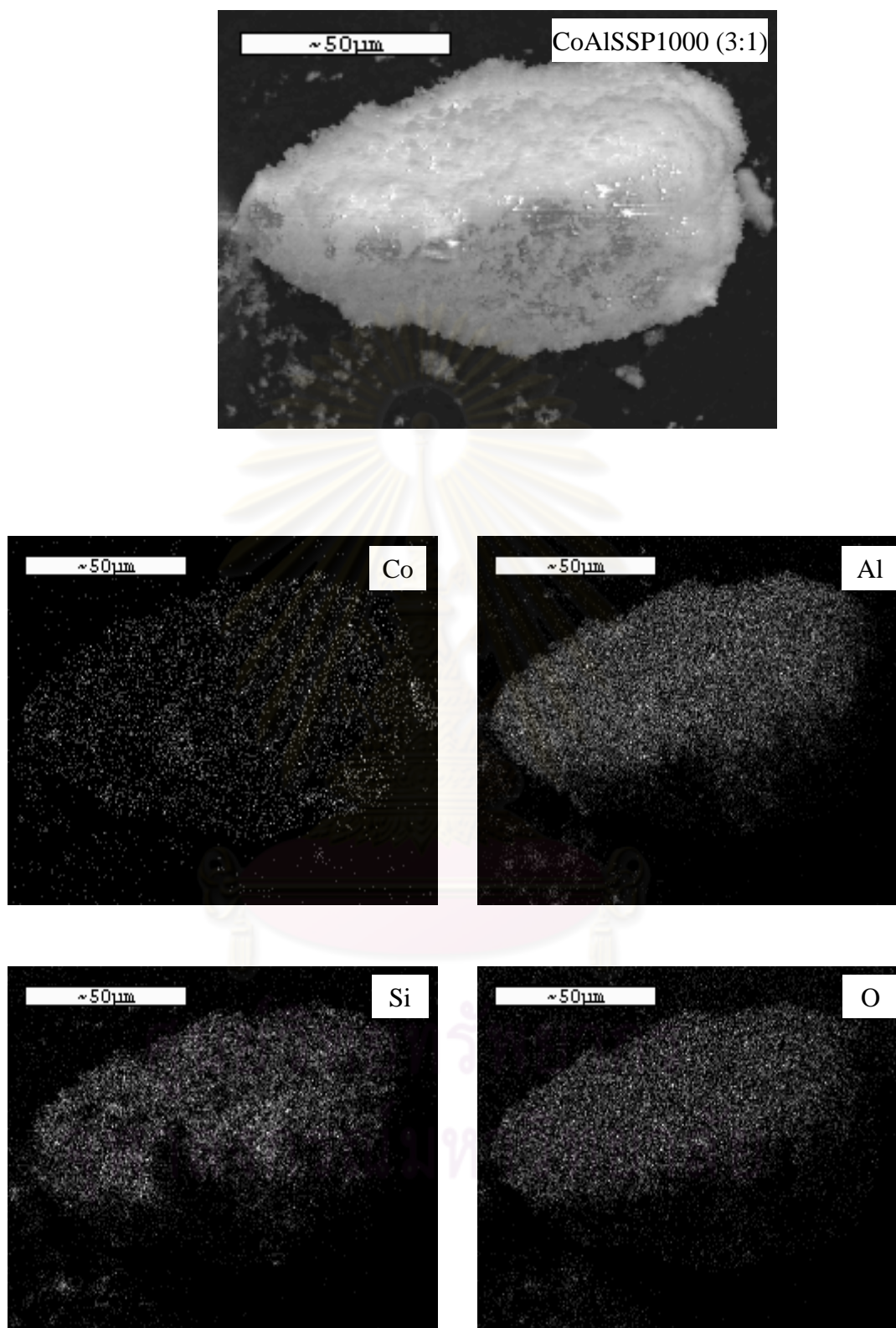
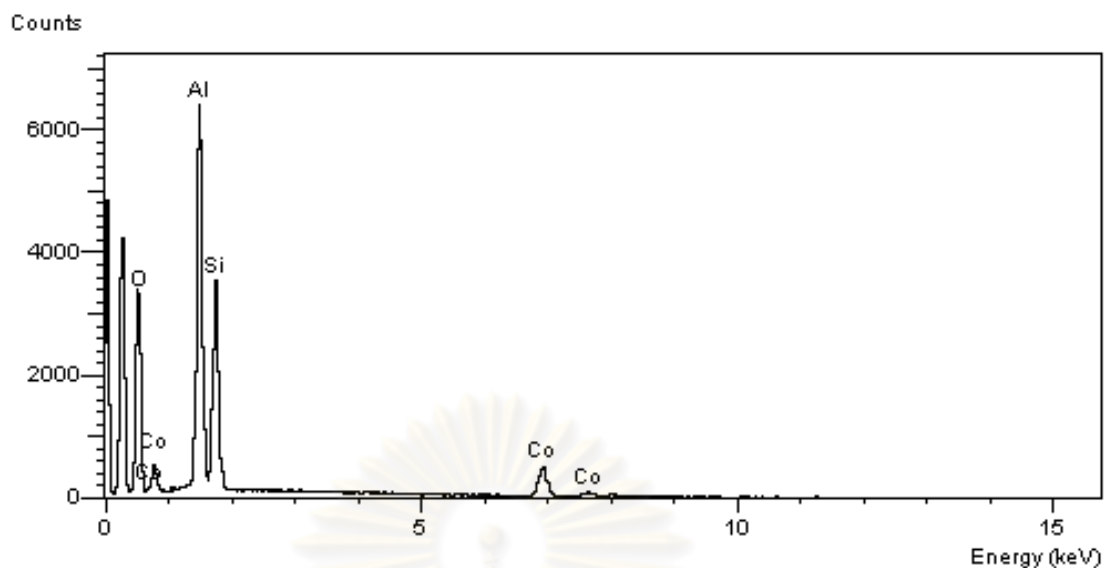


**Figure 5.15** SEM micrograph and EDX mapping of CoAlSSP1000 (3:1) catalyst.

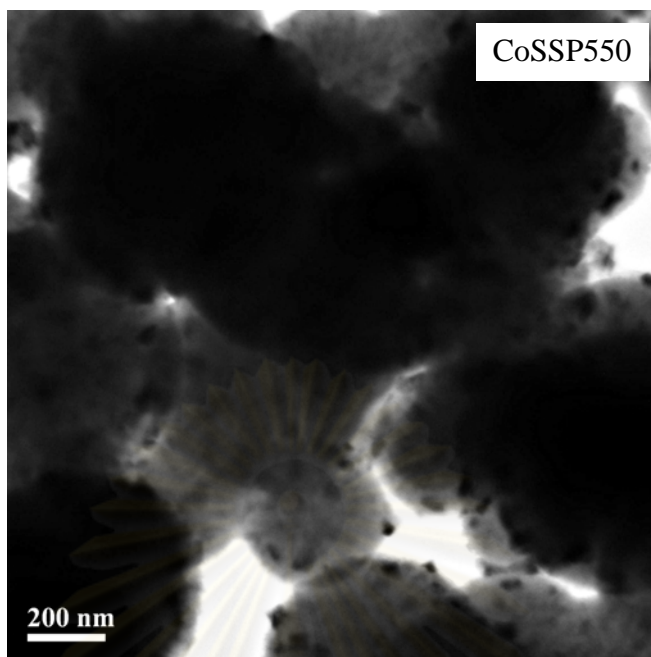


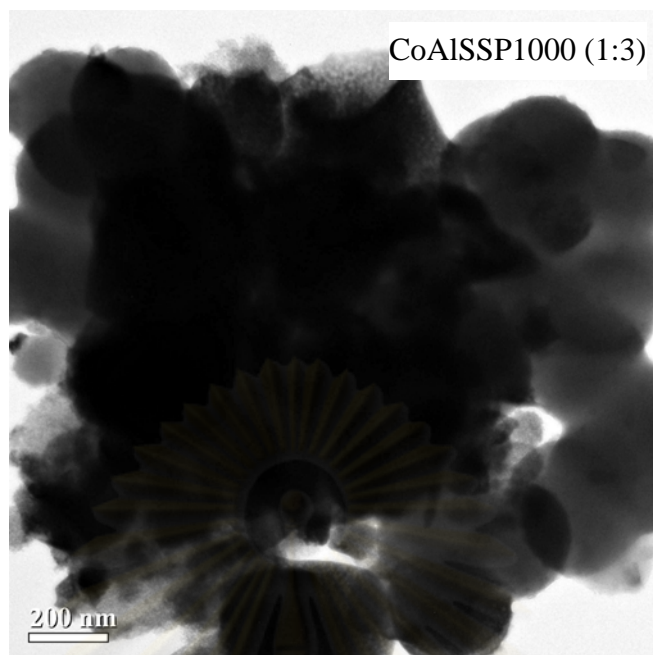
Element	Element (%)	Atomic (%)
Si	16.62	12.43
Al	24.61	19.16
Co	9.16	12.43
O	49.61	65.14

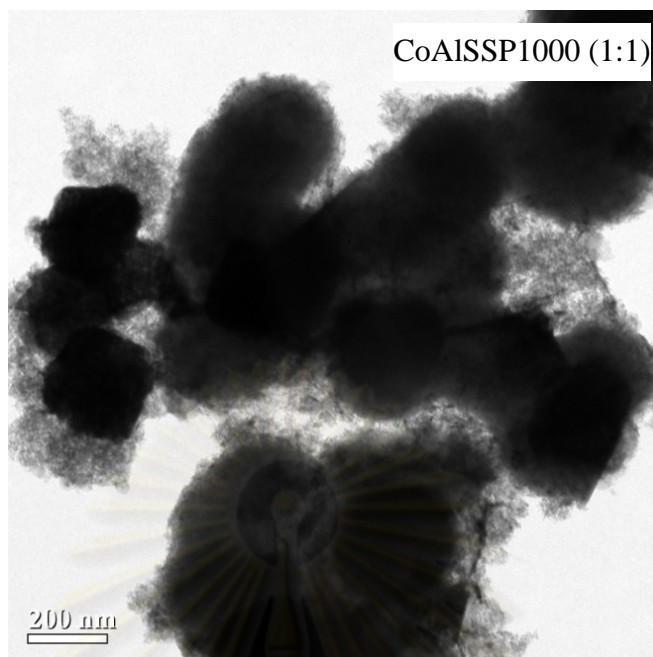
**Figure 5.16** A typical spectrum of the CoAlSSP650 (3:1) catalyst from EDX analysis.

#### 5.2.4 Transmission electron microscope (TEM)

In order to determine the dispersion and crystallite size of cobalt oxides species dispersed on the spherical silica support and alumina-silica composites supports, TEM of samples are shown in Figure 5.17. Apparently, the cobalt oxide species on the spherical silica and alumina-silica composites supports were well dispersed.







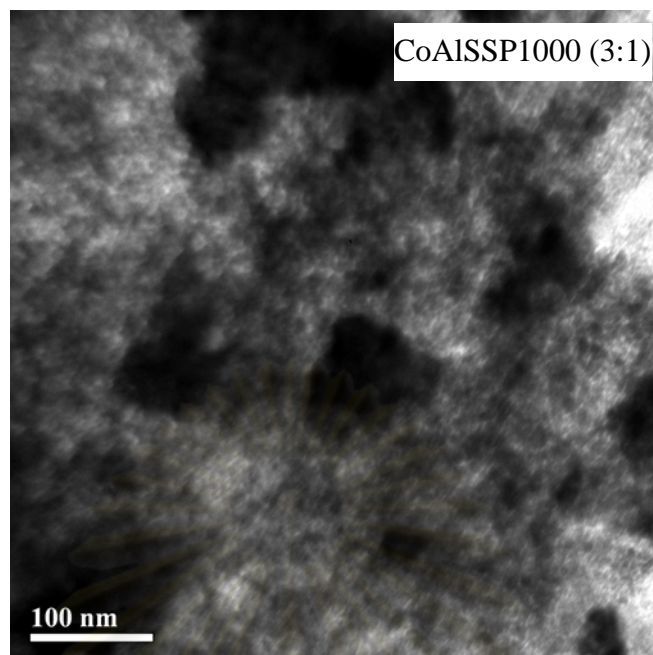


**Figure 5.17** TEM micrograph for the silica and alumina-silica composites supported cobalt catalysts.

### 5.2.5 Temperature Programmed Reduction (TPR)

As mentioned, TPR was performed in order to determine the reduction behaviors of cobalt oxides species on various supports. The TPR profiles for cobalt supported on spherical silica and alumina-silica composites supports were shown in Figure 5.18. Based on these profiles, the reducibilities for each catalyst are also given in Table 5.4. Reduction was observed for all catalysts, which can be assigned to the overlap of two peak reduction. The first peak has been ascribed the reduction of  $\text{Co}_3\text{O}_4$  to  $\text{CoO}$ , followed by the second peak which corresponds to the reduction of  $\text{CoO}$  to  $\text{Co}^0$  [Saib et al., 2002]. Besides reduction behaviors obtained from TPR results, reducibility of the catalysts can be measured based on the peak area below TPR curve. From the silica supported cobalt catalyst result, the TPR peak located at 200 to 800°C. However, this reduction peak was slightly shifted to higher temperatures with increasing the amount of alumina present in the composite supports. In addition, increased amounts of alumina caused in the decreased

reducibility due to strong support interaction between cobalt oxide species and the support [Marie et al., 2009; Sun et al., 2010].

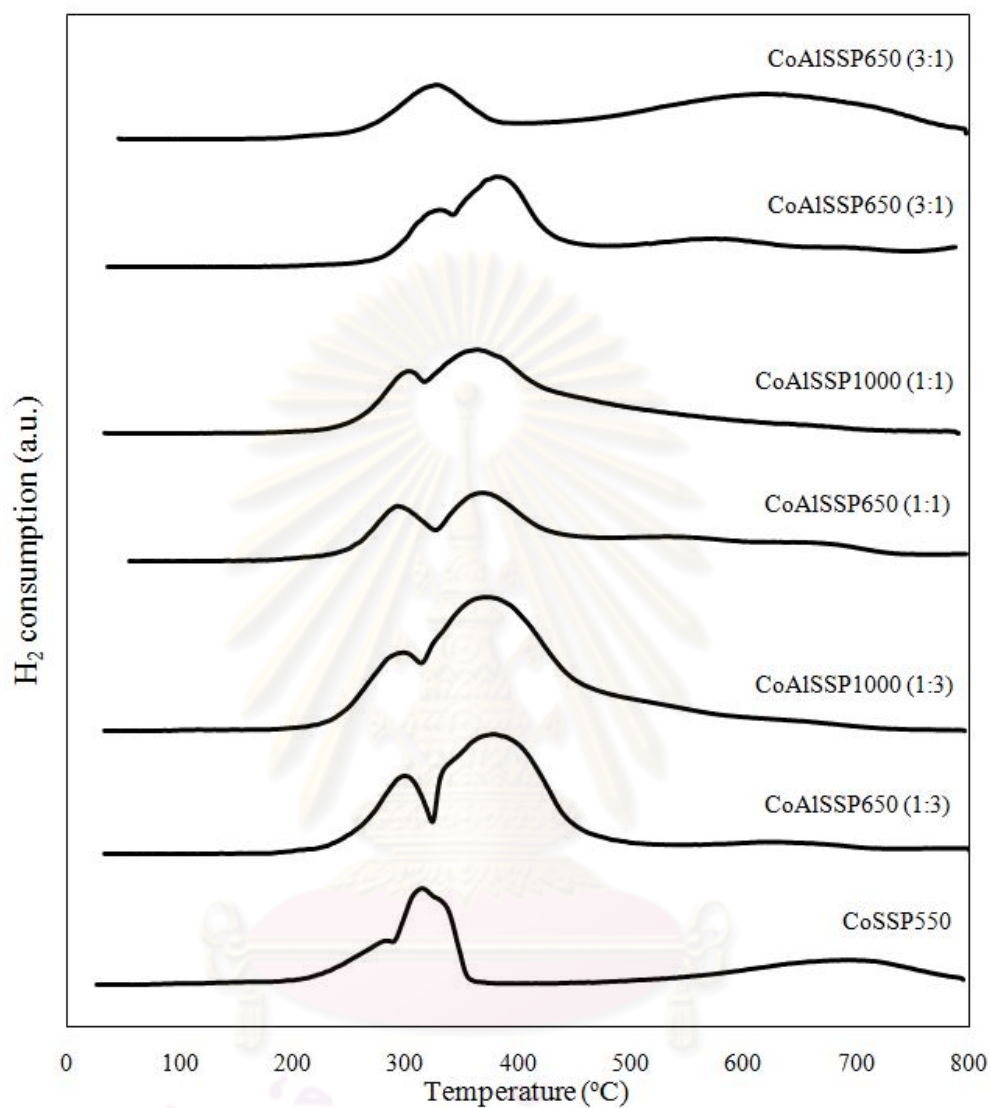


**Figure 5.18** TPR patterns of the silica and alumina-silica composites supported cobalt catalysts.

**Table 5.4** H<sub>2</sub> consumption from TRP profiles of silica and alumina-silica composites-supported cobalt catalysts.

<b>Samples</b>	<b>Total H<sub>2</sub> consumption (<math>\mu\text{mol H}_2/\text{g.cat}</math>)</b>	<b>Reducibility (%)</b>
CoSSP550	1538	33.98
CoAlSSP650 (1:3)	1948	43.04
CoAlSSP1000 (1:3)	2124	46.95
CoAlSSP650 (1:1)	1324	29.25
CoAlSSP1000 (1:1)	953	21.07
CoAlSSP650 (3:1)	1523	33.66
CoAlSSP1000 (3:1)	1308	28.90

### 5.2.6 CO-chemisorptions

Active site of catalysts can be determined by calculation from amount of carbon monoxide adsorption on catalysts. The calculation of active site for all catalysts is shown in Appendix B. Absorbed amount of carbon monoxide is directly proportional to the active site. The higher absorbed amount of carbon monoxide means the higher active site. The characterization results of CO chemisorptions for the catalyst samples are illustrated in Table 5.5.



**Table 5.5** Amount of carbon monoxide adsorbed on silica and alumina-silica composites-supported cobalt catalysts.

Sample	Active site molecule <sup>10<sup>18</sup></sup> per g.cat	Total CO chemisorption $\mu\text{mol CO /g. cat}$	% Dispersion of Cobalt
CoSSP550	12.8	21.27	0.63
CoAlSSP650 (1:3)	12.71	21.11	0.62
CoAlSSP1000(1:3)	11.24	18.66	0.55
CoAlSSP650 (1:1)	8.45	14.04	0.41
CoAlSSP1000 (1:1)	7.33	12.17	0.36
CoAlSSP650 (3:1)	6.14	10.2	0.30
CoAlSSP1000 (3:1)	9.7	16.11	0.47

From the result, the amounts of CO adsorbed were  $12.8 (\times 10^{18} \text{ mol g cat}^{-1})$  for spherical silica supported catalyst and in the range of  $6.14$  to  $12.71 (\times 10^{18} \text{ mol g cat}^{-1})$  for alumina-silica composited supported catalysts. It revealed that the number of reduced cobalt metal surface atoms slightly decreased with increasing the amount of alumina present in the composites supports. Since only Co metal has significant activity for CO hydrogenation, these results were consistent with CO chemisorption results.

ศูนย์วิจัยทรัพยากร  
จุฬาลงกรณ์มหาวิทยาลัย

### 5.2.7 Catalytic activity for CO<sub>2</sub>-hydrogenation over spherical silica and alumina-silica composites supported cobalt catalyst.

In order to determine the catalytic behaviors of the cobalt supported on spherical silica and alumina-silica composites supports, CO<sub>2</sub> hydrogenation (H<sub>2</sub>/CO<sub>2</sub> = 10.36/1) under methanation condition was performed to determine the overall activity and product selectivity of the samples. Before reaction, the catalysts were reduced in-situ in H<sub>2</sub> flow 50 ml/min at 350°C for 3 h in order to obtain metallic phase cobalt. Hydrogenation of CO<sub>2</sub> was carried out at 220°C. A flow rate of H<sub>2</sub>/CO<sub>2</sub>/Ar = 19.3344/1.8656/8.8 cm<sup>3</sup>/min in a fixed-bed flow reactor was used. The resulted reaction test is shown in Table 5.6 and Figure 5.19.

**Table 5.6** Activity and product selectivity of spherical silica and alumina-silica composites supported cobalt catalysts.

Samples	CO <sub>2</sub> Conversion <sup>a</sup> (%)		Selectivity <sup>c</sup> (%)		Rate <sup>c</sup> (x10 <sup>2</sup> gCH <sub>4</sub> / gcat. h)
	Initial <sup>b</sup>	SS <sup>c</sup>	CH <sub>4</sub>	CO	SS <sup>c</sup>
CoSSP550	18.84	19.97	91.77	8.23	10.85
CoAlSSP650 (1:3)	33.97	19.98	91.26	8.74	10.09
CoAlSSP1000 (1:3)	35.85	26.12	94.02	5.96	14.21
CoAlSSP650 (1:1)	29.93	24.26	93.30	6.69	14.35
CoAlSSP1000 (1:1)	16.99	11.78	85.20	14.80	6.30
CoAlSSP650(3:1)	29.94	21.16	91.73	8.27	11.15
CoAlSSP1000 (3:1)	17.38	18.08	90.83	9.17	10.85

<sup>a</sup> CO<sub>2</sub> hydrogenation was carried out at 220°C, 1 atm, H<sub>2</sub>/CO<sub>2</sub>/Ar = 19.3344/1.8656/8.8, and F/W = 18L/ gcat. h.

<sup>b</sup> After 5 min of reaction.

<sup>c</sup> After 4 h of reaction.

Table 5.6 shows the results from hydrogenation of CO<sub>2</sub> that was performed at 220 °C. It indicated that the steady state CO<sub>2</sub> conversions were ranged between 11.78 to 26.12% with corresponding to the reaction rate at 6.30 to 14.35 (x10<sup>2</sup> g CH<sub>2</sub>/g cat.h) of cobalt supported on spherical silica and alumina-silica composites supported catalysts. It was found that at the reaction conditions used, the use of CoAlSSP1000 (1:3) exhibited a much higher CO<sub>2</sub> hydrogenation conversion and CH<sub>4</sub> selectivity than all other catalysts in this study. On the other hand, for used of CoAlSSP1000 (1:1) resulted in lowest activity and selectivity. It was found that the alumina significantly enhanced the activity and selectivity to methane of CO<sub>2</sub> hydrogenation, indicating the balance among dispersion of alumina, reduction degree of silica and BET surface area in term of pore size can be facilitate [Sun et al., 2010]. The rate vs. time on stream of cobalt supported on spherical silica and alumina-silica composites supported catalysts with reaction temperature at 220°C is illustrated in Figure 5.19.

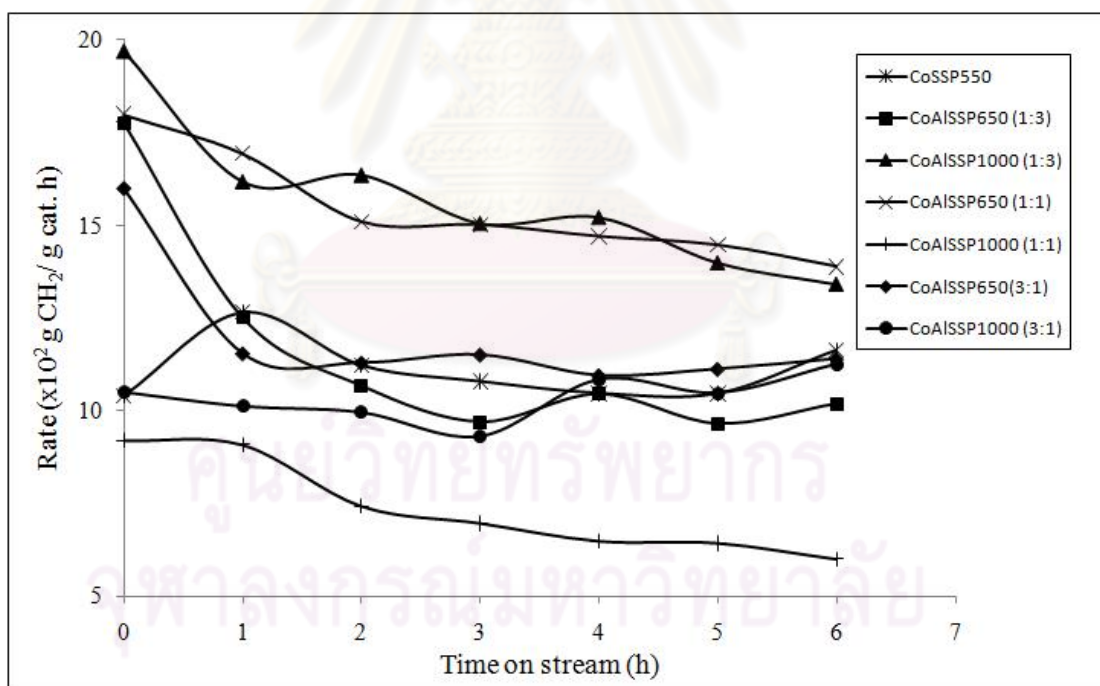


**Figure 5.19** Reaction rate at 220°C vs. time on stream of silica and alumina-silica composites supported cobalt catalysts.

## CHAPTER VI

### CONCLUSIONS AND RECOMMENDATIONS

This chapter was focused on the conclusion of the experimental results of spherical silica and alumina-silica composites supports on characteristics and catalytic properties of supported cobalt for CO<sub>2</sub> hydrogenation reaction which were described in section 6.1. Additionally, recommendations for further study are given in section 6.2.

#### 6.1 Conclusions

1. The DTA/TG and XRD patterns indicated that thermal stability of  $\gamma$ -alumina can be enhanced when adding on the spherical silica. At various compositions of alumina-silica, increased amount of alumina exhibited a larger crystalline size of  $\gamma$ -alumina.
2. The alumina distribution on the Al<sub>2</sub>O<sub>3</sub>-SiO<sub>2</sub> composite supports prepared by deposition of Al<sub>2</sub>O<sub>3</sub> particles on the spherical silica particle (SSP) using hydrolysis of aluminium isopropoxide, was uniform.
3. At high calcination temperature, increased amount of alumina obstructed the sintering effect.
4. The presence of alumina in Al<sub>2</sub>O<sub>3</sub>-SiO<sub>2</sub> composite supports caused in the decreased reducibilities of cobalt catalysts.
5. The amount of reduced cobalt metal surface atoms slightly decreased with increasing the amount of alumina present in the composite supports.
6. The alumina significantly enhanced the conversion and selectivity to methane of CO<sub>2</sub> hydrogenation, indicating the balance among dispersion

of alumina, reducibilities of silica, and pore diameter of alumina-silica composite supported cobalt catalysts.

## 6.2 Recommendations

1. The CO<sub>2</sub> hydrogenation performed at higher temperature should be further studied.
2. Besides Co, other metals such as Ni, Fe, Cu and etc should be further investigated with Al<sub>2</sub>O<sub>3</sub>-SiO<sub>2</sub> composites on the supports.
3. The Balance among dispersion, reducibilities, and pore diameter of composite supported metal catalysts should be further investigated.



## REFERENCES

- Adesina, A.A. Hydrocarbon synthesis via Fischer-Tropsch reaction: travails and triumphs. Appl. Catal. A: General 138 (1996): 345-367.
- Arakawa, H. Dubois, J.L., and Sayama, K. Selective conversion of CO<sub>2</sub> to methanol by catalytic hydrogenation over promoted copper catalyst. Energy Convers 33 (1992): 521-528.
- Baca, et al. Characterization of mesoporous alumina prepared by surface alumination of SBA-15. Microporous and Mesoporous Mat. 110 (2008): 232-241.
- Backman, L.B., Rautiainen, A., Krause, A.O.I., and Lindblad, M. A novel Co/SiO<sub>2</sub> catalyst for hydrogenation. Catal. Today 43 (1998): 11-19.
- Choi, J.G. Reduction of support cobalt catalysts by hydrogen. Catal Lett. 35 (1995): 291-296.
- Chu, W., et al. Cobalt species in promoted cobalt alumina-supported Fischer-Tropsch catalysts. J. Catal. 252 (2007): 215-230.
- Dagle, R.A., et al. Selective CO methanation catalysts for fuel processing applications. Appl. Catal. A: General 326 (2007): 213-218.
- Daniell, W., et al. Enhanced surface acidity in mixed alumina-silicas: a low-temperature FTIR study. Appl. Catal. A: General 196 (2000): 247-260.
- Dry, M.E. Practical and theoretical aspects of the catalytic Fischer-Tropsch process. Appl. Catal. A 138 (1996): 319-334.
- Evans, K.A.; 1993. Properties and uses of oxides and hydroxides. Downs, A. J.; Chemistry of aluminium gallium indium and thallium 248. 1st ed. :Blackie Academic and Professional.
- Frohlich, G., et al. Activation and deactivation of cobalt catalysts in the hydrogenation of carbon dioxide. Appl. Catal. A: General 134 (1996): 1-19.
- Grzechowiak, J.R., Szyszka, I., and Masalska, A. Effect of TiO<sub>2</sub> content and method of titania-silica preparation on the nature of oxidic nickel phases and their activity in aromatic hydrogenation. Catal. Today 137 (2008): 433-438.
- Gu, F.N., Zhou, Y., Wei, F., Wang, Y., and Zhu, J.H. Creating the adsorptive sites with high performance toward nitrosamines in mesoporous silica MCM-41 by alumina modifier. Microporous and Mesoporous Mat. 126 (2009): 143-151.
- Iglesia, E. Design, synthesis, and use of cobalt-based Fischer-Tropsch synthesis catalysts. Appl. Catal. A: General 161 (1997): 59-78.

- Jacobs, G., et al. Fischer-Tropsch synthesis: support, loading, and promoter effects on the reducibility of cobalt catalysts. Appl. Catal. A 233 (2002): 263-281.
- Jongsomjit, B., Wongsalee, T., and Praserttham, P. Catalytic behaviors of mixed TiO<sub>2</sub>-SiO<sub>2</sub> supported cobalt Fischer-Tropsch catalysts for carbon monoxide hydrogenation. J. of Mat. Chem. and Phys. 97 (2006): 343-350.
- Khodakov, A.Y., et al. Reducibility of Cobalt Species in Silica-Supported Fischer-Tropsch Catalysts. J. Catal. 168 (1997): 16-25.
- Khodakov, A.Y. Fischer-Tropsch synthesis: Relations between structure of cobalt catalysts and their catalytic performance. Catal. Today 144 (2009): 251–257.
- Kogelbauer, A., Weber, J.C., and Goodwin, J.G., Jr. The formation of cobalt silicates on Co/SiO<sub>2</sub> under hydrothermal condition. Catal Lett. 34 (1995): 259-267.
- Kusuma, H., Okabe, K., and Arakawa, H. Characterization of Rh-Co/SiO<sub>2</sub> catalysts for CO<sub>2</sub> hydrogenation with TEM, XPS and FT-IR. Appl. Catal. A: General 207 (2001): 85-94.
- Lahtinen, J., Anraku, T., and Somorjai, G.A. CO and CO hydrogenation on cobalt foil model catalysts: evidence for the need of CoO reduction. Catal. Lett. 25 (1994): 241-255.
- Lebedev, O.I., Tendeloo, G.V., Collart, O., Cool, P., and Vansant, E.F. Structure and microstructure of nanoscale mesoporous silica spheres. Solid State Sci. 6 (2004): 489–498.
- Liu, H., Ning, G., Gan, Z., and Lin, Y. A simple procedure to prepare spherical  $\alpha$ -alumina powders. Mat. Research Bulletin 44 (2009): 785-788.
- Liu, S., et al. The Influence of the Alcohol Concentration on the Structural Ordering of Mesoporous Silica: Cosurfactant versus Cosolvent. J. Phys. Chem. B 107 (2003): 10405-10411.
- Marie, A.J., Constant, A.G., Khodakov, A.Y., and Diehl, F. Cobalt supported on alumina and silica-doped alumina: Catalyst structure and catalytic performance in Fischer-Tropsch synthesis. C. R. Chimie 12 (2009): 660-667.
- Martínez, A., López, C., Márquez, F., and Díaz, I. Fischer-Tropsch synthesis of hydrocarbons over mesoporous Co/SBA-15 catalysts: the influence of metal loading, cobalt precursor, and promoters. J. Catal. 220 (2003): 486-499.
- Okabe, K., Li, X., Wei, M., and Arakawa, H. Fischer-Tropsch synthesis over Co-SiO<sub>2</sub> catalysts prepared by the sol-gel method. Catal. Today 89 (2004): 431–438.

- Panagiotopoulou, P., Kondarides, D.I., and Verykios, X.E. Selective methanation of CO over supported noble metal catalysts: Effects of the nature of the metallic phase on catalytic performance. Appl. Catal. A: General 344 (2008): 45-54.
- Riedel, T., et al. Comparative study of Fischer-Tropsch synthesis with H<sub>2</sub>/CO and H<sub>2</sub>/CO<sub>2</sub> syngas using Fe- and Co-based catalysts. Appl. Catal. A: General 186 (1999): 201-213.
- Saib, A.M., claeys, M., and Steen, E.V. Silica supported cobalt Fischer-Tropsch catalysts: effect of pore diameter of support. Catal. Today 71 (2002): 395-402.
- Somorjai, G.A. Introduction to Surface Chemistry and Catalysis, New York, Wiley, 1994.
- Son, D., and Li, J. Effect of catalyst pore size on the catalytic performance of silica supported cobalt Fischer-Tropsch catalysts. J. of Molecule Catal A: Chem. 247 (2006) 206-212.
- Storsæter, S., Borg, Ø., Blekkan, E.A., and Holmen, A. Study of the effect of water on Fischer-Tropsch synthesis over supported cobalt catalysts. J. Catal. 231 (2005): 405-419.
- Suzuki, T., Mayama, Y., Hirai, T., and Hayashi, S. Preliminary attempt to enhance the hydrogenation of carbon dioxide to methane on cobalt oxide catalyst by adding CuO-ZnO-Cr<sub>2</sub>O<sub>3</sub>. Int. J. Hydrogen Energy 18 (1993): 979-983.
- Sun, X., Zhang, X., Zhang, Y., and Tsubaki, N. Reversible promotional effect of SiO<sub>2</sub> modification to Co/Al<sub>2</sub>O<sub>3</sub> catalyst for Fischer-Tropsch synthesis. Appl. Catal. A: General 377 (2010): 134-139.
- Wittayakhun, J.; Krisdanurak, N.; 2004. Catalysis: Fundamentals and Applications, 1<sup>st</sup> ed., Thammasart university publishing.
- Xiong, H., Zhang, Y., Wang, S., and Li, J. Fischer-Tropsch synthesis: the effect of Al<sub>2</sub>O<sub>3</sub> porosity on the performance of Co/Al<sub>2</sub>O<sub>3</sub> catalyst. Catal. Comm. 6 (2005) 512-516.
- Zhang, Y., Jacobs, G., Sparks, D.E., Dry, M.E., and Davis, B.H. CO and CO<sub>2</sub> hydrogenation study on supported cobalt Fischer-Tropsch synthesis catalysts. Catal. Today 71 (2002): 411-418.
- Zhang, Y., Nagamori, S., Hinchiranan S., Vitidsant T., and Tsubaki, N. Promotional Effects of Al<sub>2</sub>O<sub>3</sub> Addition to Co/SiO<sub>2</sub> Catalysts for Fischer-Tropsch Synthesis. Energy & Fuels an American Chem. Society J. 20 (2006) 417-421.





**APPENDICES**

ศูนย์วิทยทรัพยากร  
จุฬาลงกรณ์มหาวิทยาลัย

## APPENDIX A

### CALCULATION FOR CATALYST PREPARATION

#### Calculation of Al<sub>2</sub>O<sub>3</sub>- SiO<sub>2</sub> composites supports

Preparation of alumina-silica composites support with 25% ratios of Alumina (Al<sub>2</sub>O<sub>3</sub>) by sol gel method was shown as follows:

Reagent: - Aluminium isopropoxide 98% (Al(OPr<sup>i</sup>)<sub>3</sub>)  
 Molecular weight = 204.25 g/mol  
 Alumina (Al<sub>2</sub>O<sub>3</sub>), formula weight = 101.9614 g/mol  
 - Support : SiO<sub>2</sub>

- For 25%wt of Alumina (Al<sub>2</sub>O<sub>3</sub>) was shown as follow:

Based on 75 g of silica (SiO<sub>2</sub>) used, the composition of the catalyst would be as follows:

$$\begin{array}{rcl} \text{Al}_2\text{O}_3 & = & 25 \text{ g} \\ 101.9614 \text{ g of Al}_2\text{O}_3 \text{ required} & \frac{204.25}{101.9614} & \text{g of Al(OPr}^i\text{)}_3 \\ 25 \text{ g of Al}_2\text{O}_3 \text{ required} & = 25 \times \frac{204.25}{101.9614} & \text{g of Al(OPr}^i\text{)}_3 \\ & = & 50.08 \text{ g of Al(OPr}^i\text{)}_3 \end{array}$$

$$\begin{array}{rcl} \text{Al(OPr}^i\text{)}_3 \text{ 98 g provide 98\% Aluminium isopropoxide solution} & & 100 \text{ g} \\ \text{Al(OPr}^i\text{)}_3 \text{ 50.08 g provide 98\% Aluminium isopropoxide solution} & \frac{50.08}{0.98} & \\ & & = 51.10 \text{ g} \end{array}$$

### Calculation of cobalt loading

Preparation of 20% wtCo/SiO<sub>2</sub> by the incipient wetness impregnation method was shown as follow:

Reagent:     - Cobalt (II) nitrate hexahydrate (Co(NO<sub>3</sub>)<sub>2</sub>·6H<sub>2</sub>O)  
                   Molecular weight   = 291.03 g/mol  
                   Cobalt (Co), Atomic weight = 58.933 g/mol  
 - Support:     - spherical silica support

Based on 1.00 g of catalyst used, the composition of the catalyst would be as follows:

$$\begin{aligned} \text{Cobalt} &= 0.20 \text{ g} \\ \text{SiO}_2 &= 1.00 - 0.20 = 0.80 \text{ g} \end{aligned}$$

Cobalt 0.20 g was prepared from Cobalt (II) nitrate hexahydrate

$$\begin{aligned} \text{Cobalt (II) nitrate hexahydrate required} &= \frac{0.20}{58.933} \times 291.03 \\ &= 0.9877 \text{ g} \end{aligned}$$

ศูนย์วิทยทรัพยากร  
 จุฬาลงกรณ์มหาวิทยาลัย

## APPENDIX B

### CALCULATION FOR TOTAL CO CHEMISORPTION AND DISPERSION

Calculation of the total CO chemisorption and metal dispersion of the catalyst, a stoichiometry of CO/Co = 1, was assumed. The calculation procedure was as follows:

Let the weight of catalyst used	=	W	g
Integral area of CO peak after adsorption	=	A	unit
Integral area of 100 $\mu$ l of standard H <sub>2</sub> peak	=	B	unit
Amounts of CO adsorbed on catalyst	=	B-A	unit
Concentration of Co	=	C	% wt
Volume of H <sub>2</sub> adsorbed on catalyst	=	100 $\times$ [(B-A)/B]	$\mu$ l
Volume of 1 mole of CO at 30 $^{\circ}$ C	=	24.86 $\times 10^6$	$\mu$ l
Mole of CO adsorbed on catalyst	=	[(B-A)/B] $\times$ [100/24.86]	$\mu$ mole
Total CO chemisorption	=		
		[(B-A)/B] $\times$ [100/29.93] $\times$ [1/W]	$\mu$ mole /g <sub>catalyst</sub>
	=	N	$\mu$ mole /g <sub>catalyst</sub>

$$\%Co\ dispersion = \frac{\text{The amount of cobalt equivalent to CO adsorption after reduction} \times 100}{\text{Total amount of cobalt active sites expected to exist after reduction}}$$

$$\text{Molecular weight of cobalt} = 58.93$$

$$\begin{aligned} \text{Metal dispersion (\%)} &= \frac{1 \times CO_{tot} \times 100}{\text{No. } \mu\text{mole } Co_{tot}} \\ &= \frac{1 \times N \times 100}{\text{No. } \mu\text{mole } Co_{tot}} \\ &= \frac{1 \times N \times 58.93 \times 100 \times 100}{[C \times 10^6]} \\ &= \frac{0.59 \times N}{C} \end{aligned}$$

## APPENDIX C

### CALCULATION FOR REDUCIBILITY

For supported cobalt catalyst, it can be assumed that the major species of calcined Co catalysts was  $\text{Co}_3\text{O}_4$ .  $\text{H}_2$  consumption to reduce  $\text{Co}_3\text{O}_4$  was calculated as follows:

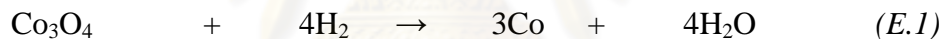
$$\text{Molecular weight of Co} = 58.93$$

$$\text{Molecular weight of } \text{Co}_3\text{O}_4 = 240.79$$

#### *Calculation of the calibration of $\text{H}_2$ consumption using cobalt oxide ( $\text{Co}_3\text{O}_4$ )*

$$\begin{aligned} \text{Let the weight of } \text{Co}_3\text{O}_4 \text{ used} &= 0.1 \text{ g} \\ &= 4.153 \times 10^{-4} \text{ mole} \end{aligned}$$

From equation of  $\text{Co}_3\text{O}_4$  reduction;



$$\begin{aligned} \text{Mole of hydrogen consumption} &= 4 \text{ Mole of } \text{Co}_3\text{O}_4 \text{ consumption} \\ &= 4 \times 4.153 \times 10^{-4} \\ &= 1.661 \times 10^{-3} \text{ mole} \end{aligned}$$

Integral area of hydrogen used to reduce  $\text{Co}_3\text{O}_4$  0.1 g = 115.63 unit

At 100 % reducibility, the amount of hydrogen consumption is  $1.661 \times 10^{-3}$  mole related to the integral area of  $\text{Co}_3\text{O}_4$  after reduction 115.63 unit.

#### *Calculation of reducibility of supported cobalt catalyst*

$$\% \text{ Reducibility} = \frac{\text{Amount of } \text{H}_2 \text{ uptake to reduce 1 g of catalyst} \times 100}{\text{Amount of theoretical } \text{H}_2 \text{ uptake to reduce } \text{Co}_3\text{O}_4 \text{ to } \text{Co}^0 \text{ for 1 g of catalyst}}$$

$$\begin{aligned}
 \text{Integral area of the calcined catalyst} &= X \quad \text{unit} \\
 \text{The amount of H}_2 \text{ consumption} &= \\
 &= [2 \times 1.661 \times 10^{-3} \times (X) / 115.63] \text{mole} \\
 \text{Let the weight of calcined catalyst used} &= W \quad \text{g} \\
 \text{Concentration of Co} &= Y \quad \% \text{wt} \\
 \text{Mole of Co} &= [(W \times Y / 100) / 58.93] \quad \text{mole} \\
 \text{Mole of Co}_3\text{O}_4 &= [(W \times Y / 100) / (3 \times 58.93)] \quad \text{mole} \\
 \text{Amount of theoretical} &= [(W \times Y / 100) \times 4 / (3 \times 58.93)] \text{mole} \\
 \text{Reducibility (\% ) of supported Co catalyst} &= \\
 &= \frac{[2 \times 1.661 \times 10^{-3} \times (X) / 115.63] \times 100}{[(W \times Y / 100) \times 4 / (3 \times 58.93)]}
 \end{aligned}$$

**Example for 20Co/ Z**

$$\begin{aligned}
 \text{Integral area of the calcined catalyst} &= 6.016 \quad \text{unit} \\
 \text{The amount of H}_2 \text{ consumption} &= [2 \times 1.661 \times 10^{-3} \times (X) / 115.63] \text{mole} \\
 \text{Let the weight of calcined catalyst used} &= 0.1 \quad \text{g} \\
 \text{Concentration of Co} &= 20 \quad \% \text{wt} \\
 \text{Mole of Co} &= [(0.1 \times 20 / 100) / 58.93] \quad \text{mole} \\
 \text{Mole of Co}_3\text{O}_4 &= [(0.1 \times 20 / 100) / (3 \times 58.93)] \quad \text{mole} \\
 \text{Amount of theoretical} &= [(0.1 \times 20 / 100) \times 4 / (3 \times 58.93)] \text{mole} \\
 \text{Reducibility (\% ) of supported Co catalyst} &= \\
 &= \frac{[2 \times 1.661 \times 10^{-3} \times (6.016) / 115.63] \times 100}{[(0.1 \times 20 / 100) \times 4 / (3 \times 58.93)]} = 34.6 \%
 \end{aligned}$$

## APPENDIX D

### CALIBRATION CURVES

This appendix showed the calibration curves for calculation of composition of reactant and products in CO hydrogenation reaction. The reactant is CO and the main product is methane. The other products are linear hydrocarbons of heavier molecular weight that are C<sub>2</sub>-C<sub>4</sub> such as ethane, ethylene, propane, propylene and butane.

The thermal conductivity detector, gas chromatography Shimadzu model 8A was used to analyze the concentration of CO by using Molecular sieve 5A column.

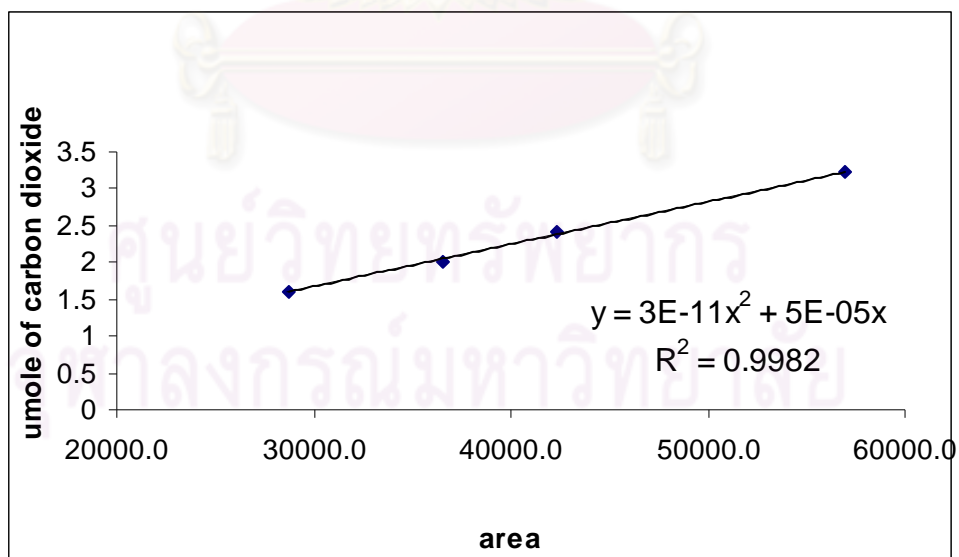
The thermal conductivity detector (TCD), gas chromatography Shimadzu model 8A was used to analyze the concentration of CO<sub>2</sub> by using porapack-Q column.

The VZ10 column are used with a gas chromatography equipped with a flame ionization detector, Shimadzu model 14B, to analyze the concentration of products including of methane, ethane, ethylene, propane, propylene and butane. Conditions uses in both GC are illustrated in Table C.1.

Mole of reagent in y-axis and area reported by gas chromatography in x-axis are exhibited in the curves. The calibration curves of CO, methane, ethane, ethylene, propane, propylene and butane are illustrated in the following figures.

**Table D.1** Conditions use in Shimadzu modal GC-8A and GC-14B.

Parameters	Condition	
	Shimadzu GC-8A	Shimadzu GC-14B
Width	5	5
Slope	50	50
Drift	0	0
Min. area	10	10
T.DBL	0	0
Stop time	50	60
Atten	0	0
Speed	2	2
Method	41	41
Format	1	1
SPL.WT	100	100
IS.WT	1	1

**Figure D.1** The calibration curve of carbon dioxide.



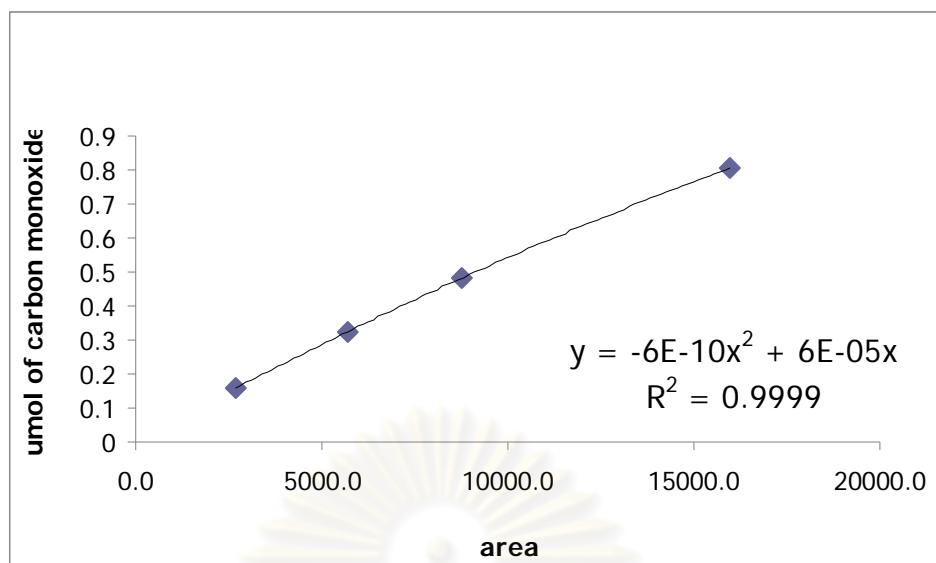


**Figure D.2** The calibration curve of carbon monoxide.

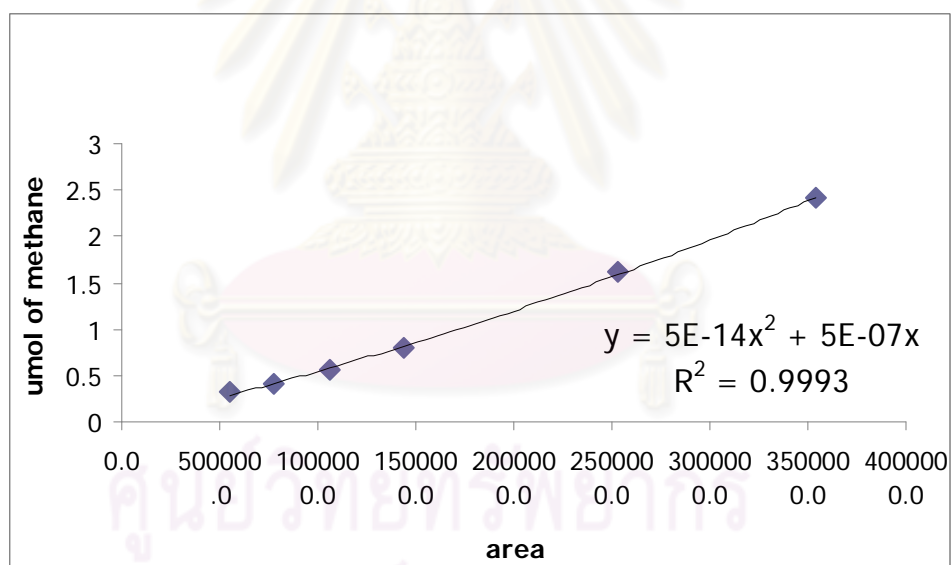


**Figure D.3** The calibration curve of methane.

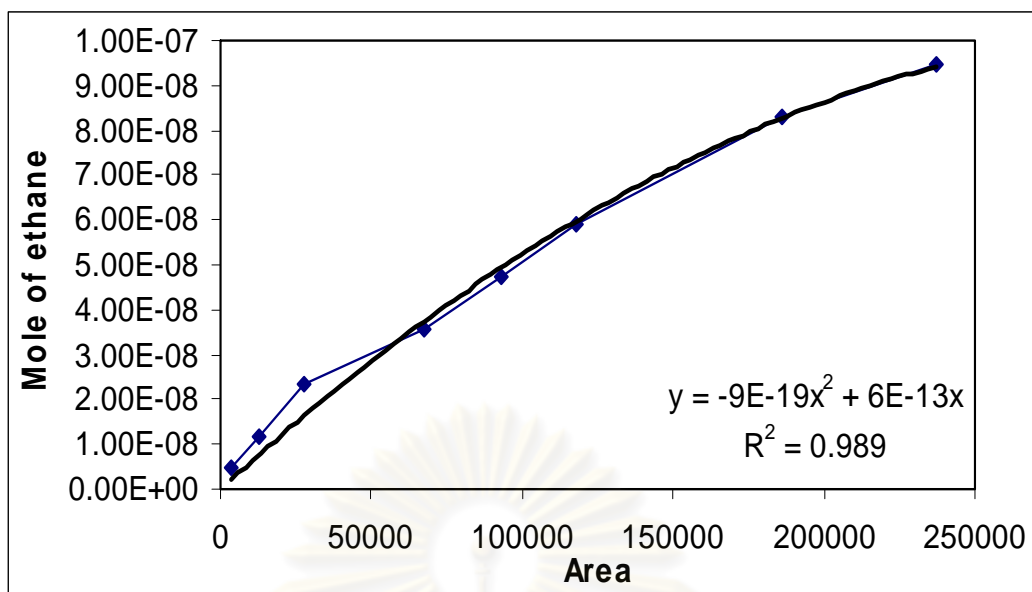


**Figure D.4** The calibration curve of ethane.

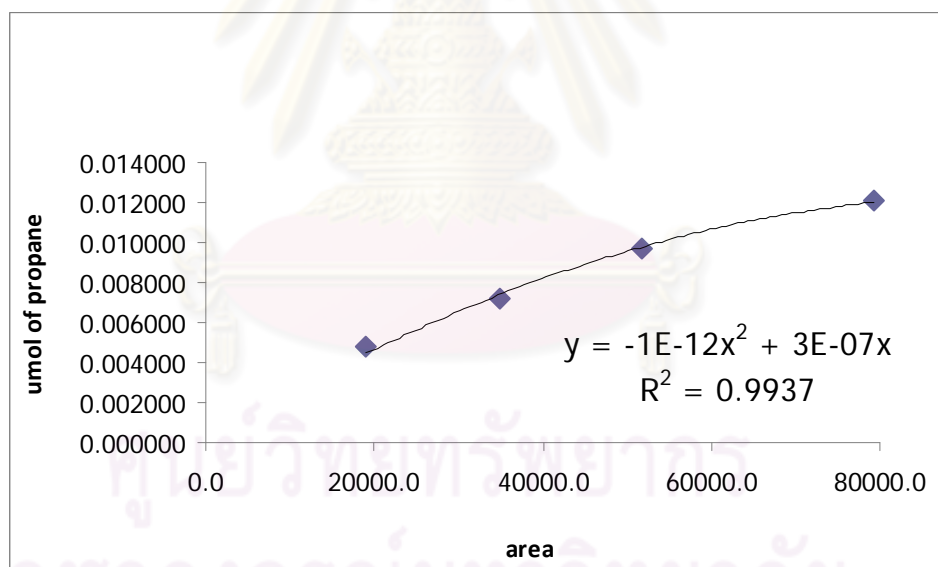


**Figure D.5** The calibration curve of propane.

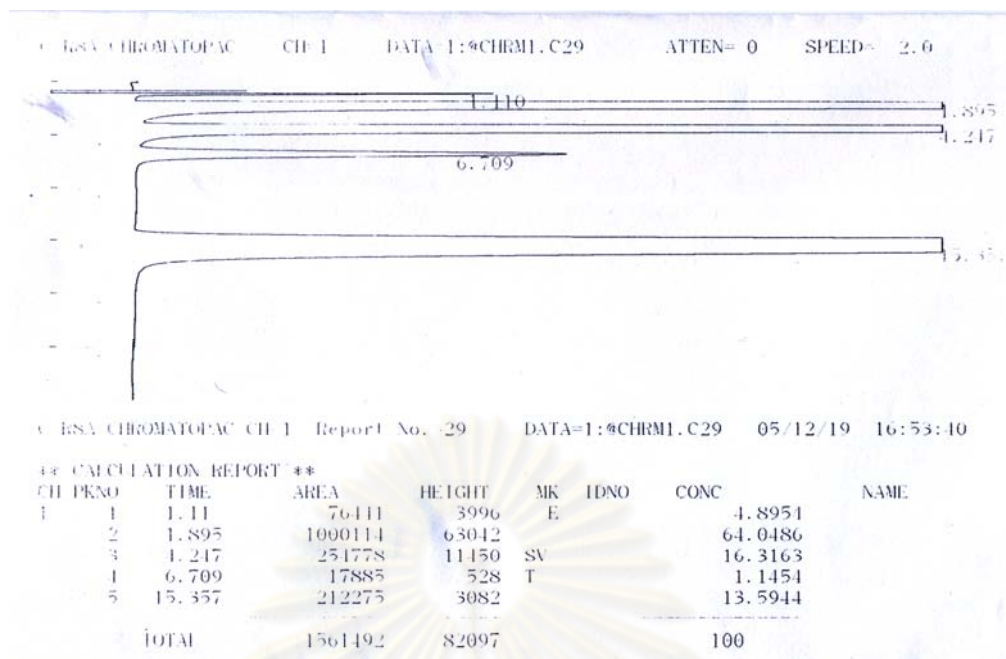


**Figure D.6** The chromatograms of catalyst sample from thermal conductivity detector, gas chromatography Shimadzu model 8A (Molecular sieve 5A column).

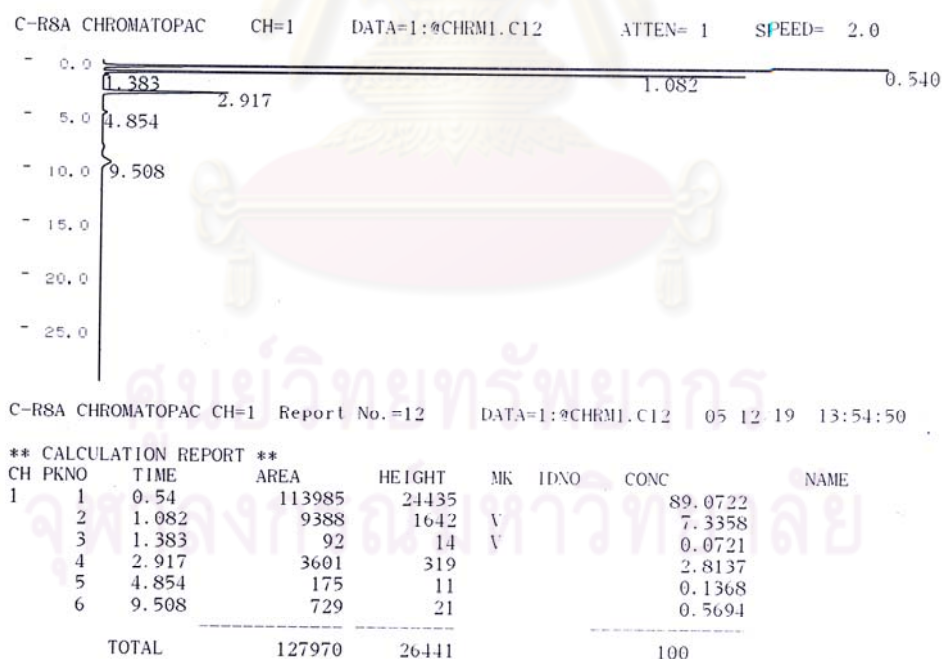


**Figure D.7** The chromatograms of catalyst sample from flame ionization detector, gas chromatography Shimadzu model 14B (VZ10 column).

## APPENDIX E

### CALCULATION OF CO<sub>2</sub> CONVERSION, REACTION RATE AND SELECTIVITY

The catalyst performance for the CO<sub>2</sub> hydrogenation was evaluated in term of activity for CO<sub>2</sub> conversion, reaction rate and selectivity.

CO<sub>2</sub> conversion is defined as moles of CO<sub>2</sub> converted with respect to CO<sub>2</sub> in feed:

$$\text{CO}_2 \text{ conversion (\%)} = \frac{100 \times [\text{mole of CO}_2 \text{ in feed} - \text{mole of CO}_2 \text{ in product}]}{\text{mole of CO}_2 \text{ in feed}} \quad (\text{i})$$

Reaction rate was calculated from CO<sub>2</sub> conversion that is as follows:

Let the weight of catalyst used	=	W	g
Flow rate of CO <sub>2</sub>	=	2	cc/min
Reaction time	=	60	min
Weight of CH <sub>2</sub>	=	14	g
Volume of 1 mole of gas at 1 atm	=	22400	cc
Selectivity to CH <sub>4</sub>	=	S	

$$\text{Reaction rate (g CH}_2\text{/g of catalyst.h)} = \frac{(\% \text{ conversion of CO}_2 / 100) \times 60 \times 14 \times 2}{W \times 22400} \times S \quad (\text{ii})$$

Selectivity of product is defined as mole of product (B) formed with respect to mole of CO<sub>2</sub> converted:

$$\text{Selectivity of B (\%)} = 100 \times [\text{mole of B formed} / \text{mole of total products}] \quad (\text{iii})$$

Where B is product, mole of B can be measured employing the calibration curve of products such as methane, ethane, ethylene, propane, propylene and butane

$$\text{mole of CH}_4 = (\text{area of CH}_4 \text{ peak from integrator plot on GC-14B}) \times 8 \times 10^{12} \quad (\text{iv})$$

## APPENDIX F

### PORE SIZE DISTRIBUTION CURVES

The pore size distribution curves derived from N<sub>2</sub> desorption from spherical silica and alumina-silica composites supports and their catalysts are illustrated in the following figures.

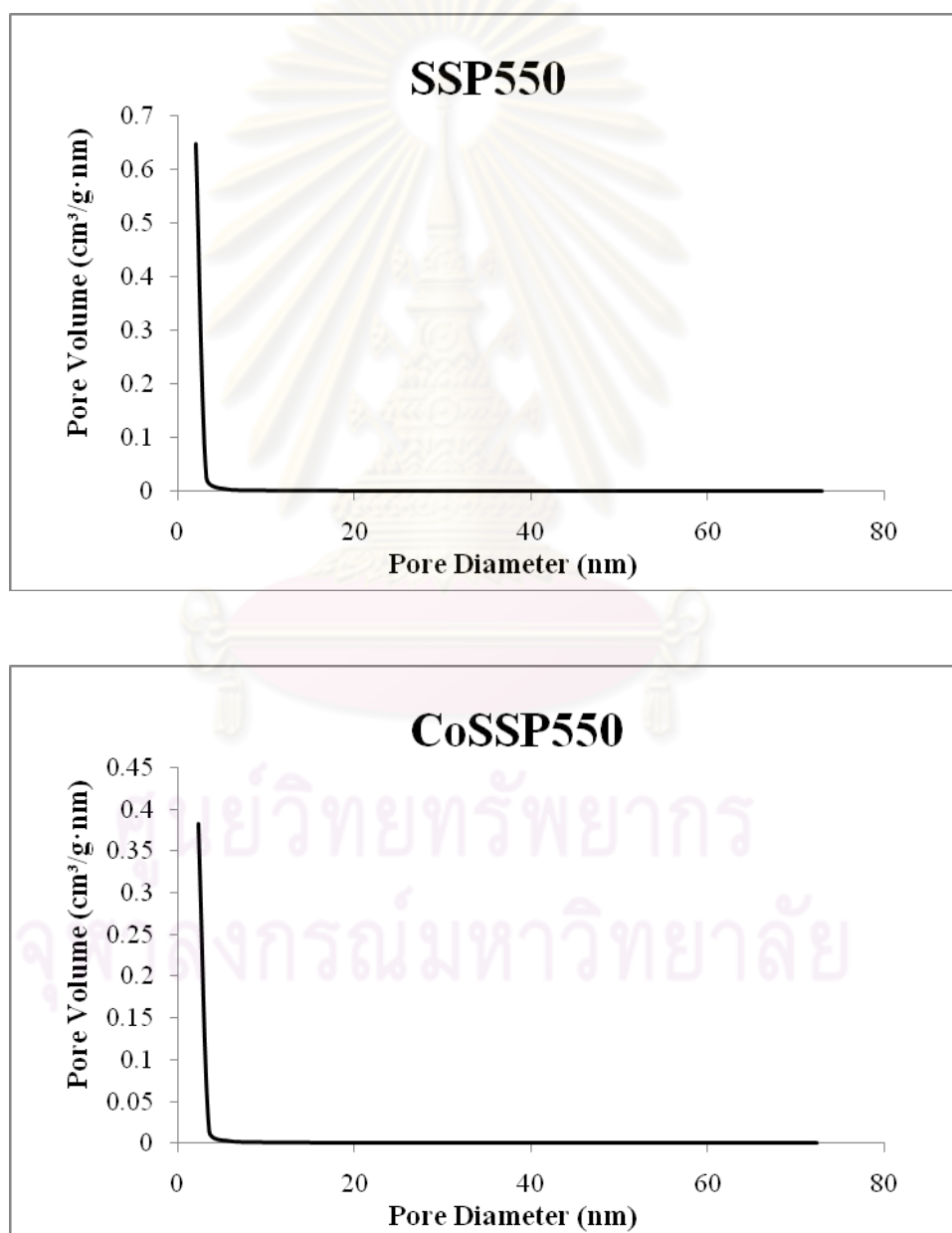


**Figure F.1** The pore size distribution of SSP550 and CoSSP550.

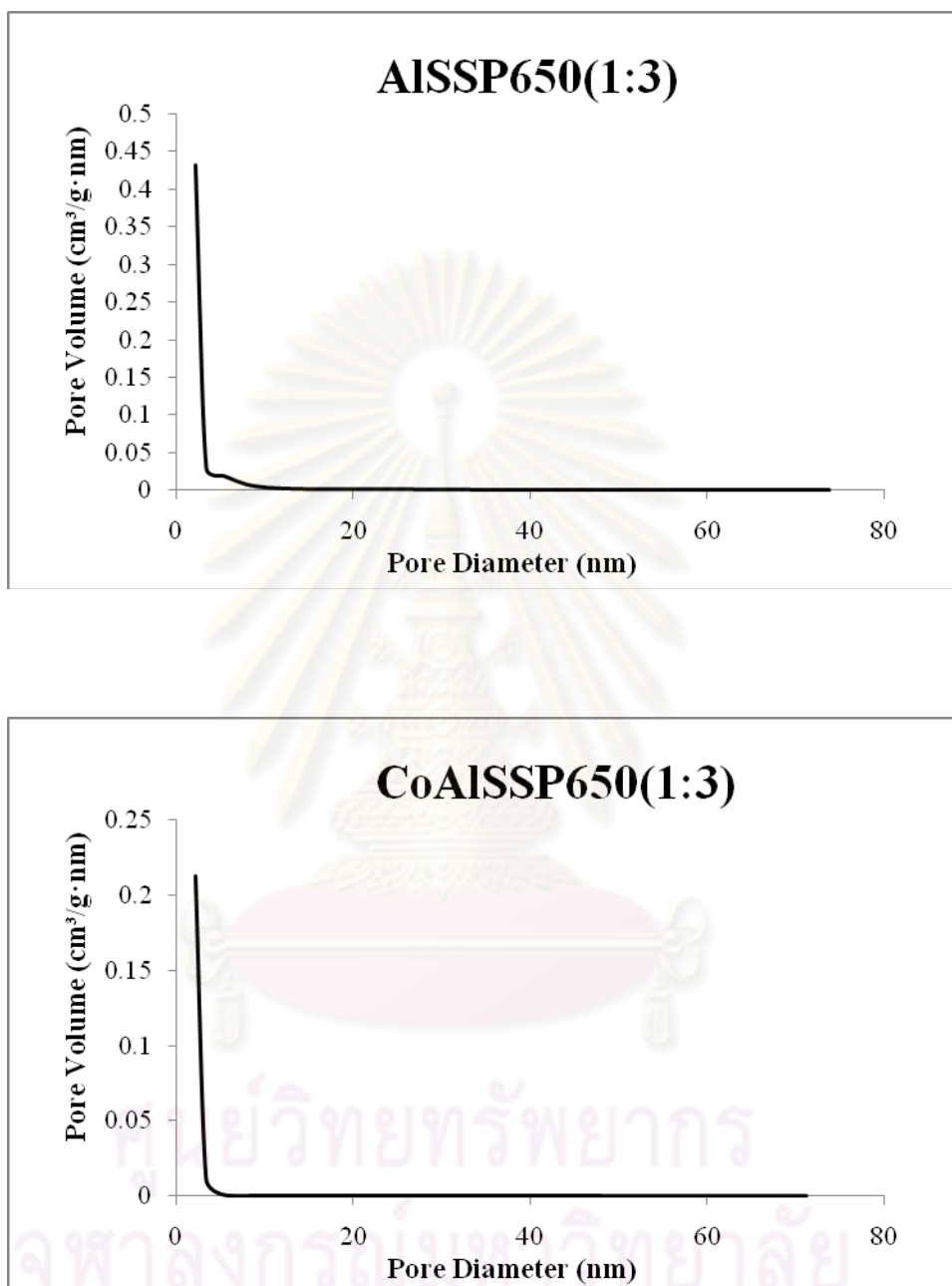


**Figure F.2** The pore size distribution of AISSP650 (1:3) and CoAISSP650 (1:3).

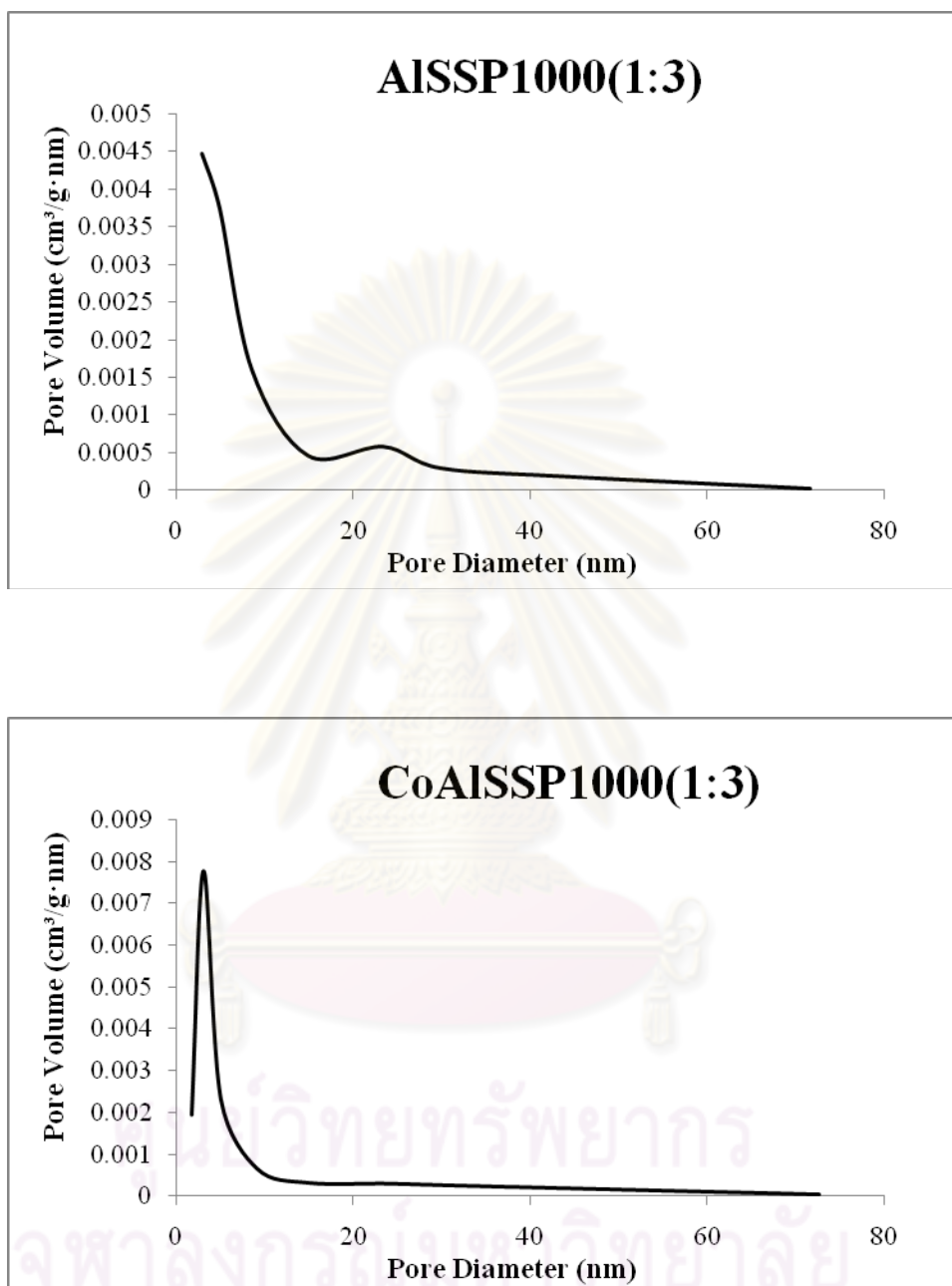


**Figure F.3** The pore size distribution of AISSP1000 (1:3) and CoAISSP1000 (1:3).

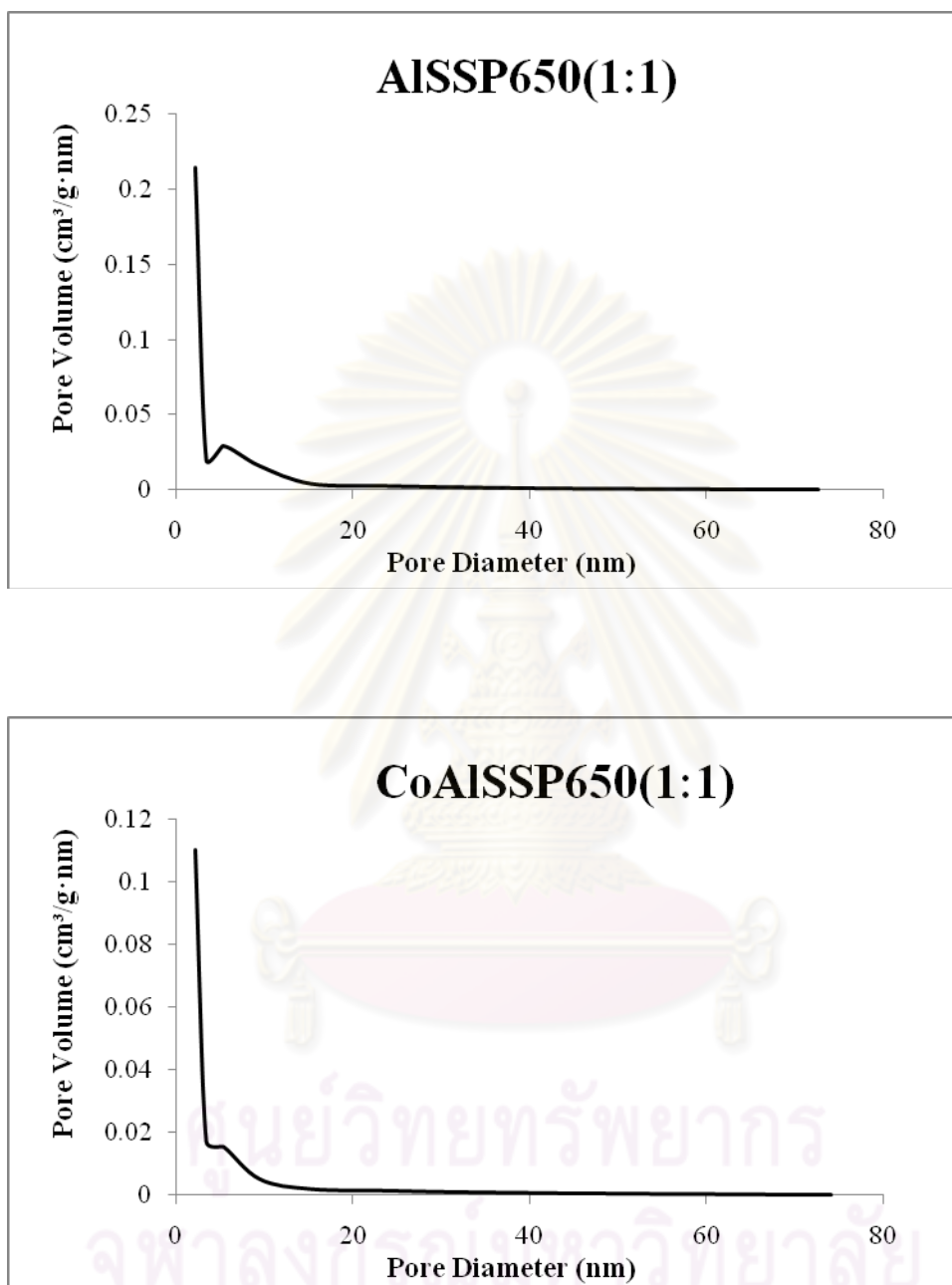


**Figure F.4** The pore size distribution of AISSP650 (1:1) and CoAISSP650 (1:1).



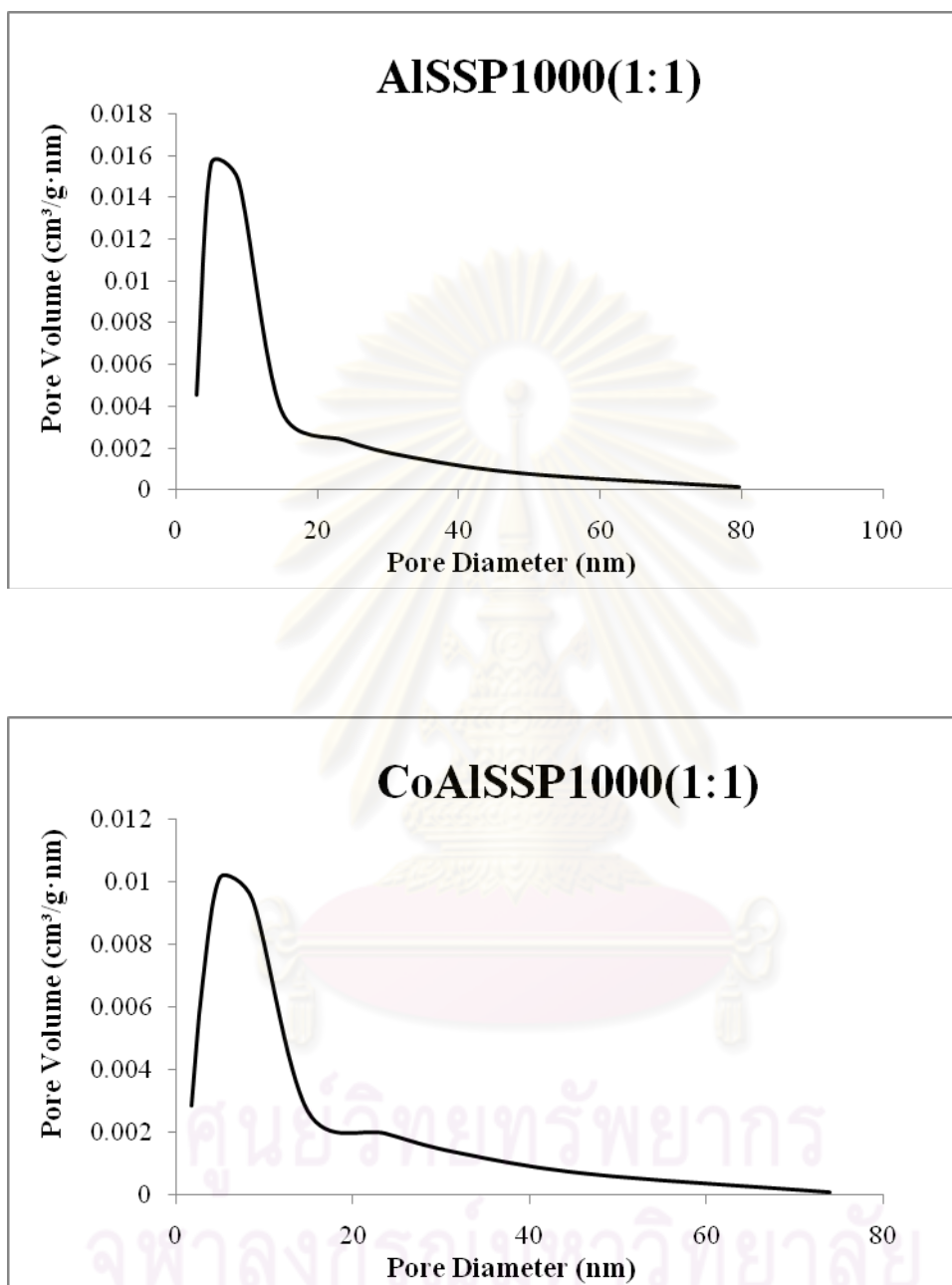


**Figure F.5** The pore size distribution of AISSP1000 (1:1) and CoAISSP1000 (1:1).

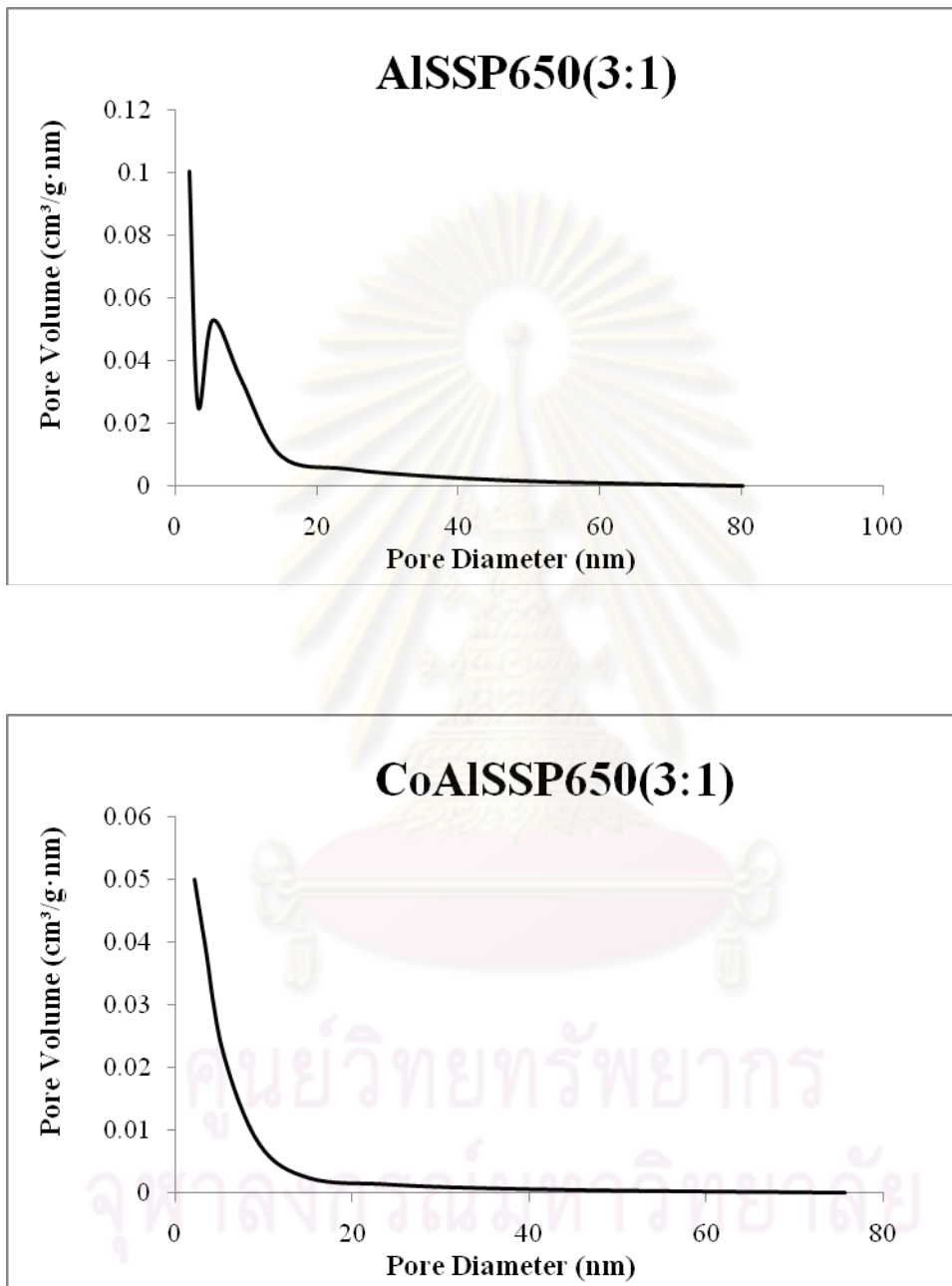


**Figure F.6** The pore size distribution of AlSSP650 (3:1) and CoAlSSP650 (3:1).

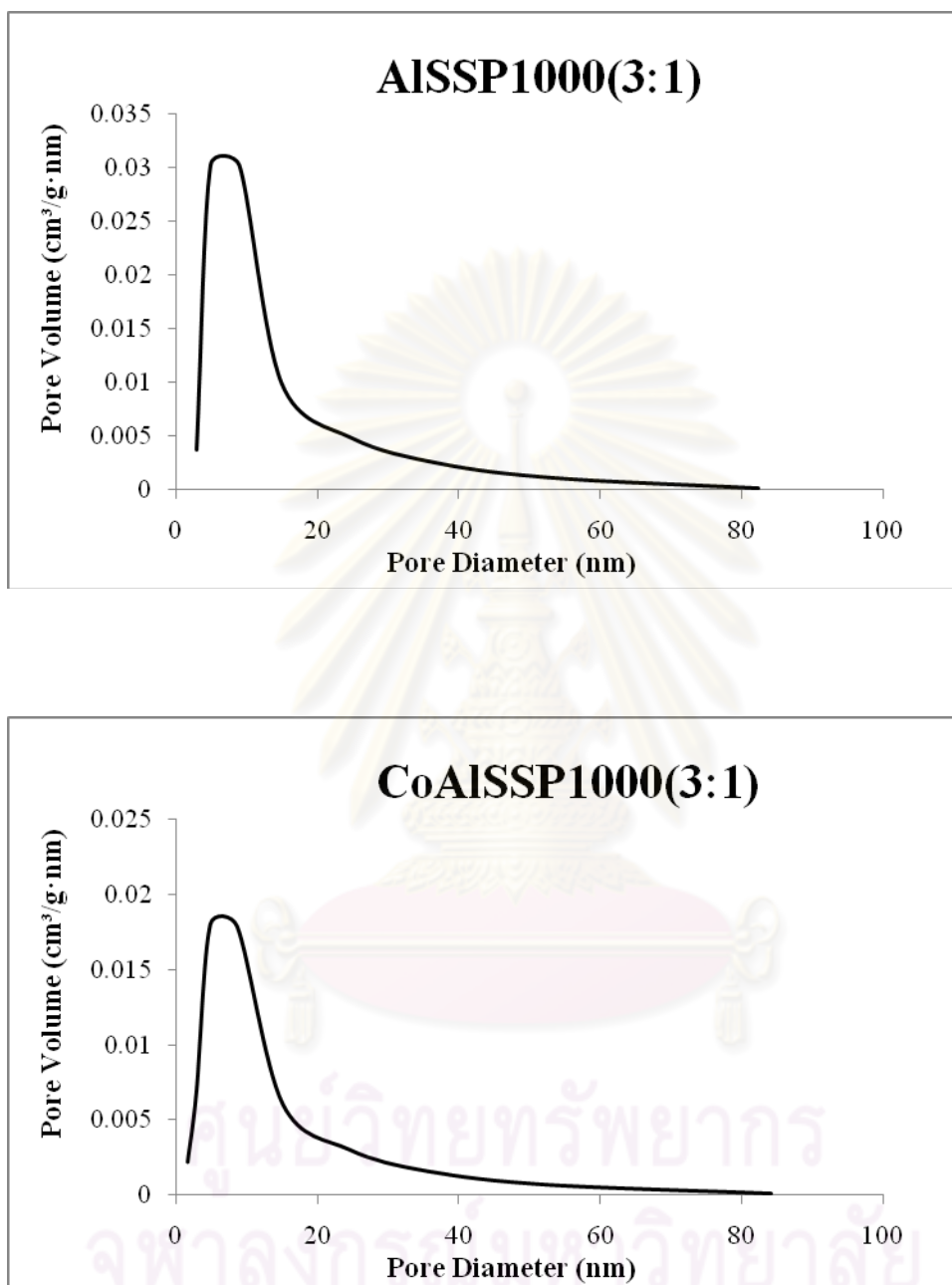


**Figure F.7** The pore size distribution of AISSP1000 (3:1) and CoAISSP1000 (3:1).

## APPENDIX G

### LIST OF PUBLICATION

- **Proceeding**

Thamonwan Jetsadanurak and Bunjerd Jongsomjit, “Carbon dioxide hydrogenation over alumina-silica composites supported cobalt catalyst.” Proceeding of the 17<sup>st</sup> Regional Symposium on Chemical Engineering, Queen Sirikit National Convention Center, Bangkok, Thailand, November, 2010.



ศูนย์วิทยทรัพยากร  
จุฬาลงกรณ์มหาวิทยาลัย

# Carbon dioxide hydrogenation over alumina-silica composites supported cobalt catalyst

Thamonwan Jetsadanurak\* and Bunjerd Jongsomjit

Department of Chemical Engineering, Faculty of Engineering,  
Chulalongkorn University, Bangkok, 10330, Thailand  
e-mail: [thamonwan.j@irpc.co.th](mailto:thamonwan.j@irpc.co.th)

## Abstract

This research focused on investigation of characteristics of the Al<sub>2</sub>O<sub>3</sub>-SiO<sub>2</sub> microparticle composites that were prepared by deposition of Al<sub>2</sub>O<sub>3</sub> particles on the spherical silica particle (SSP) surface using hydrolysis of aluminium isopropoxide with loading of 75% of SiO<sub>2</sub> and 25% of Al<sub>2</sub>O<sub>3</sub> to obtain AlSSP with calcination temperature at 650 and 1000 °C. Furthermore, the characteristics of the impregnated cobalt on spherical silica particle support (CoSSP) and alumina-silica composites support (CoAlSSP) were investigated. In addition, the catalytic activity and selectivity to methane of CoSSP and all of CoAlSSP for carbon dioxide hydrogenation with reaction temperature at 220°C was studied and characterized by X-ray diffraction (XRD), BET surface area, differential thermal analysis and thermogravimetric (DTA/TG), energy-dispersive X-ray spectroscopy (EDX), scanning electron microscopy (SEM), temperature-programmed reduction (TPR), and CO chemisorptions methods. Based on the reaction study, it revealed that the presence of alumina in the composited supports resulted in increased activity dramatically, but had slight effect on selectivity.

**Keyword:** Silica, Alumina isopropoxide, Cobalt, Carbon dioxide hydrogenation

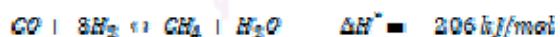
## 1. Introduction

Chemical CO<sub>2</sub> fixation has become of greater interest in recent years, primarily because of its impact on the environment through the greenhouse gases appear to warm up the atmosphere [1]. The current interest in CO<sub>2</sub> hydrogenation Fischer-Tropsch synthesis has been extensively studied for years [1]-[5].

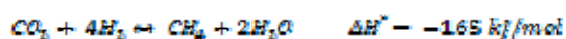
About the mechanism of CO<sub>2</sub> hydrogenation Fischer-Tropsch synthesis the general view is a first RWGS reaction as follow;



to produce CO which is subsequently consumed in the FT conversion as;



However, the additional reaction of a direct CO<sub>2</sub> hydrogenation occurs as;



In general, the catalyst properties depend on reaction conditions, catalyst compositions, metal dispersion, and types of inorganic supports used. Cobalt catalysts represent the optimal choice for

low temperature, because of higher stability, higher conversion and relatively small negative effect of water on conversion [6]. Furthermore, the supported metal catalyst has significantly enhanced the catalytic properties as well.

SiO<sub>2</sub> has been considered to be very attractive because of high surface area, thermal stability and improving the reduction degree of supported cobalt [7]. Al<sub>2</sub>O<sub>3</sub> is one of the most supports for cobalt catalyst because of its favorable mechanical properties and adjustable surface properties. In addition, it significantly improved the catalytic activity of FTS by increasing the dispersion [8].

Therefore, the main objective of this present study was to investigate the catalytic behaviors of CO<sub>2</sub> hydrogenation over alumina-silica composited supported cobalt catalyst. The composited supports and catalyst were prepared, characterized by several techniques, such as XRD, BET, DTA/TG, SEM/EDX, TPR, and CO chemisorptions methods, and tested for CO<sub>2</sub> hydrogenation reaction.

## 2. Material

Cetyltrimethylammonium bromide (C<sub>16</sub>TMABr), Tetraethoxysilane 98% (TEOS), Aluminium isopropoxide 98% (Al(OPr<sup>i</sup>)<sub>3</sub>), and

Cobalt (II) nitrate hexahydrate 98% were obtained from Aldrich. Ammonia 30% was available from Panreac. Ethanol 99.99% and Isopropanol was available from J.T. Baker and QReC, respectively.

### 3. Experimental

#### 3.1.1. Preparation of the spherical silica particle (SSP)

The composition of the synthesis gel of mesoporous SSP has following molar ratio: 1TEOS : 0.3C<sub>16</sub>TMABr : 11NH<sub>3</sub> : 58Ethanol : 144 H<sub>2</sub>O. The solution was further stirred for 2 h at room temperature. The white precipitate was then collected by filtration and washed with distilled water. Dried samples were calcined at 550°C for 6 h with a heating rate of 10 °C min<sup>-1</sup> in air.

#### 3.1.2. Preparation of the SiO<sub>2</sub>-Al<sub>2</sub>O<sub>3</sub> composites support

Calculate equivalent to the desired loading percentage of aluminium isopropoxide, diluted in isopropanol (1:3), was added to suspended silica from 3.1.1. (SiO<sub>2</sub>:i-PrOH = 1:1.5). The solution was stirred for 1 h. Hydrolysis was performed by addition of ammonia, H<sub>2</sub>O: Al(OPr<sup>i</sup>)<sub>3</sub> molar ratio being 4:1. The sol was further stirred for 20 h at room temperature. Next, the sample was dried at 110°C for 24 h. Finally, the samples were calcined at 600 and 1000 °C for 2 h with a heating rate of 10 °C min<sup>-1</sup> in air.

#### 3.1.3. Preparation of catalyst samples

A 20 wt% of Co/SiO<sub>2</sub> and Co/SiO<sub>2</sub>-Al<sub>2</sub>O<sub>3</sub> composite supports were prepared by the incipient wetness impregnation. A designed amount of cobalt nitrate [Co(NO<sub>3</sub>)<sub>2</sub>·6H<sub>2</sub>O] was dissolved in deionized water, then impregnated onto the composited oxide supports obtained from 3.1.1. and 3.1.2. The catalyst precursor was dried at 110°C for 12 h and calcined in air at 500°C for 4 h.

### 3.2. Catalyst nomenclature

The nomenclature used for the catalyst samples in this study are following:

- SSPXXX
- AlSSPXXX
- CoSSPXXX
- CoAlSSPXXX

XXX refers to calcination temperature.

### 3.3. Catalyst characterization

The specific surface area calculated by the BET method was determined from nitrogen adsorption-desorption isotherm at liquid nitrogen temperature by using a Micromeritics Pluse Chemisorb 2700 system. The sample phase and its crystalline size was examined by X-ray diffraction (XRD), which was carried out on a SIEMENS D-5000 X-ray diffractometer using Cu K $\alpha$  radiation ( $\lambda = 0.154$  nm) with a scanning angle  $2\theta = 20-80^\circ$ . SEM and EDX were used to determine the morphologies and elemental distribution throughout the granules, respectively. The SEM of JEOL model JSM-5800LV was applied. EDX was performed using Link Isis series program. DTA/TG used to determine the weight loss pattern and the reducibility of catalysts by Shimadzu TGA model 50. The reduction behaviors and reducibilities of the samples were investigated by TPR. It was carried out using 50 mg of a sample and a temperature ramp from 35 to 800°C at 10°Cmin<sup>-1</sup>. The carrier gas was 5% H<sub>2</sub> in Ar. A cold trap was placed before the detector to remove water produced during reaction. A thermal conductivity detector (TCD) was used to determine the amount of H<sub>2</sub> consumed during TPR. Static CO chemisorptions at room temperature on the reduce catalysts was used to determine the number of reduced surface cobalt metal atoms. This related to the overall activity of the catalysts during CO<sub>2</sub> hydrogenation.

### 3.4. Reaction

CO<sub>2</sub> hydrogenation (H<sub>2</sub>/CO<sub>2</sub> = 10.36/1) was performed to determine the overall activity of the catalyst samples. Hydrogenation of CO<sub>2</sub> was carried out at 220°C and 1 atm. A flow rate of H<sub>2</sub>/CO<sub>2</sub>/Ar = 10.36/1/4.72 cc min<sup>-1</sup> in a fixed-bed flow reactor under differential condition was used. Typically, 50 mg of a catalyst sample was reduced in situ in flowing H<sub>2</sub> at 350°C for 3 h prior to CO<sub>2</sub> hydrogenation. Reactor effluent samples were analyzed using gas chromatograph technique. In all case, steady-state was reached within 6 h.

#### 4. Results and Discussion

##### 4.1. Characteristics of composited support and catalyst

The XRD patterns of  $\text{Al}_2\text{O}_3\text{-SiO}_2$  composited supports before impregnation with the cobalt are shown in Fig. 1. It was observed that the SSP exhibited a broad XRD peak assigning to the conventional amorphous silica. Similar to the SSP, the different XRD patterns of pure alumina indicated the amorphous,  $\gamma$ -alumina and  $\alpha$ -alumina characteristic peaks [9]. XRD patterns of the composited supports at various calcination temperatures revealed the change of intensity of XRD characteristic peaks. At 1000 °C, the slight diffraction peak of  $\text{Al}_2\text{O}_3$  crystallite can be observed at 67°. This demonstrates that  $\text{Al}_2\text{O}_3$  had a small crystalline size of  $\gamma$ -alumina. After impregnation with the cobalt and calcinations, all samples of CoSSP and CoAlSSP catalysts were again identified using XRD. The XRD patterns of all samples are shown in Fig. 1. All samples indicated that there was no further phase transformation from amorphous to  $\gamma$ -alumina occurred after calcinations (at temperature ca. 500°C for 4 h). The amorphous silica also exhibited good stability upon the same calcination process. Besides the corresponding composited supports detected, all calcined samples also exhibited XRD peaks at 31°, 37°, and 65°, which were assigned to the presence of  $\text{Co}_3\text{O}_4$ . Based on XRD results, it indicated that the presence of  $\text{Co}_3\text{O}_4$  was apparently in the highly dispersed form.

DTA/TG curve of  $\text{Al}_2\text{O}_3\text{-SiO}_2$  composited support was shown in Fig. 2. The DTA curve displayed endothermic peak due to the evaporation of physical adsorbed water. One noticeable exothermic peak at 992°C was related to the XRD patterns as mentioned above. The DTA curve indicated the phase transformation of amorphous to  $\gamma$ -alumina.

The properties of the  $\text{Al}_2\text{O}_3\text{-SiO}_2$  composited supports and composited supported cobalt catalysts are compared in Table 1. The BET surface area of the  $\text{Al}_2\text{O}_3\text{-SiO}_2$  composited supports decreased with the increased calcination temperature. A small decrease in

surface area and pore volume was observed after cobalt addition in silica and  $\text{Al}_2\text{O}_3\text{-SiO}_2$  composited supported catalysts. This decrease is likely attributed to the effect of support dilution with cobalt. Besides, the effect of support pore size was primary important for the product selectivity related to size of the  $\text{Co}_3\text{O}_4$  cobalt particles [10].

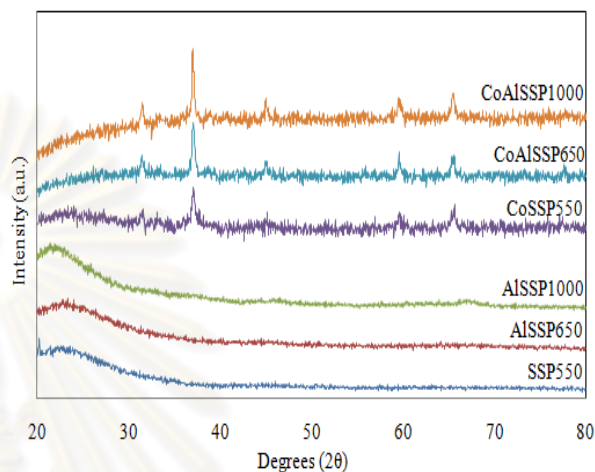


Fig. 1: XRD patterns of the  $\text{Al}_2\text{O}_3\text{-SiO}_2$  composited supports and composited supported cobalt catalysts after calcination.

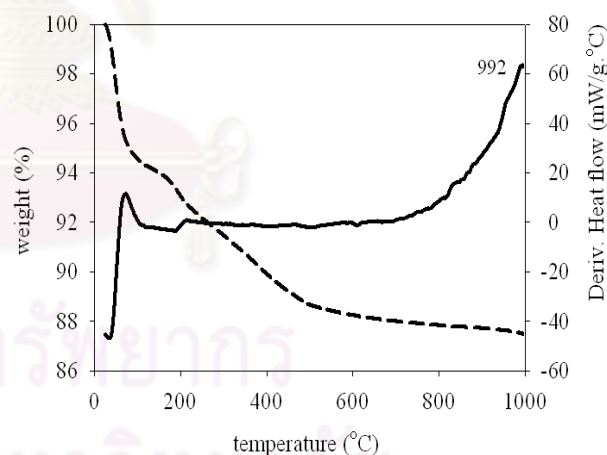


Fig. 2: DTA/TG of  $\text{Al}_2\text{O}_3\text{-SiO}_2$  composited support

SEM and EDX were also conducted in order to study the morphologies and elemental distribution of the samples, respectively. The alumina was apparently located on the outer surface of silica as shown in Fig. 3. Besides, the typical SEM micrographs along with the EDX mapping (for Co, Si, and Al) of  $\text{Al}_2\text{O}_3\text{-SiO}_2$  composited supported cobalt catalyst sample are illustrated in Fig. 4 indicating the external

Table 1: Characterization of  $\text{Al}_2\text{O}_3\text{-SiO}_2$  composited supports and composited supported cobalt catalysts

Sample	BET SA ( $\text{m}^2/\text{g}$ )	Pore size (nm)	Pore volume ( $\text{cm}^3/\text{g}$ )
SSP550	927.3	2.18	0.75
AlSSP650	769.8	2.56	0.62
AlSSP1000	23.0	6.92	0.05
CoSSP550	631.4	2.46	0.46
CoAlSSP650	489.9	2.56	0.62
CoAlSSP1000	24.5	5.16	0.04

surface of the sample granule. It can be seen that the cobalt oxides were well distributed (shown on EDX mapping) all over the sample granule.

Temperature-programmed reduction on the calcined samples needs to be performed in order to give a better understanding according to such a reduction behavior. The TPR profiles for all of samples are shown in Fig. 5. The curves recorded after calcination showed a number of reducible cobalt species present in the catalyst. The first peak has been ascribed the reduction of  $\text{Co}_3\text{O}_4$  to  $\text{CoO}$ , followed by the second peak which corresponds to the reduction of  $\text{CoO}$  to  $\text{Co}$  [10]. The reduction temperatures were found to slightly shift of to higher temperatures with increasing the amount of alumina present in the composited supports.

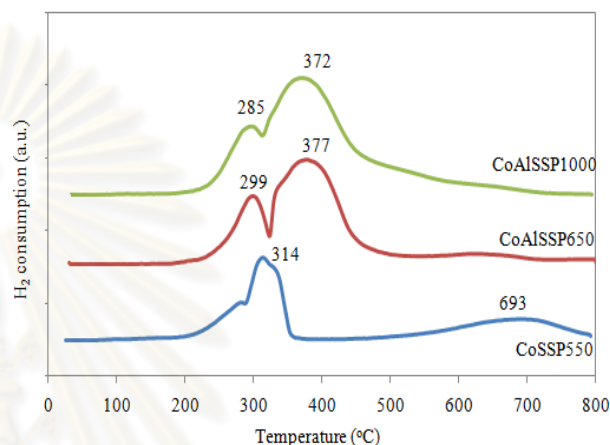


Fig. 5: TPR profiles of the  $\text{Al}_2\text{O}_3\text{-SiO}_2$  composited supported cobalt catalysts after calcination.

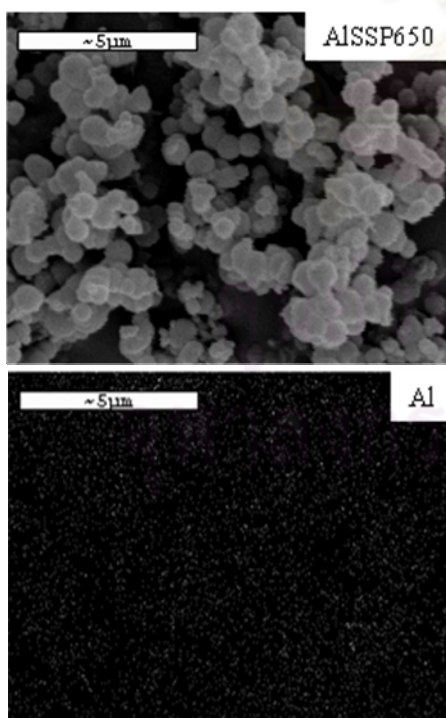


Fig. 3: A typical of SEM micrograph and EDX mapping of  $\text{Al}_2\text{O}_3\text{-SiO}_2$  composited support.

The pronounced shift of reduction temperature to higher ones found that the strong interaction between the supported cobalt and the alumina supports often results in the relative low reducibility [8]. Therefore, CO chemisorptions at room temperature on the reduce catalysts was used to determine the number of reduced surface cobalt metal atoms. The result CO chemisorptions for all samples are shown in Table 2. It revealed that the number of reduced cobalt metal atoms increase with increasing the amount of alumina present in the composited supports.

#### 4.2. Reaction study

In order to determine the catalytic behaviors of the cobalt catalyst on the alumina-silica composited supports. The resulted reaction study is also shown in Table 2. The overall activities dramatically increased with the amount of alumina present in the composited supports.



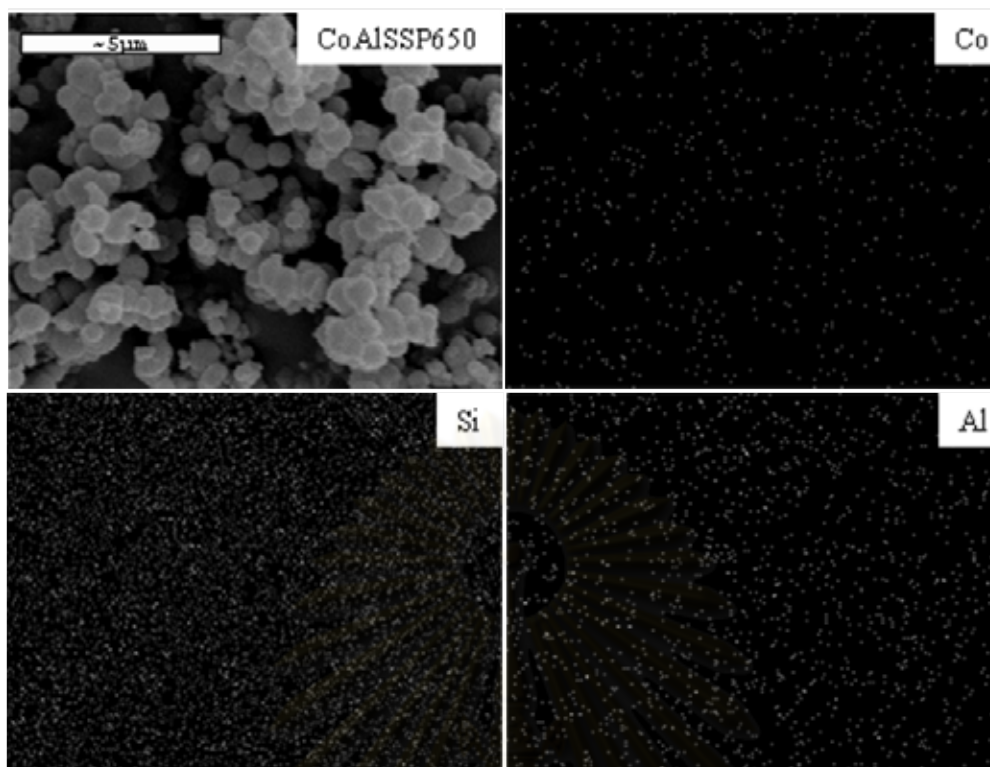


Fig. 4: SEM micrograph and EDX mapping of the calcined  $\text{Al}_2\text{O}_3\text{-SiO}_2$  composited supported cobalt catalyst.

It is known that alumina improved the catalytic activity of enhanced reaction performance by increasing the dispersion [8]. Considering the selectivity of product, it showed that the selectivity to methane also slightly increased with the the amount of alumina present in the composited supports. The cobalt particle size is primary of importance for the product selectivity. It was controlled by the support pore size [10] as seen from BET surface area results.

### Conclusion

The present study showed impact of alumina-

silica composite supported cobalt catalysts on their catalytic behaviors. It was found that the alumina significantly enhanced the activity and selectivity to methane of  $\text{CO}_2$  hydrogenation, indicating the dispersion of alumina, reduction degree of silica and BET surface area in term of pore size can be facilitate.

### Acknowledgment

The author gratefully acknowledges the financial support by the Thailand Research Fund (TRF).

Table 2: Show the dispersion, reaction rates, and product selectivity of various samples

Sample	% Dispersion of cobalt	Rate ( $\times 10^2$ g $\text{CH}_2$ /gcat·h)		Product Selectivity (%) <sup>a</sup>	
		initial <sup>a</sup>	Steady state <sup>b</sup>	$\text{CH}_4$	CO
CoSSP550	0.06	10.38	10.85	93.04	6.96
CoAlSSP650	0.2	17.75	10.09	94.44	5.56
CoAlSSP1000	0.55	19.71	14.21	95.05	4.93

<sup>a</sup> After 5 min of reaction

<sup>b</sup> After 4 h of reaction

**References**

- 1) T. Riedel, M. Claeys, H. Schulz, G. Schaub, and S. Nam: *Applied Catalysis*, **201-213** (1999) 186.
- 2) T. Suzuki, Y. Hirai, and S. Hayashi: *Int. J. Hydrogen Energy*, **979-983** (1993) 18.
- 3) A.M. Saib, M. Claeys, and E. van Steen: *Catalysis Today*, **395-402** (2002) 71.
- 4) R.A. Dagle, Y. Wang, G. Xia, J.J. Strohm, J. Holladay, and D.R. Palo: *Applied Catalysis*, **213-218** (2007) 326.
- 5) P. Panagiotopoulou, D.I. Kondarides, and X.E. Verykios: *Applied Catalysis*, **45-54** (2008) 344.
- 6) A.Y. Khodakov: *Catalysis Today*, **251-257** (2009) 144.
- 7) A. Jean-Marie, A. Griboval-Constant, A.Y. Khodakov, and F. Diehl: *C.R. Chimie*, **660-667** (2009) 12.
- 8) X. Sun, X. Zhang, Y. Zhang, and N. Tsubaki: *Applied Catalysis A: General*, **134-139** (2010) 377.
- 9) H. Liu, G. Ning, Z. Gun, and Y. Lin: *Materials Research Bulletin*, **785-788** (2009) 44.
- 10) O. Borg, S. Eri, E.A. Blekkan, S. Storsaeter, H. Wigum, E. Rytter, and A. Holmen: *Journal of catalysis*, **89-100** (2007) 248.
- 11) O.I. Lebedev, G.V. Tendeloo, O. Collart, P. Cool, and E.F. Vansant: *Solid State Sciences*, **489-498** (2004) 6.
- 12) J.R. Grzechowiak, I. Szyszka, and A. Masalska: *Catalysis Today*, **433-438** (2008) 137.

ศูนย์วิทยทรัพยากร  
จุฬาลงกรณ์มหาวิทยาลัย

## VITA

Miss Thamonwan Jetsadanurak was born on November 21<sup>st</sup>, 1983 in Songkhla province, Thailand. She finished high school from Mahidolwittayanusorn School in 2002, and received the bachelor's degree of Chemical Technology from Chulalongkorn University in 2006. She continued her master's study at Department of Chemical Engineering, Faculty of Engineering, Chulalongkorn University in 2009.



ศูนย์วิทยทรัพยากร  
จุฬาลงกรณ์มหาวิทยาลัย